Understanding movement processes underlying camera-trap data for reliable population inference

Meryl Tze Yin Theng

School of Biological Sciences

A thesis submitted to The University of Adelaide
in fulfilment of the requirement for the degree of

Doctor of Philosophy

March 2023

Declaration

I certify that this work contains no material which has been accepted for the award of any other degree or diploma in my name in any university or other tertiary institution and, to the best of my knowledge and belief, contains no material previously published or written by another person, except where due reference has been made in the text.

In addition, I certify that no part of this work will, in the future, be used in a submission in my name for any other degree or diploma in any university or other tertiary institution without the prior approval of the University of Adelaide and where applicable, any partner institution responsible for the joint award of this degree.

The author acknowledges that copyright of published works contained within this thesis resides with the copyright holder(s) of those works. I give permission for the digital version of my thesis to be made available on the web, via the University's digital research repository, the Library Search and also through web search engines, unless permission has been granted by the University to restrict access for a period of time.

Signed:

Meryl Tze Yin Theng (PhD Candidate)

Date: 14 March 2023

Acknowledgements

I acknowledge and pay my respects to the Kaurna people, the traditional custodians on whose ancestral lands the University of Adelaide's campuses at North Terrace, Waite and Roseworthy are built. I acknowledge the deep feelings of attachment and relationship of the Kaurna people to country, and I respect and value their past, present and ongoing connection to the land and cultural beliefs.

First and foremost, I express my deepest gratitude to my supervisors Steven Delean and Phill Cassey. Steve, you have guided me through the world of statistics and quantitative ecology and encouraged my interests right from the start. Your optimism and faith in me was the beacon I looked to whenever I doubted myself. Thank you for always wanting the best for me. Phill, you have always kept me grounded in real world conservation issues and offered me great ideas for applications of my work. I appreciate the research freedom you gave me, allowing me to go on crazy tangents to explore, learn and fail in the process. Thank you for welcoming me to your lab.

This thesis would not have been possible without the wonderful external collaborations I have made along the way. To my co-supervisor, Chloe Bracis, I have learned so much about movement ecology and mathematical modelling from you. You were so receptive and supportive of my ideas and worked towards my visions with me. I am so lucky to have you. To my mentors, Cyril Milleret and Pablo Palencia — each of you are respected experts in your field and it has been such a privilege to learn from you. Thank you for being so patient with my (sometimes) incessant flow of questions and for the stimulating discussions over email and Zoom.

I'm so grateful for the friends I have made during the duration of my PhD. Mingyue, Steph, Oli, Jin and Janine, thank you for being there for me, for the

adventures and the meaningful conversations. Thank you to Katie and Jacob (and other colleagues not mentioned here) for your friendship and support too. To my old friends in Singapore — Tze Kwan, Tong, Eva and Evan — thank you for being there for me through the years.

I would like to express my gratitude to my undergraduate supervisor, Sivasothi. Thank you for supporting my numerous attempts to pursue grad school, You believed in me right from the start, even though I gave you many reasons not to. You are a big reason for what I have achieved today.

I am very grateful for the financial support received from The University of Adelaide, though the Adelaide Scholarship International award.

Finally, I would like to thank my family, especially my dad. You have always supported my dreams and passions, no matter how far away it took me from you. You are the foundation that has made this all possible. Thank you.

This thesis was built using Quarto and the OxThesis LaTeX template.

Summary

Understanding how animal movement drives spatial distribution patterns and population dynamics is critically important as the consequences of ignoring movement in population models are increasingly recognised. While the gap between both fields is narrowing, the extent to which knowledge of animal movement is required for accurate population-level inferences remains unclear. This thesis harnesses advancements in animal movement modelling to evaluate the reliability of inferences obtained from population abundance (or density) estimation methods for both *marked* (i.e., individually distinguishable) and *unmarked* (i.e., not individually distinguishable) animals. The primary aim of my thesis was to explore the impact of animal movement (and other processes, e.g., imperfect detection) on population-level (i) distribution and space use patterns, and (ii) abundance estimation within the framework of camera-trap (CT) applications.

Population-level patterns are fundamentally emergent from movement decisions made at the individual animal level. The first piece of research (**Chapter 2**) explores this mechanistic link with a multi-individual movement simulation model, in which an individual's movement decisions are driven by two important biological processes: its memory of the resource landscape (i.e., resource memory) and conspecific scent environment (i.e., territorial exclusion). I used the framework to investigate how each process affects emergent space-use patterns. Both mechanisms together led to the formation of exclusive, resource- and population density-dependent utilisation distributions (UDs), which were responsive to perturbations in the conspecific environment (i.e., removing individuals). Model application to a population of feral cats demonstrates that general space-use measures (e.g., median UD area, resident and transient dynamics) can be approximated through

simulation, though finer-scale space use patterns (e.g., cumulative UD area) are poorly matched. Despite this, the model's process-based approach of simulating movement can be applied to studies that aim to evaluate the consequences of not accounting for more complex, fine-scale movement behaviours in ecological models.

In the second data chapter (**Chapter 3**), the movement simulation model (developed in **Chapter 2**) was applied in the evaluation of abundance estimation methods for *marked* populations - namely, spatial capture-recapture (SCR) models. Individual detection data was generated from simulated movement trajectories and then fitted to a basic, resource selection and transience SCR model, as well as their variants accounting for resource-driven heterogeneity in density and detectability. In general, results demonstrated that population-level inferences of abundance, and resource effect on spatial variation in density, were robust when the level of individual heterogeneity induced by the underlying movement process is low. However, my evaluation framework exposed weaknesses in current SCR models' ability to accurately reveal finer scale patterns of ecological and movement processes (e.g., resource effect on detectability and space use), and we recommend further integration of complex movement into the SCR framework to address this shortcoming.

The third data chapter (**Chapter 4**) examines the performance of CT-based abundance estimation methods for *unmarked* populations. While methods of abundance estimation of marked animals are well-established, the equivalent methods for unmarked animals are relatively new, at a stage where robustness of abundance estimates is in question. Hence, the complexity of movement simulated in **Chapter 2** and **3** was not applied here, and a simpler approach that represented a breadth of population scenarios (e.g., discrete-time biased correlated random walks, state-switching behaviour in group-living populations), was used. I evaluated abundance estimator performance from three unmarked methods (REM: random encounter model, REST: random encounter and staying time, CTDS: camera trap distance sampling) under a wide range of scenarios that vary in population densities, movement rates (i.e., speed and home-range size). Results imply that CTDS and REST can reliably estimate abundance for both solitary and group-living animals if

population densities are not low and trap effort is substantial. REM is potentially reliable under the same circumstances, but model parameters are prone to bias without careful consideration in the measurement and parameterisation process. Unmarked density estimation currently requires substantial investment of effort, thus improving their cost-effectiveness should be a priority for future research.

Finally, I synthesise the findings from my thesis and discuss the future of research at the interface of movement and population ecology, and for abundance estimation in CT applications (**Chapter 5**: General Discussion). In my view, the integration of animal movement and population dynamics models has great potential for improved inferences at the interface of population, movement and landscape ecology. As for CT-based abundance estimation, several key challenges to practical use remain, namely: (i) the substantial labour required in data collection; (ii) inconsistency in analytical approaches for unmarked animals; (iii) considerable level of statistical knowledge and computational resources required for model implementation, and; (iv) limitations in ecological inference. However, I believe that many of the solutions to these problems will be available in the near future – especially in light of rapid technological advances in data automation workflows and cloud-platform solutions.

Table of contents

List of Figures

List of Tables

1 General Introduction

Understanding the drivers of species abundance, density, spatial distribution, and habitat selection is essential to conservation and management of animal populations. Ecologists have sought to quantify these processes through both abundance estimation (e.g., Buckland et al. 2001, Royle et al. 2014a) and animal movement modelling (e.g., Hooten et al. 2017), which have independently seen widespread application and advancement in recent decades. Population modelling has traditionally focused on population-level processes, such as abundance and distribution, while movement modelling has primarily focused on the individual-level to understand movement and space use. Yet, there are clear mechanistic links between the two scales – animal movement or space use is a response to extrinsic factors (e.g., changing resource distributions, competition, group association, predation risk) that affect individual performance (e.g., survival and reproduction), and when aggregated over many individuals, population-level demography emerges (e.g., density and distribution). While these important linkages exist, it is much less clear when (or how much) knowledge of individual movement processes are required for reliable and meaningful inferences at the population level. Hence, studies at the interface of population estimation and movement ecology offer enormous potential for new insights (Morales et al. 2010).

1.1 Movement modelling

Animal movement modelling has seen rapid development and application in the past two decades, largely because of technological advances in animal tracking (e.g., GPS telemetry) and remote sensing technology (Kays et al. 2015). Conventionally, spatial point process models (assuming independent animal locations) were popular for estimating utilisation distributions (e.g., home-range size) and habitat use with resource selection functions (RSFs) (Manly et al. 2007). However, the increasing temporal resolution in telemetry data brought about the need to account for spatiotemporal autocorrelation in time series data (e.g., via step selection functions, Brownian bridges, state-space models, Horne et al. 2007, Thurfjell et al. 2014, Avgar et al. 2016, Auger-Méthé et al. 2021) and presented an opportunity for investigations into finer scale movement processes (e.g., behavioural states). This brought about a shift towards explicit models for animal movement, typically based on variations of random walk models formulated in either discrete or continuous time. One class of such models is based on multistate random walks, and more recently, hidden Markov models (HMMs), which have been developed as statistical mechanical methods that treat complex movement paths as a series of underlying behavioural states (e.g., foraging, migrating, resting) affected by changes in the internal (e.g., metabolic rate) and external (e.g., resources) environment (McClintock et al. 2012, McClintock and Michelot 2018). These movement models provide an inferential framework for understanding how individual movement processes can give rise to space use patterns and dynamics at larger scales (e.g., recharge dynamics, Hooten et al. 2019, group movement, Langrock et al. 2014).

On the more theoretical side, there have been more mechanistic formulations that describe the complex biological processes governing individual movement decisions giving rise to realistic and dynamic space use patterns. One of the key developments is the incorporation of spatial memory processes to navigate a dynamic resource landscape, in which the individual avoids a recently exploited resource locality but potentially returns to it in the long-term (i.e., expecting renewal). Home-

ranging patterns have been shown to emerge from these processes (Van Moorter et al. 2009, Bracis et al. 2015). While memory models have largely provided a mechanistic explanation for stabilising space use patterns of single individuals, one study has demonstrated how memory-mediated movement decisions at the individual level can lead to a population of individuals self-organising into spatially segregated home-ranges on a resource landscape (i.e., nonterritorial segregation, Riotte-Lambert et al. 2015). Another important development is the incorporation of inter-animal interactions, either direct or mediated by a stigmergent process, such as scent deposition or visual cues (e.g., Giuggioli et al. 2013). Territoriality mediated via scent marking and avoidance processes is a well-established mechanistic framework that gives rise to the formation of spatially distinct territorial areas at the population level (Potts and Lewis 2014). Though largely built from theory and difficult to quantify in the field, empirical evidence for these mechanisms is being uncovered one piece at a time (e.g., Moorcroft et al. 2006, Bracis and Mueller 2017, Merkle et al. 2017, Ranc et al. 2021). More importantly (and in the context of this thesis) they offer realistic starting points from which to understand the complexities of how population-level quantities, patterns and trends emerge – inferences that animal population studies seek to obtain.

1.2 Population abundance estimation

1.2.1 Marked animals

A fundamental goal of many population assessments is to obtain reliable estimates of abundance (or density) and associated ecological inferences (e.g., spatial variation in density). Capture-recapture (CR) is a foundational tool in population ecology, widely used to estimate abundance of *marked* (i.e., individually identifiable) animal populations. While early CR models ignored spatial and movement processes (e.g., Otis et al. 1978, Seber 1982, Williams et al. 2002), the introduction of the Spatial Capture-Recapture (SCR) models (Efford 2004), and subsequent expansions (Borchers and Efford 2008, Royle and Young 2008, Gardner et al.

2009), has addressed numerous deficiencies associated with non-spatial approaches, including: defining an effective sampling area for estimating density and eliminating the bias induced by unmodelled heterogeneity in detection probability attributable to individual space use (Royle et al. 2014a). Most importantly, the SCR framework links movement, space use, or resource selection to population dynamics, allowing for inference at the intersection of these components (e.g., Royle et al., 2013). Though model assumptions about animal space use and detection are simplified, abundance (the primary parameter of interest) estimation has generally proven to be robust to assumption violations, unless such violations are substantial (Royle et al. 2013b, Borchers et al. 2014, Sutherland et al. 2015, Bischof et al. 2020a, Moqanaki et al. 2021).

SCR models have been extended to address abundance estimator bias from assumption violations by incorporating ecological processes such as resource selection functions, landscape connectivity and group-living behaviour (Royle et al. 2013b, Sutherland et al. 2015, Bischof et al. 2020a). These extensions also improve ecological inference and reduce uncertainty associated with unmodelled heterogeneity. Royle et al. (2013a) went a step further and suggested that animal movement models could be integrated into SCR to represent how animals use space more realistically, and improve model inference.

More interestingly, the ongoing effort to integrate movement models and SCR provides new opportunities to explicitly link individual movement behavior (e.g., habitat selection, dispersal) to population dynamics, density and distribution (McClintock et al. 2022). While these endeavors are conceptually appealing, the data and computational and technical challenges associated with greater model complexity (McClintock et al. 2022) are likely beyond the reach (or scope) of ecological studies with limited resources. Thus, it may be first worth understanding if more complex representations of individual movement processes are required to obtain reliable abundance and ecological inference in existing SCR methods.

1.2.2 Unmarked animals

While the methods for abundance estimation in *marked* animals are well established and rapidly developing, they are, unfortunately, not applicable to many situations where animals do not possess natural markings and cannot be manually marked (i.e., *unmarked* populations). Distance sampling was one of the earliest methods developed to estimate abundance for unmarked populations (Buckland et al. 1993), which has been adapted for many sampling situations (e.g. line transects, trapping or lure point transects, plot counts, indirect surveys, cue counts, acoustic surveys, Buckland et al. 2015). Since then, numerous approaches have been developed to deal specifically (or primarily) with camera trap data. They include the following: random encounter model (REM) (Rowcliffe et al. 2008); spatial count (SC) (Chandler and Royle 2013); camera-trap distance sampling (CTDS) (Howe et al. 2017); random encounter and staying time (REST) (Nakashima et al. 2017); time-to-event (TTE), space-to-event (STE), instantaneous sampling (IS) (Moeller et al. 2018); and a space-use model (Luo et al. 2020).

Without individual identity information, the two major requirements for abundance estimation in most methods (REM, CTDS, REST, TTE, space-use model) is information about animal movement and camera detection zone. The implicit – sometimes, explicit – assumption is that the observed distributions of animal movement (e.g., speed, staying time) and detection zone data (e.g., animal distance and angle relative to camera) must fit well to the parametric distribution (or function) specified by the methods (e.g., log-normal for speed, hazard-rate function for effective detection distance, Rowcliffe et al. 2011, 2016, Howe et al. 2017).

Unlike SCR methods, these methods are relatively early in development and the ability to incorporate covariates for ecological inference (e.g., spatial variation in density) is largely limited. In fact, the performance of abundance estimates generated by the unmarked methods is still largely untested beyond simulations conducted by the original papers describing the methods.

Several empirical multi-method comparisons and a handful of simulation-based evaluations exist, but have shown mixed results. Abundance estimates produced by unmarked methods relative to that produced by reference methods (e.g., total counts, distance sampling, SCR) have been found to be comparable in some empirical studies (e.g., Zero et al. 2013, Anile et al. 2014, Cusack et al. 2015, Caravaggi et al. 2016), but biased (usually positively) in others (e.g., Rovero and Marshall 2009, Amburgey et al. 2021, Doran-Myers et al. 2021, Loonam et al. 2021, Pettigrew et al. 2021). The latter group of studies mostly suspect the source of bias to arise from violation of the assumption of random camera-trap placement with respect to animal movement (i.e., nonrandom placement; e.g., near trials, baited cameras). Under simulations of animal movement behaviours (e.g., searching, grazing, resting), Santini et al. (2022) found REM and TTE generated overestimates in abundance, while REST underestimated abundance. In contrast, Hayashi and Iijima (2022) found abundance estimates generated by REM, REST and IS to be robust to simulations of group-living animals, while STE underestimated abundance. Thus, it is unclear what conditions are required for unbiased abundance estimates of unmarked populations. A recent review noted that "a comparison of methods under a common simulation has not been performed" and that doing so under a range of movement scenarios (speeds, home-range sizes, grouping behaviours) would be valuable (Gilbert et al. 2021).

1.3 Quantifying biodiversity using camera-traps

With recent advances in remote camera technology, reduction in cost and increased interest in wildlife images, the use of camera-traps (CTs) has grown exponentially in the past 10–15 years, doubling every 2.9 years (Burton et al. 2015). CTs offer a cost-effective and standardised way to intensively survey animal populations across space and time for a variety of analytical purposes (e.g., species richness, behaviour, occupancy, abundance). The bulk of CT assessments has focused on metrics alternative to (absolute) abundance or density, such as occupancy and relative abundance (Figure 1.1), which are easier to obtain – only requiring

detection/nondetection data (Burton et al. 2015, Gilbert et al. 2021). However, measures of occupancy and relative abundance are often not directly comparable across species and populations, and across time and space. These indices tend to be markedly obscured by the numerous factors affecting detection probability – such as differences in movement, space use and body mass (Neilson et al. 2018, Broadley et al. 2019, Efford 2019). Thus, they cannot be treated as proxies of abundance (Steenweg et al. 2018, Broadley et al. 2019, Efford 2019). Essentially, occupancy is a measure of distribution and relative abundance is not an absolute quantity, which may not be sufficient information for effective population management. Such limitations in the ability to make quantitative inferences from camera-trap data may be impeding the field of applied conservation (Burton et al. 2015).

Estimates of abundance provide the gold-standard for population monitoring, providing absolute quantities that are directly comparable across populations in space and time. Despite this, applications of abundance estimation in CT assessments have been relatively few, representing just 5.5% of all applications (Gilbert et al. 2021). This dearth in CT-based abundance estimation applications is mainly attributed to the added labour required to collect the auxiliary information (e.g., individual identities, animal-to-camera distance, Figure 1.2) (McClintock et al. 2013, McClintock and Thomas 2020, Gilbert et al. 2021). Furthermore, while abundance estimates are a desirable metric for population management, reliability of estimates and associated inferences are not immune to violations of model assumptions (as discussed in the preceding section). Underlying limitations and assumptions to CT-based methods tend to be violated in the field and are often not fully considered during model application (Burton et al. 2015, Steenweg et al. 2018). Thus, addressing the current limitations and challenges with both *marked* and *unmarked* CT-based abundance estimation in the face of ecological complexities encountered in the field is a worthwhile direction.

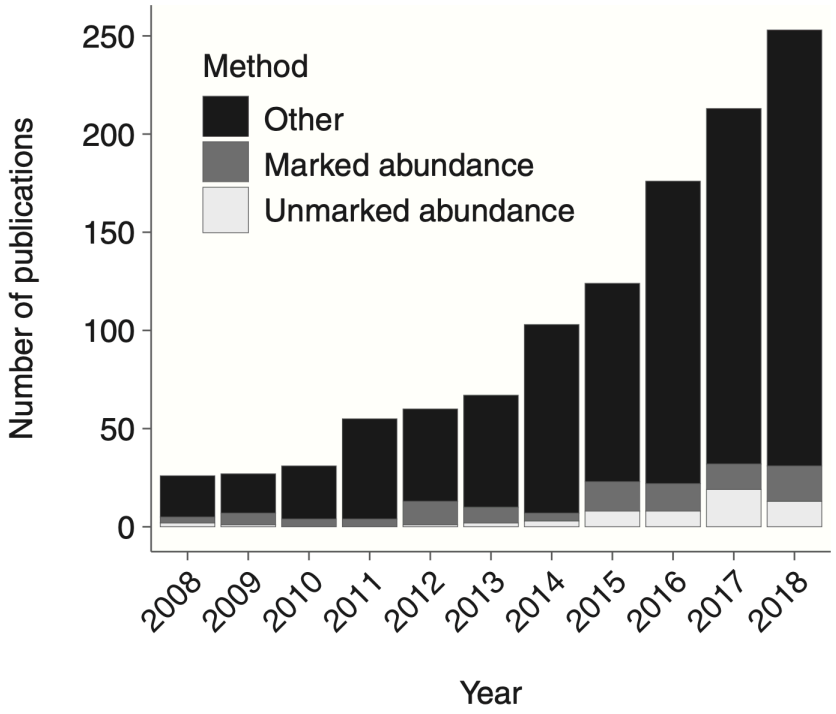

Figure 1.1: Number of peer-reviewed publications of camera-trap applications from 2008 to 2018, broken down by abundance estimation of marked (medium grey) and unmarked (light grey) animals and other applications (black), including relative abundance, behaviour, occupancy and species richness. Plot and data from Gilbert et al. (2021).

1.4 Thesis outline

The once separate fields of animal movement modelling and population modelling are seeing increasing integration to explicitly connect individual- to population-level processes (e.g., Potts et al. 2014, McClintock et al. 2022). While there is potential for improved ecological understanding, it is not clear if the benefits are worth the cost of greater model complexity (e.g., higher data, computational, statistical expertise demands). This thesis harnesses advancements in animal movement modelling to evaluate the reliability of inferences obtained from population abundance estimation methods for both *marked* and *unmarked* animals, in the context of camera-trap applications. Individual-based models present an intuitive way to model movement (i.e., as a spatiotemporally autocorrelated trajectory) from which to generate sampling data independent from the assumptions made by the

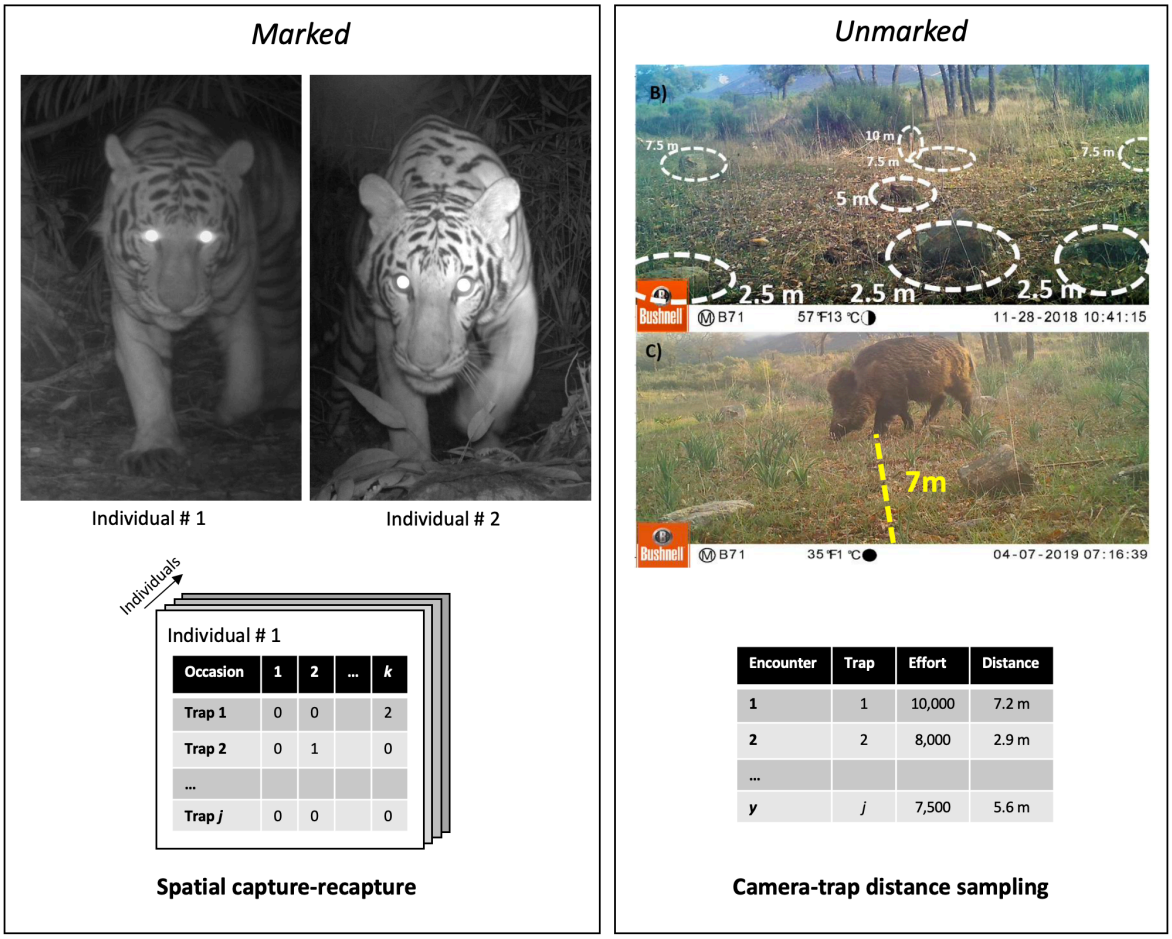

Figure 1.2: The information required for abundance or density estimation with camera-trap data for *marked* and *unmarked* animal populations. In *marked* populations (left panel), individual identity information is required. Individuals are identified and matched across images at different times and trap locations to build encounter histories for each individual (e.g., for spatial capture-recapture methods). In *unmarked* populations (right panel), animal-to-camera distances are typically required for estimation of animal movement (e.g., speed) and/or detection zone (e.g., effective detection distance). Distances are measured using known distance reference markers (e.g., stones). Camera-trap images © Meryl Theng/Pablo Palencia.

population model (e.g., SCR assumes statistically independent animal locations drawn from a spatial point process). The two overarching aims of the thesis are to: (i) develop a simulation-based approach to evaluate population abundance estimation methods under realistic movement, and (ii) interrogate the reliability of inferences obtained from abundance estimation methods with instantaneous detection data (i.e., camera-trap), identifying specific areas for improvement (Figure 1.3). This is a thesis by publication and comprises three data chapters (**Chapters 2–4**):

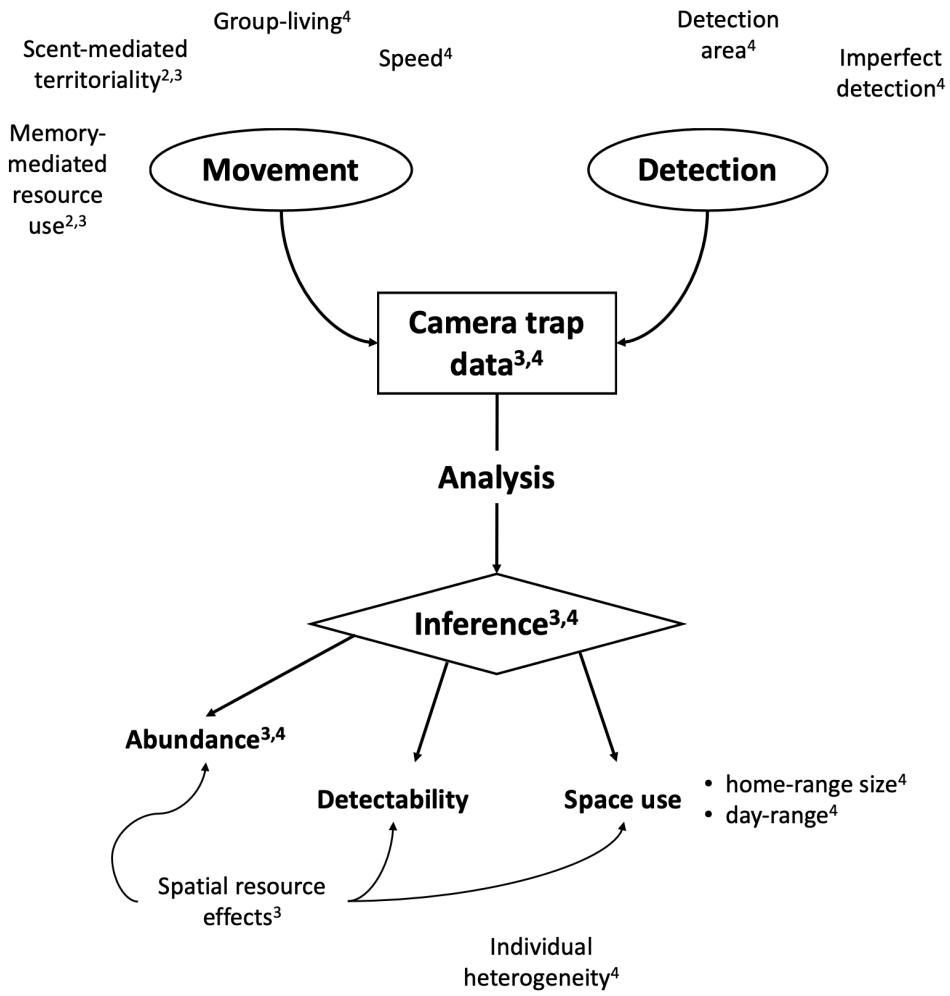

Figure 1.3: A conceptual representation of the aims of this thesis. I explore how movement (and detection) processes underlying camera trap data influences inferences obtained from population abundance estimation methods. The superscript numbers reference the thesis Chapter where each concept is investigated in.

Chapter 2. My second chapter examines the mechanistic link between individual movement processes and space-use patterns at the population scale. I describe a multi-individual movement simulation model, in which small-scale movement decisions of the individual are informed by two biological processes: its memory of the resource landscape (i.e., resource memory) and conspecific scent environment (i.e., territorial exclusion). This model builds upon a two-state memory-based foraging model (Bracis et al. 2015), extended to model multiple individuals that

interact through cue-based conspecific avoidance behaviour. These processes are evaluated across population density scenarios for their ability to replicate realistic self-organising spatial patterns of territorial animal space use (i.e., relationships between space use, population density and resource availability) and dynamic movement responses to changes in the conspecific environment (i.e., the removal of individuals). I then use the model to replicate general space-use patterns in feral cat telemetry data using a sensitivity analysis to guide model pararamterisation.

Chapter 3. My third chapter applies the movement simulation model (described in Chapter 1) as the basis for evaluating the performance of abundance estimation methods for *marked* populations, namely spatial capture-recapture (SCR) models. I was interested in examining the extent to which movement emerging from biologically driven decision processes occurring at the fine scale (i) violated SCR model assumptions and influenced abundance estimates; and (ii) was accurately interpreted by ecological (i.e., resource effect in density and detection) and space-use (i.e., home-range size) inferences obtained from the SCR methods. I generated individual detection data from simulated movement trajectories and fitted the datasets to a suite of closed population SCR methods (i.e., basic, resource selection and transience), as well as their covariate variants accounting for heterogeneity in density and detectability. These results would help determine if representations of movement in existing SCR methods require further complexity.

Chapter 4. My fourth chapter examines the performance of abundance estimation methods for *unmarked* populations. Since unmarked methods are relatively new, at a stage where robustness of abundance estimates is in question and offer limited ability to draw ecological inferences related to density, the aim was to identify the methods that provided accurate abundance estimates and under what conditions. Hence, the complexity of movement simulated in Chapters 1 and 2 was not applied here, and a simpler approach that represented a breadth of population scenarios (e.g., discrete-time biased correlated random walks, state-switching behaviour in group-living populations), was used. I evaluate abundance estimator performance from three unmarked methods (REM, REST, CTDS) under

a wide range of animal movement (speed, scale and grouping behaviour) and population scenarios.

In the final chapter (**Chapter 5**: General Discussion), I discuss the future of (i) integrating movement and population models, and (ii) abundance estimation with camera-trap data based on the insights gained from this thesis. I review the core challenges identified from conducting my research and integrate them with those from existing literature. I then discuss potential solutions and future directions, taking from emerging technologies and methodologies.

2

Integrating resource memory and cue-based territoriality to simulate individual movement dynamics

Statement of Authorship

Publication title	Integrating resource memory and cue-based territoriality to simulate individual movement dynamics
Publication status	Unpublished and Unsubmitted work written in manuscript style
Publication details	
Data and code	https://github.com/cbracis/ForagingModel https://github.com/merylltheng/movement_dynamics

Principal Author

Name of Principal Author	Meryl Theng
Contribution to Paper	Conceptualised and designed the study, performed all simulations and analysis, wrote the paper.
Overall percentage	85%

Certification	This paper reports on original research I conducted during the period of my Higher Degree by Research candidature and is not subject to any obligations or contractual agreements with a third party that would constrain its inclusion in this thesis. I am the primary author of this paper.
Date	12 March 2013

Co-author Contributions

By signing the Statement of Authorship, each author certifies that: (i) the candidate's stated contribution to the publication is accurate (as detailed above); (ii) permission is granted for the candidate in include the publication in the thesis; and (iii) the sum of all co-author contributions is equal to 100% less the candidate's stated contribution.

Name of Co-author 1	Thomas A. A. Prowse
Contribution to Paper	Supported sensitivity analysis and writing.
Signature	
Date	12 March 2013
Name of Co-author 2	Steven Delean
Contribution to Paper	Supported analysis and writing. Provided supervisory support.
Signature	
Date	12 March 2013
Name of Co-author 3	Phillip Cassey
Contribution to Paper	Supported writing. Provided supervisory support.
Signature	
Date	12 March 2013
Name of Co-author 4	Chloe Bracis
Contribution to Paper	Designed and provided the model. Supported conceptualisation, study design, analysis and writing. Provided supervisory support.
Signature	
Date	12 March 2013

Abstract. Animal movement is central to ecology and of paramount importance to understand processes underlying the emergence of empirical space-use patterns. In this study, we investigated how integrating two well-established movement processes in the field of theoretical movement ecology, (i) memory-based resource use; and (ii) cue- or scent-based territoriality, affects emergent space-use patterns. We integrated the two mechanisms of space-use into a single individual-based modelling framework, and then quantified how varying degrees of each process affects emergent space-use patterns. Both mechanisms together led to the formation of exclusive, resource- and population density-dependent utilisation distributions, which were responsive to perturbations in the conspecific environment (i.e., removing individuals). Utilisation distribution patterns (area and overlap) were primarily influenced by memory and scent decay rate parameters, controlling an animal's inherent exploratory tendency and its desire to avoid conspecifics respectively. Model application to a population of feral cats demonstrated that general space-use measures (e.g., median UD area, resident and transient dynamics) could be approximated through simulation, though replication of fine-scale space use patterns (e.g., cumulative UD area) was poorly matched. Though application of mechanistic movement models remains both challenging and limited, the potential of such endeavours to ultimately predict population responses cannot be overstated.

2.1 Introduction

Movement is fundamental to understanding the ecology of many animal populations. It emerges from individual behaviours with consequences for population- and community-level processes. A growing awareness of the conceptual significance of individual-level movement processes in animal movement studies is reflected by the burgeoning literature on the subject (Péron 2019), facilitated by the increasing

availability of high-resolution tracking data (Cagnacci et al. 2010). Understanding the biological mechanisms underlying animal space-use patterns is necessary to predicting their responses to external factors such as environmental change, and hence critical to the management of wild populations (Grimm and Railsback 2012). While the conventional approach of using simpler correlative movement models may be sufficient for predicting short-term space-use patterns (e.g., habitat use), it cannot by itself predict space-use responses, which process-explicit or mechanistic movement models have the potential to do (Powell and Mitchell 2012).

With a process-based approach to modelling space-use, movement patterns emerge from decisions of individual animals driven by behavioural processes inherently linked to survival and reproduction, such as accessing resources while avoiding costly interactions with conspecifics and predators (Moorcroft et al. 1999, Börger et al. 2008, Nathan et al. 2008). Two well-established processes are proposed to play important roles in creating emergent spatiotemporal space use patterns: namely (1) resource use mediated by cognitive memory (i.e., resource memory); and (2) spatial segregation of individual space use via resource competition through defensive cues (i.e., territoriality) (Börger et al. 2008, Powell and Mitchell 2012, Spencer 2012, Fagan et al. 2013).

Animal cognition is increasingly recognised as a key feature in movement decisions (Fagan et al. 2013), notably providing a plausible biological explanation for animals constraining movement to familiar locations (a.k.a. 'site fidelity'), a hypothesis that has received empirical support (Bracis and Mueller 2017, Merkle et al. 2017, Ranc et al. 2021). While quantifying memory processes empirically remains particularly challenging, theoretical analyses have demonstrated that memory-based foraging processes can produce emergent home-ranges and more efficient resource use (Van Moorter et al. 2009, Riotte-Lambert et al. 2015, Bracis et al. 2015). Modelling memory mechanisms captures the underlying process bounding space use, and creating spatio-temporal patterns of site use and fidelity. It results in dynamic space-use in response to a changing environment (e.g., Potts et al. 2013, Bateman et al. 2015), which is a key advance from many models that

assume home-range existence *a piori* (such as home-range centres or boundaries) to achieve stable but unrealistically static home-ranges (Börger et al. 2008).

How individuals spatially organise themselves across a landscape is largely influenced by the availability of unoccupied habitat or presence of competitors. Competition is a key driver of spatial segregation between individuals in a population and has been demonstrated to arise in both territorial and non-territorial contexts (Potts 2012, Riotte-Lambert et al. 2015). Here, we focus on territorial animals that maintain and defend exclusive territories against conspecifics. In classical mechanistic models of animal movement, territoriality is modelled as scent-mediated conspecific avoidance (Giuggioli et al. 2013, Potts and Lewis 2014), which has been demonstrated as a significant underlying driver of observed variation in individual space use and changes in space use patterns following population change in territorial carnivores (Lewis and Murray 1993, Moorcroft et al. 2006, Bateman et al. 2015). The scent-marking model has also been applied in an analogous way to model memory of direct territorial conflicts or vocalisations in bird flocks (Potts and Lewis 2014). While these models have led to realistic patterns of space use, most have postulated a redirect-to-centre response to scent, which has limited application to species with central place attraction (i.e., to den or nest site). Furthermore, these species tend to exhibit it only when rearing offspring (e.g., wolves during pup-rearing (Mech and Boitani 2010), red foxes (Giuggioli et al. 2011), starlings (Kacelnik 1984). Moreover, an organising centre is not necessary for stable space use patterns to emerge when memory and learning are modelled (Van Moorter et al. 2009).

Though critical insight has been gained from modelling resource memory and territoriality separately, the integration of the two important aspects of space-use into a single modelling framework to understand how animals balance multiple motivators has remained unexplored (Potts and Lewis 2014). Here we advance toward a more holistic understanding of the emergence of animal space-use patterns, by developing what is, to our knowledge, the first theoretical model integrating these two well-established processes to simulate realistic patterns of space-use by

territorial animals. We move away from traditional approaches where steady-state space-use (e.g., home-range or territory) is the only goal and explore the transient dynamics of space-use modulated by varying degrees of philopatric/exploratory tendencies (i.e., via resource memory) and scent avoidance behaviour. To explore and illustrate the effects of integrating these two components, we investigate how the interplay of resource memory and territoriality influences: (1) the emergence of individual space use areas; (2) the relationship between space use area, population density and resource availability; and (3) the response of animal space use to changes in the conspecific environment (i.e., removing individuals). Next, we used a pattern-oriented modelling approach (Grimm and Railsback 2012) to explore the potential of using our general process-based model to replicate empirical space use patterns in a specific population. We first conducted a sensitivity analysis on the movement model to assess parameter importance for space-use area patterns (size, skewness and overlap) and other metrics of movement (step-length, step-length distribution skewness, daily distance) to guide model parameterisation to reproduce these general patterns in feral cat telemetry data.

2.2 Methods

We first describe the conceptual movement model (Section 2.2.1; summarised in Figure 2.1), and then detail the parameterisation process used for simulations in the following Sections 2.2 and 2.3. All parameter values used in simulations are collated in Table 2.1.

2.2.1 Movement model description

Our model builds upon a two-state memory-based foraging model (Bracis et al. 2015) to include multiple individuals that interact through scent-based conspecific avoidance behaviour (Figure 2.1 a). In memory-based movement, individual movement is influenced by current resource quality and spatial memory, and are navigated towards previously learned resource areas. The model is a two-dimensional

in space $z \in R^2$ with time t (e.g., $f(z,t)$, though dependent variables z and t are omitted from some equations for clarity).

2.2.1.1 Resource memory

Resource quality Q is modelled as continuously varying in space across the landscape. The resource landscape is simulated on a discretised grid with two-dimensional coordinates z. The dynamic resource landscape is characterised by the sum of n animals' consumption of resources (at a rate of β_C and according to a spatial kernel) and logistic regeneration over time at a rate of β_R to the initial landscape quality Q_0:

$$\frac{\partial Q}{\partial t} = \left(\overbrace{\beta_R(1 - \frac{Q}{Q_0})}^{\text{regeneration}} - \underbrace{\sum_n \beta_C f_C(\|z - Z_i\|)}_{\text{consumption}} \right) Q. \tag{2.1}$$

The spatial kernel $f_C(\|z - Z_i\|)$ follows a bivariate normal distribution $\frac{\exp\left(\frac{\|z-Z_i\|}{\gamma_C}\right)}{2\pi\gamma_C}$ with length scale γ_C. Thus, $\|z - Z_i\|$ is the Euclidean distance between z and the current location of individual i, Z_i.

Animals have a resource memory $M(z,t)$ consisting of two streams of information: a short-term stream $S(z,t)$ that pushes the animal away from recently visited locations even if they are attractive, and a long-term stream $L(z,t)$ that attracts the animal back to high quality areas (Van Moorter et al. 2009). The two streams are combined into a single memory map M, which is used to inform the movement process:

$$M = L - \psi_M S, \tag{2.2}$$

where ψ_M is the short-term memory factor which ensures that the value at a just-visited location will initially be negative (repulsive), with $\psi_M > 1$. Each stream is characterized by learning the intrinsic quality of the resource landscape (i.e., initial quality at Q_0) at rates of $\beta_{S,L}$ (with bivariate normal spatial kernels describing learning $f_{S,L}$; similar to Equation 2.9) and forgetting at rates $\phi_{S,L}(\phi_L < \phi_S)$:

$$\frac{\partial L}{\partial t} = \overbrace{\beta_L f_L(\|z - Z\|)(Q_0 - L)}^{\text{learn}} - \overbrace{\phi_L(L - \mathrm{M}^*)}^{\text{forget}}, \tag{2.3}$$

$$\frac{\partial S}{\partial t} = \overbrace{\beta_S f_L(\|z - Z\|)(Q_0 - S)}^{\text{learn}} - \overbrace{\phi_L S}^{\text{forget}}. \tag{2.4}$$

L can either be initiated fully informed, with the intrinsic resource quality Q_0, or naively, with a homogenous map of value $M*$ indicating the animal's expectation for unvisited areas which can be more optimistic or pessimistic and thus affect exploratory tendency (see Bracis and Wirsing 2021). $M*$ is also the value to which long-term memory L decays.

The resource memory contribution to this angular probability distribution is computed by integrating transects of individual i's resource memory map (M_i) radiating out with radius r from the individual's location with the memory value at each point weighted by distance,

$$g(\theta)_i = \frac{\int_0^r M_i(r, \theta) f_z(r) dr}{\int_0^{2\pi} \int_0^r M_i(r, \theta') f_z(r) dr d\theta'}, \tag{2.5}$$

where θ represents the angle, and $f_z(r)$ is the kernel function that weights according to distance (here exponential with length scale γ_z). The foraging memory movement model is described in further detail in Bracis et al. (2015).

2.2.1.2 Scent-marking (territoriality)

As individuals move about the landscape, they also deposit scent, which decays over time, thereby marking their territory. The amount of scent on the landscape, D, is governed by the deposition rate, β_D, (i.e., how much scent is deposited), the deposition spatial scale, γ_D, (i.e, how broadly the scent is deposited in the vicinity of the forager) and the exponential decay rate ϕ_D. D is limited to a maximum value of D_0 and we take D_0 to be one. Thus, the change in scent for each individual i at location Z_i is given by the equation

$$\frac{\partial D_i}{\partial t} = \beta_D f_D(\|z - Z_i\|)(D_0 - D) - \phi_D(D), \tag{2.6}$$

where f_D is the spatial kernel (here exponential with scale γ_D). Scent deposition is tracked per individual, and individuals are indifferent to their own scent, but repulsed by the scents of all other conspecifics.

The repulsion of individuals by the scent of conspecifics is represented with an angular conspecific safety metric that scales between 0–1 but is not constrained to sum to 1 (like predation risk in Bracis et al. 2018b). This value represents the relative 'safety' in each direction in terms of avoiding conspecifics, with 0 meaning unsafe (high levels of conspecific scent) and 1 meaning safe (no conspecific scent). Safety for individual i is calculated by integrating the summed values of all other individuals' ($n \neq i$) deposited scent according to

$$d_i(\theta) = 1 - \max(1, \int_0^r \psi_D \sum_{n \neq i} D_n(r', \theta) f_w(r') dr'), \tag{2.7}$$

where ψ_D is the response strength and $f_w(r)$ is a spatial kernel (here the exponential kernel with length scale γ_w) that represents that decay of scent perception with increasing distance.

2.2.1.3 Decision rules

To create the final angular probability distribution from which the angle θ is drawn to inform the movement process, the angular probability distribution based on the resource memory $g(\theta)_i$ is multiplied by the conspecific safety metric $d_i(\theta)$ for individual i, then normalised, giving

$$h_i(\theta) = \frac{g_i(\theta) d_i(\theta)}{\int_0^{2\pi} g_i(\theta') d_i(\theta') d\theta'}. \tag{2.8}$$

and the orientation angle of the bias term $\theta(t) = \angle\mu(t)$, in the movement process is then drawn from $h_i(\theta)$, which is specific for each individual at a given time t and location $z = (x, y)$.

2.2.1.4 Movement process

An animal's movements through the landscape are described by a continuous trajectory with a current position of $Z(t) = \int_0^t V(t')\,dt' + Z_0$, with a velocity of $V(t)$ and initial position of Z_0. The autocorrelated, directed, continuous movement process is given by

$$dV = \frac{1}{\tau}(\mu(t) - V)dt. \tag{2.9}$$

This is similar to the Ornstein-Uhlenbeck process where τ is the time scale of autocorrelation and instead of the white noise component, stochasticity is introduced through the bias vector $\mu(t) = (\upsilon, \angle\theta)$ of magnitude $\upsilon = \|\mu(t)\|$ (controlling average speed) and angle θ (direction). A Poisson process with rate parameter λ determines when angle θ is updated, which is then selected from an angular probability distribution derived from resource memory or scent processes, depending on the behavioural state. Finally, individuals switch between feeding and searching states, characterised by different values for τ and υ, based on the current resource consumption $C(t)$ (Figure 2.1 b). The switch occurs when $C(t)$ crosses the average consumption rate, $\bar{C} = \beta_C f_C(\|z - Z\|)\bar{Q}_0$, where $\bar{Q}_0$ is the average resource quality over the landscape. In the feeding state, movement is tortuous (i.e., undirected) and slow as the animal exploits the local high-quality resource. The searching state is characterised by faster speeds and directional persistence towards high quality resources determined from the memory map (see Equation 2.5).

2.2.2 Theoretical examples

The movement model was simulated on a 200 × 200 pixel heterogenous resource landscape, generated with the function `nlm_fbm` in R package `NLMR` (fractal dimension = 0.75). Initial locations of animals were random, and the landscape boundaries were reflective.

2.2.2.1 Impacts of resource memory and territoriality

To demonstrate the effect of resource memory and territoriality on emergent space-use, we simulated animal movement trajectories for three scenarios: (1) territoriality only, (2) memory only; and (3) territoriality and memory in concert. In scenario 1, the movement process was a resource-dependent two-state random walk, with $g(\theta)$ in Equation 2.8 being uniform while scenarios 2 and 3 use the memory process of Equation 2.5. All three scenarios were run across three different densities of individuals ($n = 5, 10, 15$), creating 100 replicate simulations for each combination of scenario and density. We characterised space-use by calculating individual utilisation distribution (UD) area estimated from the simulation outputs using a kernel density estimator function `kernelUD` in the R package `adehabitatHR`. The 95% UD polygons were used to extract resource values within the landscape using the R packages `sp` and `raster`, after which the mean resource value within each UD was computed. Variance in each individual's UD size was also visualised with respect to density and resource availability. A two-way ANOVA was used to evaluate the effect of density and scenario on $\log_{10}$-scaled UD area.

2.2.2.2 Impacts of population manipulation

To demonstrate that space-use is both an emergent property and dynamic when conditions change in our model, we tested the effect of individual removal on remaining individuals' UDs. We first simulated 100 datasets with a density of 10 individuals (i.e., a control setting). We simulated a further 100 datasets with the same parameters and starting conditions as the control setting, and then used a three-phase approach to remove individuals and quantify the effects of their removals on the UDs of the remaining individuals. The three phases were: (Phase 1) establishment of stable UD (t = 1–20,000, indicated by a plateau in UD area in at least five individuals; Figure A.2); (Phase 2) removal of four out of ten individuals ($t = 20,001$), followed by a transition period to allow the scent of removed individuals to decay to near zero (t = 20,001–30,000); and (Phase 3) exploration and establishment of new UD by remaining individuals (t

= 30,001–50,000). To quantify the effects of removal, we compared the aggregate overlap in area (95% UD) between initial area covered by removed individuals (calculated from Phase 1 with 5,000 timesteps burn-in) and the area covered by remaining individuals before and after removal (calculated from Phase 1 and 3 respectively with 5,000 timesteps burn-in). A paired t-test was used to compare differences between the dependent before-after samples. For comparisons in the control setting, four of the 10 individuals were randomly "marked for removal" (but not actually removed). Aggregate overlap in area covered between "marked for removal" and "unmarked" individuals was then calculated using the function `over` from R package `rgeos`.

2.2.3 Model calibration using sensitivity analysis

To facilitate a better mechanistic understanding of emergent properties of the model and to examine model application, we: (1) conducted a sensitivity analysis (SA) to evaluate input parameter influence; and (2) used the SA results to guide setting of parameters to match general patterns in an empirical case study that consisted of GPS-locations from 11 adult female and male feral cats (*Felis catus*) from a 2019 eradication operation conducted on Kangaroo Island (South Australia) by the Department for Environment and Water South Australia (Hodgens 2019, see Text A.1 for details on the empirical study and simulation setup).

2.2.3.1 Sensitivity analysis

We assessed the relative influence of the following nine input parameters on emergent movement patterns: resource regeneration rate, searching speed, feeding speed, short-term memory decay rate, long-term memory decay rate, memory expectation, scent deposition rate, scent decay rate and scent response spatial scale. Emergent patterns were summarised with six summary statistics for 1,000 sampled input parameter combinations (one replicate simulation per combination): step-length, step-length distribution skewness, daily distance, UD area, UD area distribution skewness and UD overlap. The influence of input parameters on each

respective summary statistic was estimated with boosted regression trees (BRT) to account for complex, non-linear relationships and parameter interactions (Elith et al. 2008, Prowse et al. 2016). We calculated the relative influence of each parameter (scaled to sum to 100), with higher numbers indicating stronger influence on the response. In models with interactions, we measured the interaction strength for top pairwise interactions between input parameters, with values near zero representing negligible interactions. Details on summary statistic calculation and model fitting are in Text A.2 and A.3 respectively.

2.2.3.2 Parameter calibration to match empirical data

We proceeded with parameter calibration via a multi-step process: (1) optimising to a parameter set that best achieved the target values for the six summary statistics simultaneously (using respective BRT models); and (2) manual calibration to five target criteria: UD area and UD area skew (quantitatively evaluated), UD overlap, cumulative UD area and spatial distribution of locations (visually evaluated). The second step was iterated until no further improvement was found (i.e., improving one metric made another worse). We then ran 10 simulations using our final set of parameters and compared the outcomes with the empirical data. Details for this procedure are in Text A.4.

All simulations (Section 2.2.2 and Section 2.2.3) were performed using Java `v. 13.0.2` on a High-Performance Computing cluster. Analyses of model outputs were performed in R `v. 3.6.1` (R Core Team, 2020). Note that we reported statistics obtained from our quantitative comparisons between simulation scenarios (two-way ANOVA, paired T-test) because we ran a small number of simulations (100 each scenario). However, we recognise that statistical significance from simulations should be interpreted with care, especially when applied to large numbers of simulations (Grimm and Railsback 2005), and thus focused on reporting the biological significance of results (i.e., magnitude of differences) instead of simply the strength of evidence against the null hypothesis.

Table 2.1: Overview of simulation parameters used in all four sets of simulations in the study. In theoretical example 1 (TE1), we tested the impacts of resource memory and territoriality on emergent home-ranges across three scenarios (territoriality only, resource memory only, territoriality and memory) and densities ($n = 5, 10, 15$). In theoretical example 2 (TE2), we test the impact of population manipulation by removing four out of ten individuals mid-simulation on emergent space use, and compare it with a control scenario without individual removal. In the sensitivity analysis (SA), we assessed the relative influence of nine parameters across a range of values. Finally, we ran simulations with a set of parameters calibrated to the empirical feral cat data (Cat). Units are arbitrary in the simulations, L is used for generic length units and T is used for generic time units. † L = long-term resource memory, S = short-term resource memory. ‡ S = searching, F = feeding.

Parameter	Definition	Units	TE1	TE2	SA	Cat
Simulations						
Δt	Model time step	T	1	1	1	1
T	Simulation length (time steps)	T	25,000	50,000	21,600	21,600
	Burn-in (time steps)	T			5,040	5,040
n	Number of individuals		5, 10, 15	10	30	30
	Number of individuals removed		-	4 (removal), 0 (control)	-	-
Landscapes						
	Dimensions	L	200×200	200×200	400×600	400×600
Consumption						
β_R	Resource regeneration rate	1/T	0.01	0.01	10^{-3}–10^{-1}	0.01
β_C	Consumption rate	1/T	0.5	1	1	1
γ_C	Consumption spatial scale	L	1	1	1	1
Resource memory †						
ϕ_L	Long-term memory decay rate	1/T	10^{-5}	10^{-6}	10^{-7}–10^{-3}	10^{-7}
ϕ_S	Short-term memory decay rate	1/T	0.01	0.01	10^{-4}–10^{-1}	0.005
ψ_M	Short-term memory factor		2	2	2	2
β_L, β_S	Learning rates	1/T	1	1	1	1
γ_L, γ_S	Learning spatial scale	L	1	1	1	1
γ_z	Memory spatial scale foraging	L	10	10	10	10
$M*$	Memory expectation (value uninformed)		$5E^{-5}$	$5E^{-4}$	0–$2E^{-4}$	$5E^{-5}$

Parameter	Definition	Units	TE1	TE2	SA	Cat
	Memory fully informed?	Boolean	True	True	True	True
Scent behaviour						
	Switched on?	Boolean	True, False, True	True	True	True
β_D	Deposition rate	1/T	3	3	0–5	4
γ_D	Deposition spatial scale	L	1	1	1	1
ϕ_D	Decay rate	1/T	10^{-5}	10^{-4}	10^{-6}–10^{-2}	10^{-6}
ψ_D	Response strength		2	2	2	2
γ_w	Response spatial scale	L	2	2	0.5–10	3
Movement ‡						
	Type	Category	Kinesis, Memory, Memory	Memory	Memory	Memory
τ_S, τ_F	Autocorrelation time scale	T	4,2	4,2	4,2	4,2
v_S	Search speed	L/T	2	2	1–6	5
v_F	Feed speed	L/T	0.2	0.2	0–0.5	0.05
λ	Mean time to update θ	T	1	1	1	1

2.3 Results

2.3.1 Resource memory and territoriality lead to exclusive UDs shaped by resource quality and population density

Individuals in the territoriality-only scenario established distinct non-overlapping UDs and space use was independent of resource (Figure 2.2 a). In the memory-only scenario, individual space use favoured high resource areas but overlapped substantially (Figure 2.2 b). With both territorial and resource memory processes operating in concert, individuals established distinct UDs that utilised high resource areas with relatively little overlap (Figure 2.2 c).

Across all three scenarios, individuals in low resource areas tended to have larger UDs than in high resource areas (Figure 2.2 d). This relationship was strongly log-linear in the memory-only and territoriality + memory scenarios (Pearson's

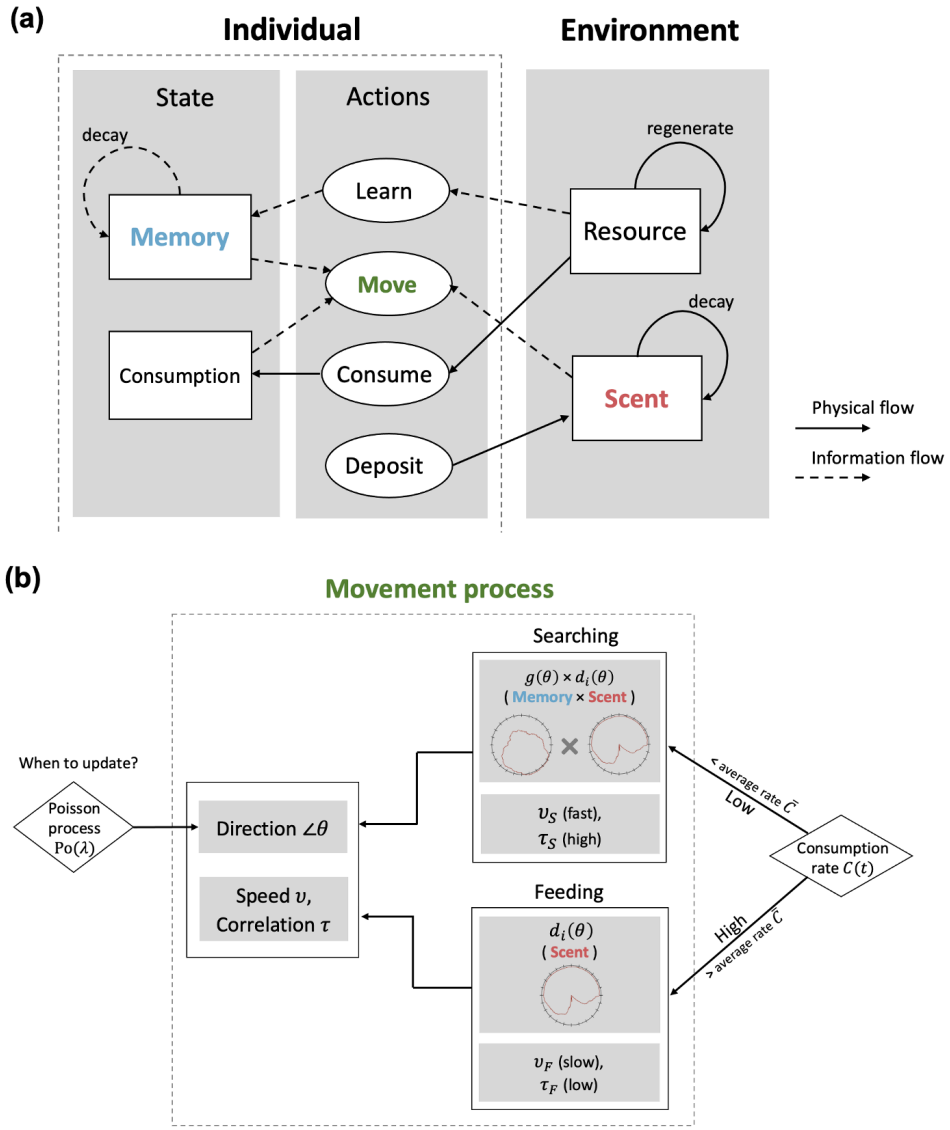

Figure 2.1: A conceptual representation of the movement model. (a) An overview of the individual-environment processes. The individual interacts with the external environment through a series of actions, which serve to update its internal state and ultimately influence movement decisions. Solid arrows show the flow of a physical process and dotted arrows are show the flow of information. (b) The movement process is formulated on continuous time, where updating of the individual's direction and behavioural state are independent processes. Behavioural state (Searching and Feeding) ultimately determines the processes used in selecting the next direction (represented by an angular probability density function of resource memory $g(\theta)$ and scent $d_i(\theta)$ and the speed (v)/correlation (τ) values. The component processes of Memory (i.e., resource memory; blue) and Scent (red) in (a) are highlighted in the movement process model (b).

$r = -0.75$), though variation in both UD area and mean resource were larger for the latter. The resource and UD area relationship in the territoriality-only scenario was consistent with the other scenarios at mid to high resource areas but starts to trend towards a positive UD-resource relationship in low resource areas, with a much smaller lower-limit of mean resource compared to the other two scenarios.

An increase in density caused a decrease in mean UD area in the territoriality-only (mean(UD area)$_{\text{density=5/10/15}}$ = 11,860/6,670/4,600 unit^2) and territoriality + memory (mean(UD area)$_{\text{density=5/10/15}}$ = 6,730/4,200/2,840 unit^2) scenarios, while it caused a slight increase in mean UD area in the memory-only scenario (mean(UD area)$_{\text{density=5/10/15}}$ = 11,230, 12,080, 12,730 unit^2; two-way ANOVA, $F_{2,899} = 450$, $p < 0.001$; Figure 2.2 e). Overall, the smallest UDs were observed in the territoriality + memory scenario (two-way ANOVA, $F_{2,8995} = 2,580$, $p < 0.001$).

2.3.2 Individuals move into recently occupied areas

Aggregate UD overlap between remaining individuals and removed individuals was two times higher in Phase 3 compared to Phase 1 (mean(UD overlap) = 7,000/14,430 unit^2; paired t-test: t_{99} = -19.9, $p < 0.001$) in the removal simulations, while there was a 14% increase in the overlap between individuals (mean(UD overlap) = 6,580/8,980 unit^2; paired t-test, t_{99} = -8.2, $p < 0.001$) in the control simulations (Figure 2.3). Removal simulations showed space use shifts in remaining individuals into areas previously occupied by removed individuals. Individuals in the control example demonstrated smaller shifts in space use on average, explaining the small increase in aggregate UD overlap from Phase 1 to 3.

2.3.3 Sensitivity analysis

UD area was strongly influenced by memory decay rates and scent decay rate (Figure 2.4 a). Short-term memory decay rate had a strong negative effect on UD area, whereas long-term memory and scent decay rates had strong threshold effects from around the mid-points of their parameter ranges, which increased constantly for long-term memory decay but tended to plateau at higher rates of scent decay

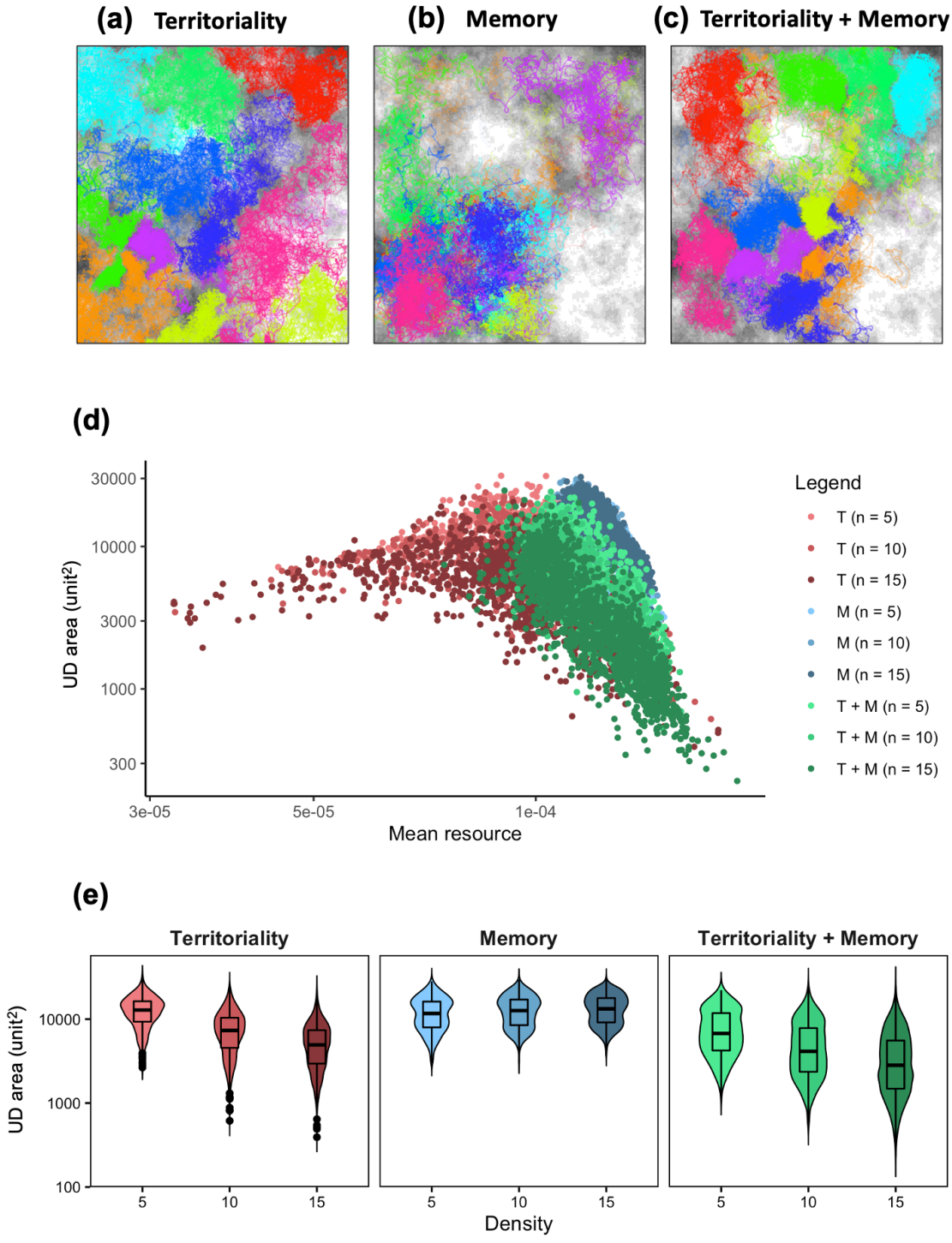

Figure 2.2: Simulation results of movement and utilisation distribution (UD) from three scenarios (territoriality, memory, territoriality and memory). (a–c) sample realisations of animal movement trajectories ($n = 10$) from each scenario, where individual trajectories start at random (colours represent individuals) within the heterogeneous resource landscape (shades of grey corresponding to resource quality; refer to Figure A.1 for resource map only); relationship between UD area and (d) mean resource value within the UD (T: territoriality, M: memory, T + M: territoriality + memory) and (e) animal density ($n = 5, 10, 15$) from 100 replicates.

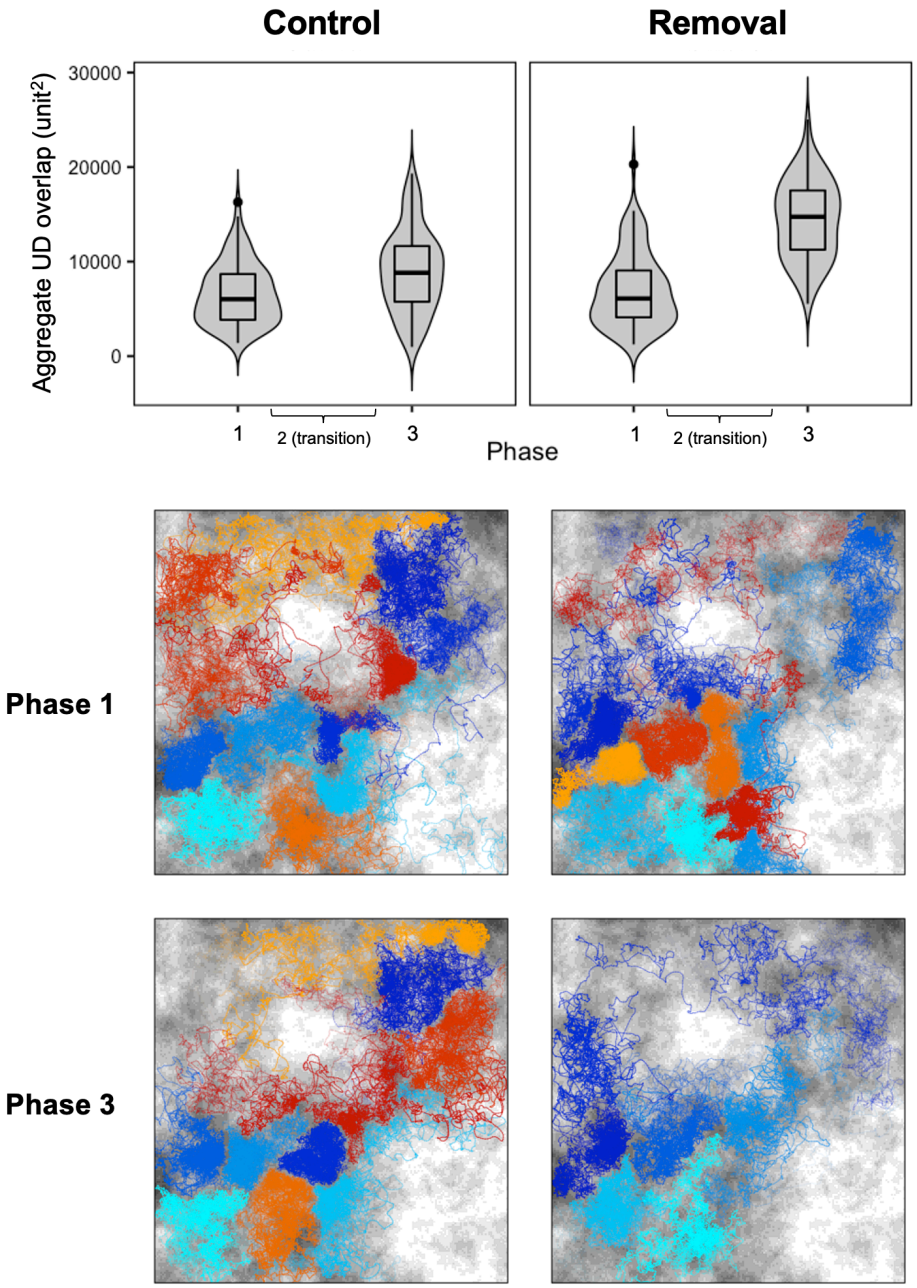

Figure 2.3: Aggregate utilisation distribution (UD) overlap between removed and remaining individuals. Before (Phase 1; t = 5,001–20,000) and after removal (Phase 3; t = 35,001–50,000) in the control and removal scenarios (100 replicates each). Beneath each scenario is a sample realisation of movement trajectories in Phase 1 (top panel) and 3 (bottom panel) of the control (left panel) and removal (right panel) simulation. Individual trajectories decrease in opacity according to time. Cool colours represent remaining individuals, warm colours represent removed individuals (in the control scenario, individuals were randomly grouped as remaining or removed for a comparison to be made). The heterogeneous resource landscape is represented by shades of grey corresponding to resource quality, from none (white) to high (dark grey).

(Figure 2.4 b). Interactions led to a combined effect that if scent decay rate was high, and either short- or long-term memory decay rate was low or high respectively, a 4–6 times increase in UD area was observed (Figure A.10). Longer right-tailed skews in UD area distribution were primarily caused by slower rates of scent decay, faster rates of short-term memory decay and larger scent response spatial scales (Figure 2.4 c). Smaller overlaps in UD were predominantly associated with slow scent decay rates and fast short-term memory decay rates (Figure 2.4 d).

Distance metrics (step-length, step-length skewness, daily distance) were mainly influenced by resource regeneration rate and search speed (Figure 2.4 a). Step-length and daily distance increased, while step-length skewness decreased, with lower resource regeneration rates and higher search speeds (Figures A.5 – A.7).

2.3.4 Empirical application

The simulated data generally captured the long right-tailed distribution of UD area that reflected populations of predominantly resident individuals (with smaller and distinct UDs), and a small number of transient individuals (with larger and less distinct UDs, and sparser location density) observed from the empirical cat movement data (Figure 2.5 a). Median UD area was the same in the simulated and empirical data (1.9 km^2). However, simulated UD area range tended to be smaller than the empirical data (0.5 vs. 1.3 km^2 respectively) – approximately a tenth of simulated individuals had UDs smaller than one km^2 and few ranged wider than nine km^2 across the replicates. Furthermore, the cumulative UD in the simulations reflected a less stable system compared to the empirical data (i.e., curves did not approach a plateau for most individuals; Figure 2.5 b). Spatial patterns of simulated locations resembled empirical movement patterns in that locations tended to cluster linearly along high resources, but to a markedly lesser extent. The intense clustering of locations in specific sites observed for cats was not reproduced in the simulated data (Figure 2.5 c).

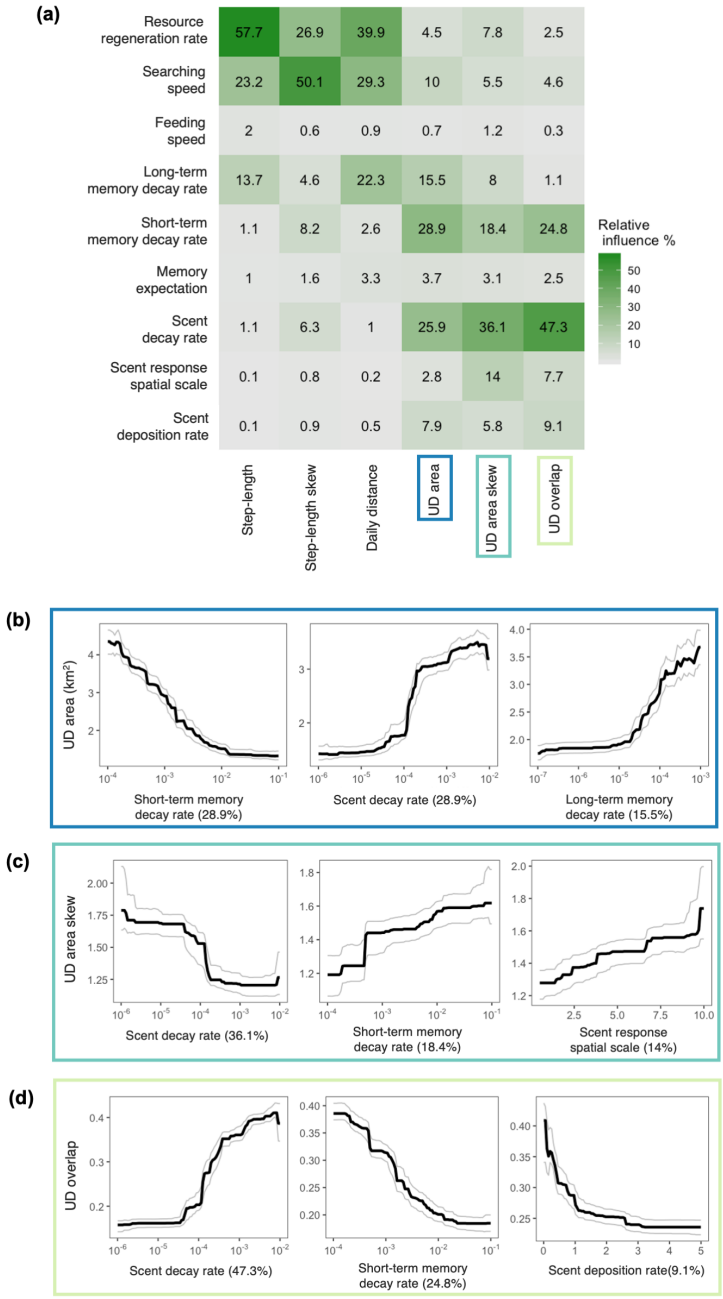

Figure 2.4: Results from the sensitivity analysis. (a) Relative influence (%) of nine model input parameters (rows) on six emergent movement summary statistics (columns) from a boosted regression tree (BRT) analysis. Partial dependency plots showing effects of the top three contributing input parameters on (b) utilisation distribution (UD) area, (c) UD area skew and (d) UD overlap. Partial dependency plots show the effect of a given explanatory variable on each UD metric, while holding the effects of other explanatory variables at their average (black lines). We used 500 bootstrap replicates to calculate the 95% confidence intervals, depicted in grey. Note that some of the x–axes are on a log-10 scale. Full plots showing partial effects of all parameters on each summary statistic can be found in Figures A.5 – A.11.

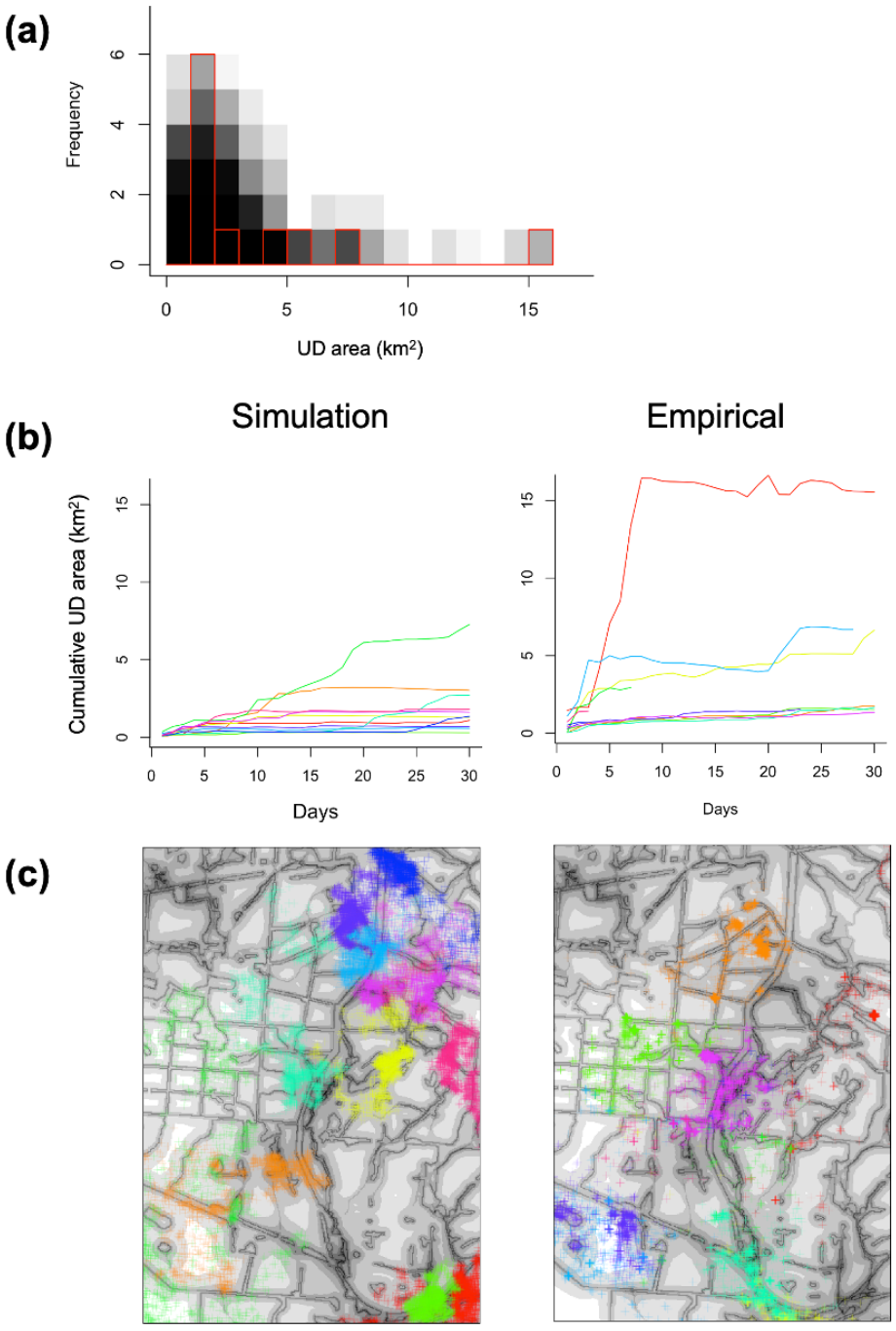

Figure 2.5: A comparison of movement patterns from parameterised simulations and the empirical feral cat data: (a) frequency distribution of utilisation distribution (UD) area of simulated individuals obtained from 10 replicates bootstrap sampled 10 times each (samples represented as 100 histograms in translucent black fill) to match the empirical sample of 11 tagged feral cats in Kangaroo Island, South Australia (histogram with empty fill and red border); (b) one realisation of cumulative UD area over time of 11 randomly selected individuals (left; individuals shown in different colours) against that of the observed feral cat ranges (right); and (c) their corresponding simulated movement locations (left) vs. observed feral cat movement locations (right; note that some cat locations go beyond the landscape shown here). The heterogeneous resource landscape is represented by shades of grey corresponding to resource quality, from none (white) to high (dark grey).

2.4 Discussion

Understanding the relative contributions of multiple processes driving empirical patterns in wild animal populations for predictive response modelling remains one of the prime challenges in conservation biology (Grimm and Railsback 2005). In movement ecology, theoretical models have separately demonstrated how modelling key processes general to many species — e.g., memory-based resource use (Van Moorter et al. 2009, Bracis et al. 2015), nonterritorial conspecific avoidance (Riotte-Lambert et al. 2015), scent-based conspecific avoidance (Potts 2012), and memory-based conspecific avoidance based on past interactions (Potts and Lewis 2016) — can simulate realistic animal space-use patterns. We built on existing knowledge by integrating multiple drivers of space-use (memory-based resource use and cue-based conspecific avoidance) into a single modelling framework that simulates fine-scale movement trajectories in continuous space and time. The model could replicate the emergence of exclusive UDs whose areas were negatively related to resource and population density, and was responsive to a changing conspecific environment, consistent with empirical patterns in multiple species. We also demonstrated a pattern-oriented calibration approach to parameterise our process-based model to empirical data, without requiring direct measurement of memory or scent capacities. While application of our model to reproduce general spatial measures and patterns of feral cat space use was limited, we identified several potential areas for improvement.

In our multi-individual simulation environment, both mechanisms were required to replicate patterns of stable UD formation in territorial animals: one that tended towards fidelity to previously visited, high quality areas (resource memory); and another that drove spatial avoidance between individuals (territoriality). The model captured realistic responses to density with the emergence of transient behaviour by some individuals as density increased and all high-quality areas were occupied. Without territoriality individuals acted independently of conspecifics, which caused large overlaps in emergent UDs (Figure 2.2 b). Without resource

memory, unrealistic UDs emerged that were independent of resource quality; movement was only constrained by the scent of surrounding conspecifics (Figure 2.2 a). The combination of both mechanisms led to the emergence of distinct individual UDs distributed across high resource areas of the landscape (Figure 2.2 c). However, note that other modelling work has shown that resource memory alone can lead to nonterritorial spatial segregation through a long-term adaptive attribute memory storing the average of previous experience and the resource amount actually found (Riotte-Lambert et al. 2015, 2017).

In addition to being spatially realistic, biologically meaningful relationships were also captured. Simulated individuals' UD areas correlated negatively with both resource availability and population density, which is congruent with ecological evidence from both field and experimental studies (Baker et al. 2000, Santangeli et al. 2012, Sálek et al. 2015, Schoepf et al. 2015). This result is biologically intuitive. Namely, when resources are abundant, an individual needs less space to meet its metabolic needs (Mcloughlin and Ferguson 2000); when population density is high, the amount of available, unoccupied space is smaller, which limits individual home-range sizes (Schradin et al. 2010).

The stable and exclusive individual UDs were a dynamic property emerging from our model, continuously adapting to the dynamic resource landscape and presence of surrounding conspecifics. This pattern was emphasised in our removal simulations, where remaining individuals migrated into areas previously occupied by removed individuals once their scent decayed. The phenomenon of expanding into newly vacated habitat can be found in numerous species, such as mice (Schoepf et al. 2015), chipmunks (Mares et al. 1976), coyotes (Moorcroft et al. 2006), and red foxes (Potts et al. 2013). Non-mechanistic models (e.g., with imposed home-range centres and/or boundaries) fail to respond to changing environments (e.g., individuals leaving or dying, fluctuating resource availability), whereas in our model dynamic behaviour arises directly from underlying mechanisms. Notably, the memory mechanism in our model provides the basis for UD stabilisation in the absence of territoriality, which existing mechanistic territorial models either lacked or imposed

through the assignment of home-range centres (Potts and Lewis 2014). Moreover, the ability to control the relative strengths of each mechanistic component allows modulation of remaining individuals' spatio-temporal responses to vacancies, which can vary according to sociodemographic factors (Frank et al. 2018).

The sensitivity analysis revealed that emergent UD areas were most sensitive to memory (short- and long-term) and scent decay rates. These rate parameters essentially control the decay in effects (i.e., time-scale of effects) of modelled mechanisms that act on space use. Short-term memory is a repulsive force pushing the individual to move beyond areas it has visited, where a slower decay results in more exploratory (or diffusive) movement leading to larger UD areas. On the other hand, long-term memory is an attractive force that directs the individual to areas, based on either an informed memory of previously visited high resource areas, or an uninformed expectation that areas beyond the local area of movement (that are unexplored or forgotten) are better. If the animal's expectation for unexplored area matches the mean resource value, faster long-term memory decay rates led to larger UD areas because the memory expectation was generally better than most individuals' local area of movement (i.e., resource distribution was skewed so the mean was greater than the median value). If unexplored area expectations were low, we expect long-term memory decay to have the opposite negative effect on UD area. Unlike resource memory, the effect of scent is externally conferred by conspecifics. When conspecific scent lingers at slower decay rates, it acts as an external negative pressure limiting UD areas. While most individuals have smaller UD areas with slow scent decay rates, a few individuals ranged widely in low resource areas, causing the longer right-tailed skew in overall UD area distribution.

The effects of resource memory and scent on emergent UDs from our model raises an interesting point: territorial formation in territorial animals can be attributed to both memory-mediated philopatric behaviour operating at the individual-level (i.e., inherent exploratory vs. recursive tendency) and spatial competition at the population-level. Existing theoretical models have independently demonstrated that distinct and stable UDs (i.e., home-ranges) can form from either resource

memory-mediated movement (Van Moorter et al. 2009, Bracis et al. 2015) or scent- or memory-mediated conspecific avoidance (Potts 2012, Giuggioli et al. 2013, Ellison et al. 2020) alone. In territorial species, both mechanisms are likely crucial to home-range formation. While site revisits owing to memory processes are commonly observed (Bracis et al. 2018a), it is also common for animals to 'probe' the boundaries of their home-range and expand into newly unoccupied habitat. Thus, to consider the degree to which each component drives space-use patterns (e.g., home-ranging, transience), it is important to combine them within the same modelling framework to understand how territorial animals integrate the opposing motivators and the relative strengths of each response, which is possible with different component parameterisations in our model. Mechanistic home-range analyses (MHRAs) on carnivores have integrated and disentangled the effects of scent-mediated conspecific avoidance from other drivers of home-range formation (e.g., resource selection and steep terrain avoidance) in their modelling frameworks (Moorcroft et al. 2006, Bateman et al. 2015). However, the use of memory as a mechanistic basis for philopatry (e.g., site fidelity) within analytical models is still in development. The analytical framework used in recent studies to incorporate memory-mediated behaviours (e.g., step selection and conspecific avoidance, Oliveira-Santos et al. 2016, Ellison et al. 2020) can plausibly be extended to memory-mediated philopatry.

Using a pattern-oriented calibration approach (Grimm and Railsback 2012), we demonstrated how a process-based movement model could be parameterised from testing a range of 'guesstimated' parameter values against a set of criteria. This comes in especially useful when parameters related to memory and territoriality are challenging to obtain empirically. Parameterising our process-based movement model allowed us to simulate movement data and hence evaluate the model's ability to capture feral cat space-use from an independent dataset.

Movement models built from first principles with wide generality are not often tested this way, and when they are, often reveal limited performance (e.g., Avgar et al. 2013, 2015). In some ways, this appeared to be the case here with the model able

to replicate broad patterns but not some specific features of feral cats' movements. While our parameterised model could reproduce the target median and positively skewed variation in UD area of the empirical dataset, the upper limit of UD area was underestimated. We suspect this is due to the spatial limitation of the truncated simulation landscape (to prevent long simulation times) from the total landscape covered by the tagged feral cats. Nonetheless, the model could replicate the emergence of wide-ranging individuals (or transients) amidst resident individuals, as seen by the positively skewed variation in individual UD area, reflecting a real phenomenon observed in our data and many other territorial species (Holmes et al. 1996, Mitchell et al. 2015, Hinton 2016). While transience itself is a complex movement phenomenon, it emerged without modelling further complexities such as individual differences in motivation (e.g., varying exploratory tendencies).

Next, finer scale spatio-temporal patterns estimated for feral cats (i.e., cumulative UD) were poorly matched. First, the less stable simulated cumulative UD curves could indicate that our burn-in period was not long enough for individuals to establish stable UDs and that burn-in time should be considered in parameter calibration. However, the simulated patterns were also not unrealistic and have been observed in real populations such as the Eurasian lynx (Breitenmoser-Würsten et al. 2007) and several Brazilian mesocarnivore species (Bianchi 2016). Secondly, we were not able to quantitatively describe the cumulative UD curves despite efforts to do so (Text A.4). Quantitative characterisation of such curves (including similar metrics such as net squared displacement) is a challenging and active area of research (Spitz et al. 2017). Ultimately, improving resemblance to the empirical data likely requires additional mechanisms for movement behaviours common in carnivores. For example, the lack of location point clusters and concentrations along linear resources in our simulated data suggests that we did not account for intermittent resting behaviour and preferential use of corridors respectively (Noss et al. 1996). Integrating rest site and corridor layers into the resource map could potentially improve emergent spatial patterns. However, the underlying utilisation mechanism is different from modelled behaviours (of continuous resource

consumption), which may warrant building additional mechanisms and landscape layers into the model (e.g., a resting state dependent on the animal's internal bioenergetic state; landscape permeability). Additionally, methods that attempt to identify site fidelity and quantify recursions can potentially be used to parameterise and evaluate such a model (e.g., Richardson et al. 2017, Bracis et al. 2018a).

Our flexible modelling framework simulates continuous-time movement trajectories from general mechanisms that can be applied to a variety of populations exhibiting cue-based, and potentially memory-based territorial behaviour (e.g., Potts and Lewis 2016). Models can be calibrated and validated against empirical movement data, which is becoming increasingly available (Kays et al. 2015). While further development and testing may be necessary to replicate fine-scale movement patterns, our model can be used to simulate generic memory-informed resource and territorial space use, and broadly match space-use characteristics. Potential applications include simulation-based evaluations of behavioural structure in animal movement (Gurarie et al. 2016) and population estimation of mobile animals (e.g., Theng et al. 2022). Another potential application is in animal-mediated seed dispersal research, which has identified the need to integrate frugivory and disperser movement and to consider more process-based movement approaches (Nield et al. 2020).

We developed a broadly applicable modelling framework that demonstrates how animals integrate and modulate two key motivators of space-use, resource memory and territoriality, to simulate complex patterns of territorial animal space-use. Though parametrisation of process-based models to replicate empirical space use patterns of specific populations remains difficult, overcoming these challenges potentially opens up the powerful ability to predict population responses to environmental change. Thus, we urge researchers to continue to pursue the challenging task of understanding the processes underlying space-use patterns in the wild.

3

Confronting spatial capture–recapture models with realistic animal movement simulations

Statement of Authorship

Publication title	Confronting spatial capture–recapture models with realistic animal movement simulations
Publication status	Published
Publication details	Theng, Meryl, Milleret, Cyril, Bracis, Chloe, Cassey, Phillip, and Delean, Steven. 2022. Confronting spatial capture–recapture models with realistic animal movement simulations. Ecology 103(10): e3676. https://doi.org/10.1002/ecy.3676
Data and code	https://doi.org/10.5281/zenodo.6104214 https://doi.org/10.5281/zenodo.5209568

Principal Author

Name of Principal Author	Meryl Theng
Contribution to Paper	Conceptualised and designed the study, performed all simulations and analysis, wrote the paper.
Overall percentage	85%

Certification	This paper reports on original research I conducted during the period of my Higher Degree by Research candidature and is not subject to any obligations or contractual agreements with a third party that would constrain its inclusion in this thesis. I am the primary author of this paper.
Date	12 March 2023

Co-author Contributions

By signing the Statement of Authorship, each author certifies that: (i) the candidate's stated contribution to the publication is accurate (as detailed above); (ii) permission is granted for the candidate in include the publication in the thesis; and (iii) the sum of all co-author contributions is equal to 100% less the candidate's stated contribution.

Name of Co-author 1	Cyril Milleret
Contribution to Paper	Supported study design, analysis and writing.
Signature	
Date	12 March 2023
Name of Co-author 2	Chloe Bracis
Contribution to Paper	Designed and provided the model. Supported movement simulation design.
Signature	
Date	12 March 2023
Name of Co-author 3	Phillip Cassey
Contribution to Paper	Supported writing. Provided supervisory support.
Signature	
Date	12 March 2023
Name of Co-author 4	Steven Delean
Contribution to Paper	Supported analysis and writing. Provided supervisory support.
Signature	
Date	12 March 2023

Abstract. Spatial capture-recapture (SCR) models have emerged as a robust method to estimate population density of mobile animals. However, model evaluation has generally been based on data simulated from simplified representations of animal space use. Here, we generated data from animal movement simulated from a mechanistic individual-based model, in which movement emerges from the individual's response to a changing environment (i.e., from the bottom-up), driven by key ecological processes (e.g., resource memory and territoriality). We drew individual detection data from simulated movement trajectories and fitted detection datasets to a basic, resource selection and transience SCR model, as well as their variants accounting for resource-driven heterogeneity in density and detectability. Across all SCR models, abundance estimates were robust to multiple, but low-degree violations of the specified movement processes (e.g., resource selection). SCR models also successfully captured the positive effect of resource quality on density. However, covariate models failed to capture the finer-scale effect of resource quality on detectability and space use, which may be a consequence of the low temporal resolution of SCR datasets and/or model misspecification. We show that home-range size is challenging to infer from the scale parameter alone, compounded by reliance on conventional measures of 'true' home-range size which are highly sensitive to sampling regime. Additionally, we found the transience model challenging to fit likely due to data sparsity and violation of the assumption of normally distributed inter-occasion movement of activity centers, suggesting further development of the model is required for general applicability. Our results show that further integration of complex movement into SCR models may not be necessary for population estimates of abundance when the level of individual heterogeneity induced by the underlying movement process is low, but appears warranted in terms of accurately revealing finer-scale patterns of ecological and movement processes. Further investigation into whether this holds true in populations with other types of realistic movement characteristics is merited. Our study provides a framework to generate realistic SCR datasets to develop and evaluate more complex movement processes in SCR models.

3.1 Introduction

Estimating abundance or density of mobile animals requires an understanding of the ecological and movement processes underlying detection data. Spatial capture-recapture (SCR) models have emerged not only as a robust method to estimate animal abundance, but also as a flexible framework that scales individual level processes (e.g., movement, resource selection) to the population level (Royle et al. 2018). This has enabled the integration of increasingly realistic movement processes into SCR models and expanded the scope of inferences possible from detection data (summarized by McClintock et al. 2022).

The key feature of the SCR framework is the ability to account for imperfect detectability by spatially linking individual detection data with underlying movement processes. Animal movement is conceptualized as each individual having an 'activity center' where detection probability (analogous to space use probability) is a function of the distance to the activity center (Efford 2004). In a basic SCR model, individuals are assumed (i) to possess a stationary activity center, which is uniformly distributed within the study area for the entire sampling duration; from which (ii) space use probability symmetrically declines; and (iii) to move independently of each other. Because these assumptions are likely to be violated in wild populations, tests to assess the robustness of the SCR models have been conducted (Efford 2019, Bischof et al. 2020a, Dey et al. 2022), and model extensions have been developed (Royle et al. 2013b, 2016, Reich and Gardner 2014, Sutherland et al. 2015).

While SCR model assumptions are known to be violated frequently in the real-world, evaluation of model performance remains largely based on data generated from a deterministic process centered on the concept of activity centers, which is the same process assumed by the models. In reality, movement of individuals

and their distribution in the landscape emerge from the biological characteristics of the species and the spatio-temporal pressures to which individuals are exposed. As a consequence, animal movement rarely conforms to static structures defined by existing SCR methods in a number of ways. Firstly, movement is dynamic as animals constantly adjust the space they use as a response to ever-changing environments at spatio-temporal scales much finer than SCR data and existing models allow. Secondly, animals often may not possess a single activity center during the sampling duration or occasion (or interval); there may be multiple asymmetric areas of activity (Mueller and Fagan 2008). Thirdly, movement is ultimately a continuous and autocorrelated trajectory that is not captured by statistically independent locations generated from a spatial point process (Fleming et al. 2015).

Density estimates obtained from SCR models appear relatively robust when only a single model assumption is violated (Borchers et al. 2014, Efford 2019, Bischof et al. 2020a, Moqanaki et al. 2021, Dey et al. 2022). However, simplified representations of space use cannot capture the breadth of ecological processes that underpin encounter history data collected in the field (i.e., reality), and the robustness of SCR models to multiple violations of model assumptions remains limited. When models perform poorly with field data, it is often difficult to diagnose how model assumptions were violated or why models failed to produce satisfactory results (Gerber and Parmenter 2015, Moqanaki et al. 2021, Dey et al. 2022). Moreover, as the field of SCR modelling continues to integrate increasingly complex movement processes (McClintock et al. 2022), the data generation methods used to evaluate these models need to advance accordingly.

Despite increasing efforts to account for the complexity and variability of animal movement in SCR models, the use of realistic animal movement behavior as the basis for a simulation-based model evaluation has not been undertaken. New advances in animal movement modelling present an opportunity to simulate realistic animal movement and evaluate the robustness of SCR models under controlled conditions. The fundamental concept underpinning these advances is that space use emerges from an individual's interactions with its changing environment – a significant

improvement from phenomenological models of movement constructed using a top-down approach (e.g., pre-defined activity centers, home-range boundaries and step-selection functions). Modelling movement as emergent from bottom-up processes (i.e., starting from the individual responding to its environment) is not only a more intuitive way to approach individual movement, but it can also reproduce complex and dynamic patterns observed in real animal populations (Moorcroft et al. 2006, Bateman et al. 2015, Bracis et al. 2015). For example, the common phenomenon of an animal's repeated returns to an 'activity center' is its memory of a previously visited resource location (e.g., foraging sites, dens, watering holes). Stable home-ranges with distinct boundaries can also form through territorial processes, which fundamentally arise from the avoidance of competitors (e.g., via direct encounter or scent-marking, Potts and Lewis 2014). The key to modelling mechanisms that capture underlying behaviors of observed movement is to treat them as emergent properties that are not static, but change over time.

Here, we evaluate the performance of a suite of SCR models in estimating population-level parameters from detection SCR data generated using a mechanistic individual-based model to simulate animal movement trajectories. Simulated movement is driven by two key biological processes, resource memory and territoriality (Bracis et al. 2015 chap. 2). We evaluate the performance of a basic SCR model, and SCR models that account for spatial heterogeneity in (i) density and (ii) detection, and (iii) behavioral heterogeneity in movement (i.e., resident vs. transient). We measure bias, precision and coverage of abundance estimates to quantify the performance of SCR models. Additionally, we evaluate the extent to which SCR models can reveal ecological patterns that are simulated from bottom-up processes in terms of estimates of home-range size and effects of resources on both density and detection.

3.2 Methods

3.2.1 Movement simulations

SCR models have been commonly used to estimate density in many territorial animals including tigers (Karanth et al. 2006, Gardner et al. 2018), leopards (Goldberg 2015), small cats (Reppucci et al. 2011, Mohamed et al. 2013), coyotes (Morin et al. 2016), foxes (Jimenez et al. 2019), and mustelids (Lampa 2015, Fuller et al. 2016). Thus, we simulated individual movement trajectories using a mechanistic individual-based model that integrates two key processes of territorial animal space use: resource memory and territoriality.

Animal memory not only provides a plausible biological explanation for the emergence of activity centers and other stabilizing movement behaviors (e.g., home-ranging, trapline foraging, Fagan et al. 2013), but recent empirical evidence also supports this hypothesis (Polansky et al. 2015, Bracis et al. 2015, Merkle et al. 2017, Ranc et al. 2021). Resource memory can be modelled with a component that preserves the long-term attractive quality of good resource locations (as there is a cognitive expectation for its utility to be replenished) and a component where attraction to a good quality location waxes and wanes with a utility that changes over relatively short-term scales (e.g., resource consumption and regeneration, predator risk, intraspecific competition) (Van Moorter et al. 2009, Bracis et al. 2015). The inherently stabilizing behavior of site fidelity (leading to home-ranging) that emerge from these models are behaviors that have been recorded in numerous carnivores such as coyotes, cougars (Mahoney and Young 2017), wolverines (Aronsson and Persson 2018) and mongooses (Palomares 1994). Moreover, the memory mechanism can control the degree to which individuals exhibit the opposing diffusive (exploratory) behavior that is reflective of dispersal (Bracis and Wirsing 2021). This tendency to explore has been commonly observed; animals tend to 'probe' home-range boundaries and move into areas previously occupied by conspecifics (Mares et al. 1976, Moorcroft et al. 2006, Potts et al. 2013, Schoepf et al. 2015).

The other process underlying stability in space use is externally conferred through competitive interactions, as territorial individuals maintain and defend exclusive territories against conspecifics. The competitive process of territoriality is classically modelled as scent deposition, decay, and avoidance (Moorcroft et al. 2006, Giuggioli et al. 2013), a behavior that has been recorded in numerous felid (Allen et al. 2016), canid and mustelid species (Macdonald 1980). In the conspecific scent avoidance model, the territorial individual will continuously perceive the presence and strength of conspecifics' scent in its vicinity, avoiding areas where they are strong (i.e., a competitor was recently present). This reproduces the dynamism of distinct home-range boundaries in territorial animals, that may be distinct in a finite time window, but start to overlap with time (Giuggioli et al. 2013). The mechanistic territorial framework also potentially allows more complex behaviors to emerge, such as the emergence of 'floater' or transient individuals when high resource areas have all been occupied (i.e., by residents, Pitt et al. 2003, Tao et al. 2016).

The integrated resource memory and territoriality movement framework has been shown to produce emergent space use patterns broadly representative of territorial animals (Chapter 2). The conceptual model is illustrated in Chapter 2 and is described in detail in the following sub-sections. Note that we reformulated some of the original model's mathematical and parameter notations according to the notations used in the Special Feature (McClintock et al. 2022).

3.2.1.1 Resource memory

The resource landscape is modelled as a continuous scalar measure of heterogenous resource quality Q. We simulate the resource landscape on a discretized grid with two-dimensional coordinates x. The resource landscape is dynamic as N animals consume those resources (at a rate of β_C and according to a spatial kernel), which regenerate over time at a rate of β_R according to:

$$\frac{\partial Q}{\partial t} = \left(\overbrace{\beta_R(1 - \frac{Q}{Q_0})}^{\text{regeneration}} - \underbrace{\sum_N \beta_C f_C(\|x - \mu_t\|)}_{\text{consumption}} \right) Q, \tag{3.1.1}$$

where Q_0 is the initial landscape quality. The spatial kernel $f_C(\|x-\mu_t\|)$ follows a bivariate normal distribution $\frac{\exp\left(\frac{\|x-\mu_t\|}{\gamma_C}\right)}{2\pi\gamma_C}$ with length scale γ_C. Thus, $\|x - \mu_t\|$ is the Euclidean distance between x and the current location of the animal μ_t at time t.

The resource memory mechanism M consists of two streams that track the heterogenous landscape: a long-term stream L, which decays slowly at rate ϕ_L and attracts the animal to high quality habitat, and a short-term stream S, which decays more quickly at rate ϕ_S and repels the animal from depleted habitat that it has recently occupied:

$$M = L - \psi_M S, \tag{2.1.2}$$

where ψ_M is the short-term memory factor which ensures that the value at a just-visited location will initially be negative (repulsive), with $\psi_M > 1$. Each stream is characterized by learning the intrinsic quality of the resource landscape (i.e., initial quality at Q_0) at rates of $\beta_{S,L}$ (with bivariate normal spatial kernels describing learning $f_{S,L}$; similar to Equation 3.1.1) and forgetting at rates $\phi_{S,L}$ ($\phi_L < \phi_S$):

$$\frac{\partial L}{\partial t} = \overbrace{\beta_L f_L(\|x - \mu_t\|)(Q_0 - L)}^{\text{learn}} - \overbrace{\phi_L(L - \text{M}^*)}^{\text{forget}}, \tag{3.1.3}$$

$$\frac{\partial S}{\partial t} = \overbrace{\beta_S f_L(\|x - \mu_t\|)(Q_0 - S)}^{\text{learn}} - \overbrace{\phi_L S}^{\text{forget}}. \tag{3.1.4}$$

For our model, we started individuals with a fully informed long-term memory of the intrinsic resource landscape quality Q_0 that decays to the uninformed memory parameter value of M*.

3.2.1.2 Scent marking (territoriality)

As animals move about the landscape, they mark their territory on scent map D by depositing scent at a rate of β_D with a bivariate normal spatial kernel of f_D (of spatial scale of γ_D), and decays at a uniform rate of ϕ_D,

$$\frac{\partial D}{\partial t} = \beta_D f_D(\|x - \mu_t\|)(D_0 - D) - \phi_D(D), \tag{3.1.5}$$

Here, maximum scent amount D_0 is taken to be 1, as animals adjust the amount of scent deposited based on the scent amount already present through $(D_0 - D)$.

3.2.1.3 Movement process

An animal's movements through the landscape are described by a continuous-time trajectory with a current location of

$$\mu_t = \int_0^t V_{t'}\, dt' + \mu_0, \tag{3.1.6}$$

at time t, with a velocity of V_t and initial position of μ_0. The autocorrelated, directed, continuous movement process is given by

$$dV = \frac{1}{\tau}(b_t - V)dt, \tag{2.1.7}$$

similar to the Ornstein-Uhlenbeck process where instead of the white noise component, stochasticity is introduced through the bias vector, described by its magnitude and angle as $b_t = (\upsilon, \angle\Omega)$. The movement process is parameterized by τ, the time scale of autocorrelation, $\upsilon = \|b_t\|$, the magnitude of the bias vector which controls average speed, and Ω, the angle which controls direction. A Poisson process with rate parameter λ determines when angle Ω is updated, which is then selected from an angular probability distribution derived from resource memory or scent maps, depending on the behavioral state.

The animal switches between feeding and searching states, based on the instantaneous resource consumption $C(t)$, and is characterized by state-specific parameters for b_t and τ. While $\upsilon_{F,S}$ and $\tau_{F,S}$ are fixed parameters, angle $\angle\Omega$ is set

from an angular probability distribution that is made up of the contribution of only conspecific scent in the feeding state, and both conspecific scent and resource memory in the searching state.

The resource memory component for individual i is given by the angular probability density function

$$g_i(\Omega) = \frac{\int_0^r M_i(r,\Omega) f_z(r) dr}{\int_0^{2\pi} \int_0^r M_i(r,\Omega') f_z(r) dr d\Omega'}, \tag{3.1.8}$$

which is computed by integrating transects of the resource memory map M_i radiating out with radius r from the animal's location ($r = \|x - \mu_t\|$) with the memory value at each point weighted by distance, represented by the spatial kernel f_z (here exponential with length scale parameter γ_z).

Since animals ignore their own scent but are repulsed by scents of all other conspecifics, the angular conspecific avoidance metric for individual i of population size N is calculated by integrating the summed values of all other individuals' deposited scent according to

$$d_i(\Omega) = 1 - \max(1, \int_0^r \Psi_D \sum_{N \neq i} D_N(r', \Omega) f_w(r') dr'), \tag{3.1.9}$$

where Ψ_D is the scent response strength and $f_w(r)$ is a spatial kernel (here the exponential kernel with length scale γ_w) that represents that decay with distance of scent perception. The avoidance metric scales between 0 and 1 (but is not constrained to sum to 1), representing the relative 'safety' in each direction in terms of avoiding conspecifics, with 0 meaning not safe (high levels of conspecific scent) and 1 meaning safe (no conspecific scent).

Finally, the angular probability distribution from which angle Ω is drawn (in the searching state) is a combination of the angular probability distribution based on the resource memory $g(\Omega)$ multiplied by the conspecific avoidance metric $d_i(\Omega)$ for individual i, then normalized (to sum to 1), giving

$$h_i(\Omega) = \frac{g_i(\Omega) d_i(\Omega)}{\int_0^{2\pi} g_i(\Omega') d_i(\Omega') d\Omega'}. \tag{3.1.10}$$

In the feeding state, $g_i(\Omega)$ is replaced with 1. The angle of bias term $\Omega_t = \angle b_t$ in the movement process (Equation 3.1.6) is then drawn from $h_i(\Omega)$, which is specific to each animal.

3.2.1.4 Simulation design

We parameterized the model to simulate movement trajectories for species typically analyzed using SCR models, which are solitary and territorial with the following general characteristics: (i) individuals of the same sex avoid each other, otherwise they overlap; (ii) males have larger territories compared to females; and (iii) individuals are solitary.

Within a squared landscape of 300 × 300 units, we simulated the movement of a population of 100 individuals ($N = 100$, density = $1.11e^{-3}$/unit area) with parameters given by Table 3.1. To account for sex differences in space use, and opposite-sex overlap in movement, we simulated independent sets of movements for females ($N = 60$) and males ($N = 40$) (Figure 3.1). Males were parameterized to be relatively wider ranging with a higher consumption rate relative to females (Table 3.1). We treated the duration of a single timestep as one minute. We first ran the simulations for 21,600 timesteps as burn-in, which was the timeframe empirically determined to allow initial conditions to disappear (e.g., long enough for territories to be established). A further 21,600 timesteps were run that constituted our movement dataset (corresponding to 30 days, assuming 12-hours of activity per day). Scent was parameterized to decay substantially on the order of a week, loosely based on empirical data (Potts et al. 2013). Long-term memory decay was set near 0 ($\phi_L = 1e^{-10}$) to ensure individuals readily moved into unoccupied areas perceived as available due to weak conspecific scent.

We implemented our movement model in the programming language Java `v. 13.0.2` and ran 100 replicated simulated populations on a High-Performance Computing cluster. Preparation of model input and subsequent analysis of model output was conducted in R `v. 3.6.1` (R Core Team 2020). Movement was simulated on a resource landscape generated by the fractional Brownian motion function `nlm_fbm`

in the R package `NLMR` (Sciaini et al. 2018), and mean resource per cell was set to a value of 1×10^{-4} (range = 8.8×10^{-6} – 1.7×10^{-4}). Individual starting locations were biased randomly towards resource values (manually sampled in R) to allow individuals to establish territories faster. To minimize edge effects of a hard boundary and to keep the population geographically closed, individuals were allowed to move into an empty border of 50 units surrounding the resource landscape, which represents accessible but undesirable habitat that is rarely used (i.e., habitat boundary; Figure 3.2).

Three individual-level measures of 'area of use' ($A_{0.95}$) were calculated as outcomes of simulation runs with the `kernelUD` function in R package `adehabitatHR` (using the default bandwidth estimation method 'href'): (i) 95% minimum convex polygon (MCP) of all locations, (ii) 95% kernel density estimate (KDE) of locations subsampled hourly and (iii) daily. The MCP estimator was used to observe total area covered (TAC) over time, while the hourly-sampled KDE estimator was used to characterize area of use and its relationship with resource quality (mean resource value within area of use).

Table 3.1: Parameters used in the mechanistic individual-based movement model and values used to parameterize the simulations. Note: Units are arbitrary in the simulations, L is used for generic length units and T is used for generic time units. [a] L = long-term resource memory, S = short-term resource memory [b] S = searching, F = feeding.

	Parameter	Definition	Units	Values
Simulations				
	Δt	Model timestep	minutes	1
		Simulation length (timesteps)	minutes	43,200 (60 days)
	N	Number of individuals		Female 60; Male 40
Consumption				
	β_R	Resource regeneration rate	1/minute	0.01
	β_C	Consumption rate	1/minute	Female 0.5; Male 0.7
	γ_C	Consumption spatial scale	L	1
Memory[a]				
	ϕ_L	Long-term memory decay rate	1/minute	1E^{-10}

	Parameter	Definition	Units	Values
	ϕ_S	Short-term memory decay rate	1/minute	0.01
	ψ_M	Short-term memory factor		2
	β_L, β_S	Learning rates	1/minute	1, 1
	γ_L, γ_S	Learning spatial scale	L	1
	γ_z	Memory spatial scale foraging	L	1
		Memory fully informed?	boolean	True
Scent behaviour				
	β_D	Deposition rate	1/minute	1
	γ_D	Deposition spatial scale	L	1
	ϕ_D	Decay rate	1/minute	1.98E^{-4}
	ψ_D	Response strength		1.5
	γ_w	Response spatial scale	L	5
Movement[b]				
	τ_S, τ_F	Autocorrelation time scale	T	4, 2
	v_S	Search speed	L/T	3
	v_F	Feed speed	L/T	0.05
	λ	Mean time to update Ω	T	1

3.2.1.5 Emergent movement characteristics

The parameters used in the model led to a population with a positively skewed distribution of space use area (Figure 3.1 a). Females had an overall median space use area of 2,230 unit^2 (overall range = 323 – 39,192 unit^2; based on hourly sampled $A_{0.95}$) across all 100 replicates. Males had space use areas almost 1.5 times larger than females, with a median of 3,738 unit^2 (range = 648 – 46,603 unit^2). Daily sampled $A_{0.95}$ returned larger overall estimates of space use for both females (median = 2,898, range = 403 – 52,208 unit^2) and males (median = 4,878, range = 583 – 71,250 unit^2).

Most individuals maintained fairly stable territories over time (i.e., asymptotic space use area) but a small proportion (approximately 10–20%) of individuals exhibited relatively less stable and wider-ranging movements (Figure 3.1 c). The

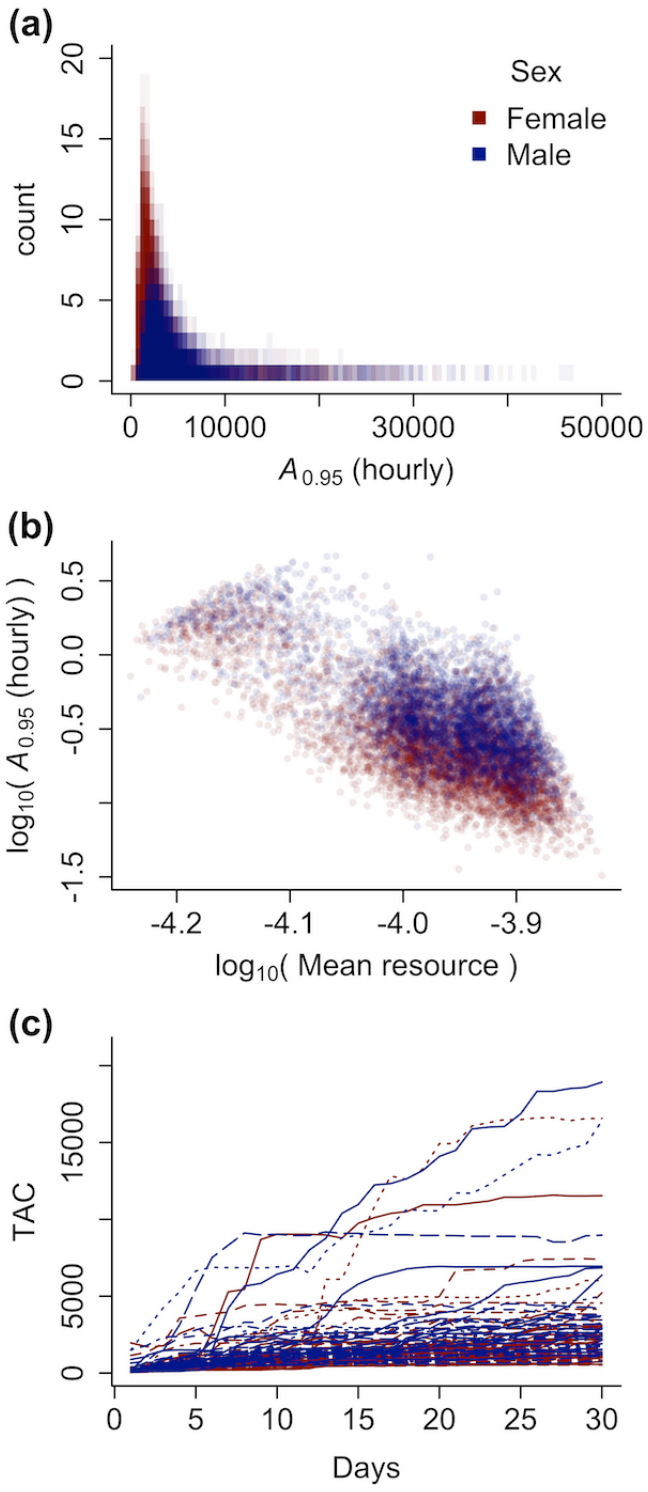

Figure 3.1: Movement characteristics from the 100 simulated populations of females ($n = 60$) and males ($n = 40$). (a) overlaid replicate-specific distributions of area of use (hourly-sampled) and (b) relationship between area of use (hourly) and mean resource value (within area of use) on a log-scale (points represent individuals). Additionally, (c) total area covered (TAC; 95% MCP estimator) over the sampling duration of one replicate.

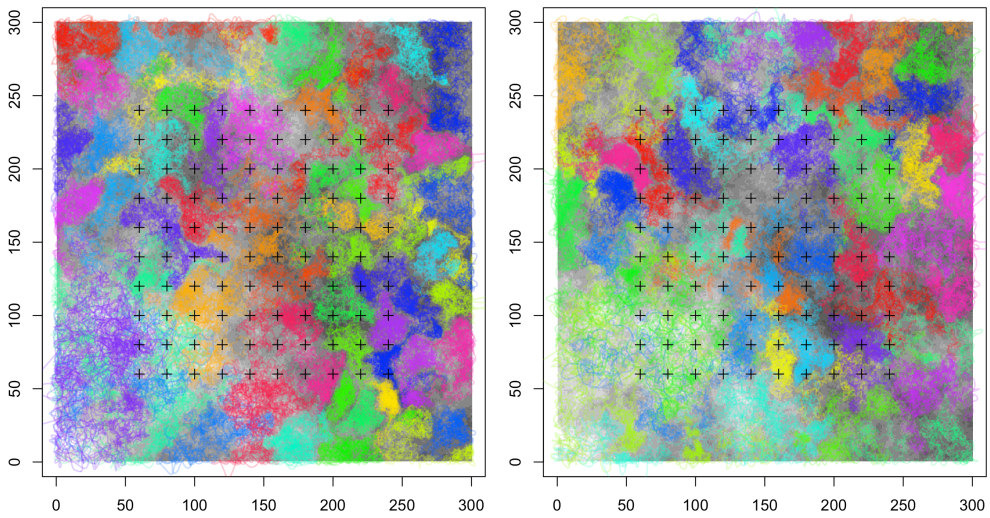

Figure 3.2: One realization of simulated movement trajectories for females (left) and males (right). Configuration of the simulation trap array (black crosses), and the heterogeneous resource landscape state-space (shade of grey corresponding to resource quality) used to simulate populations.

negative correlation between space use area and resource quality indicated that smaller and more stable territories were formed in high resource areas by resident individuals, whilst wider-ranging, transient individuals tended to be located in low resource areas (Figure 3.1 b).

3.2.2 Spatial capture-recapture analyses

3.2.2.1 Model description

We considered the following five different SCR models:

i. basic0: a basic null single-session SCR model (generally referred to as a null model);

ii. basic1: a basic single-session SCR model accounting for spatial heterogeneity in detectability and inhomogeneous density (Borchers and Efford 2008);

iii. rsf0: a resource selection (RSF) SCR model accounting for spatial heterogeneity in detectability (Royle et al. 2013b);

iv. rsf1: a resource selection (RSF) SCR model accounting for spatial heterogeneity in detectability and inhomogeneous density;

v. transience0: a Markovian transience model accounting for inter-occasion movement of activity centers (Royle et al. 2016).

All five SCR models assume a closed population (i.e., no mortality or emigration, recruitment or immigration) where the activity center of each individual (s_i) is contained within the state space ($\mathcal{M}$) during the sampling period. SCR models typically have two components: an ecological model of density describing the spatial distribution of N individuals' activity centers (s_i), and a detection model that relates the spatial encounter history for each individual (y_{ij}) to the distance between s_i and detector j. In the following model descriptions, we assume that J traps occur over T consecutive sampling intervals (i.e., occasions), and detections of individual i at trap j at occasion t follows the outcome of independent Bernoulli trials ($y_{ijt} \in [0, 1]$), constituting its detection (a.k.a. encounter) history. For numerical integration, we defined the state-space ($\mathcal{M}$) as the entire simulation landscape, represented by a 60×60 pixel landscape with a resolution of five units (3,600 grid cells). Here, x denotes the center coordinates of each landscape pixel. In the inhomogeneous density models, we used a coarse version of the resource landscape to match the resolution of the state-space (mean values aggregated by factor = 5). The resource covariate was scaled to zero-mean and unit-variance.

The basic null model (basic0) In the basic SCR model, detection probability $p_{ij} = \Pr(y_{ijt} = 1)$ for individual i at trap j is a function of the location of the activity center s_i and the location of trap x_j (constituting a subset of coordinates x), given by,

$$p_{ij} = p_0 \exp\left(- \frac{\|x_j - s_i\|^2}{2\sigma^2_{\text{det}}} \right) \tag{3.2.1}$$

where $\|x_j - s_i\|$ is the Euclidean distance between s_i and x_j, and p_0 is the baseline detection probability at distance zero (Borchers and Efford 2008). The scale parameter σ_{det}; typically denoted as "σ" in SCR literature) controls the rate of probability decline as a function of distance, with the assumption that

it arises from a bivariate, isotropic normal distribution of space use centered on a singular and static activity center s_i. Here, s are assumed to be homogenously distributed within $\mathcal{M}$.

The basic covariate model (basic1) We hypothesized baseline detection probability p_0 and density D should correlate positively with resources because movement and ultimately distribution of individuals in the landscape emerges from individuals' decisions (made at fine spatio-temporal scales) based on resource quality z. We used the same formulation as basic0 except that we accounted for spatial heterogeneity in the baseline encounter p_0 via its linear predictor, $\text{logit}(p_0) = \alpha_0 + \alpha_z z(j)$, where α_0 is the (logit-scale) intercept term, $z(j)$ is the value of the resource covariate z at trap j, and α_z is the corresponding slope parameter. Additionally, inhomogeneous density is accounted for by $D(s) = \exp(\beta_0 + \beta_z z(s))$, where $D(s)$ represents pixel density at activity center location s, β_0 is the (log-scale) intercept term, $z(s)$ is the value of the resource covariate z at location s, and β_z the corresponding coefficient.

The resource selection (RSF) homogenous density model (rsf0) In the RSF model, detections (y_{ij}) are individual (i) and trap-specific (j) counts, which are binomial with sample size T and detection probabilities $p_{ij} = 1 - \exp(-\lambda(x|s_i))$. The underlying Poisson space use model is given by,

$$\lambda(x|s_i) = \exp\left(a_0 - \frac{\|x_j - s_i\|^2}{2\sigma^2_{\text{det}}} + \alpha_2 z(j)\right) \tag{3.2.2}$$

where parameter α_2 is the effect of landscape covariate $z(j)$ at trap j, on the relative probability of use. Similar to baseline detection probability, we hypothesized p to correlate positively with resources z.

The resource selection (RSF) inhomogenous density model (rsf1) The pixel-specific landscape covariates $z(x)$ induce spatial heterogeneity in density in the same fashion as in basic1.

The transience model (transience0) The Markovian transience model extends the basic model by allowing activity centers to shift between occasions (Royle et al. 2016). At the first occasion, $s_{i,1}$ are assumed to be uniformly distributed within $\mathcal{M}$.

For $t > 1$, transience is modelled by assuming that activity centers for all individuals are transient, moving within $\mathcal{M}$ according to a Gaussian random walk centered on $s_{i,t-1}$,

$$s_{i,t} \sim \text{Normal}(s_{i,t-1}, \sigma^2 \text{I}) \tag{3.2.3}$$

where I is an identity matrix. The random walk variance is denoted by σ^2 to distinguish it from the scale parameter of the SCR detection probability model, σ^2_{det}.

As a consequence, detection probability for individual i at trap j depends on occasion t, and occasion-specific $s_{i,t}$,

$$p_{ijt} = p_0 \exp\left(- \frac{\|x_j - s_{i,t}\|^2}{2\sigma^2_{\text{det}}} \right) \tag{3.2.4}$$

3.2.2.2 Detection data generation

Detections were loosely modelled after camera traps, which have a small detection zone relative to the landscape, and theoretically capture any movement within that zone (i.e., assuming perfect detection). Our detection (or trap) array was a square grid of 100 points ($J = 100$) spaced 20 units apart. We ensured that detector spacing was smaller relative to the 95% space use radius ($r_{0.95} = \sigma_{\text{det}}\sqrt{5.99}$, see Royle et al. 2014b sec. 5.4) of simulated individuals (26.6 units based on female median in Section 3.2.1.5) to minimize estimator bias (Sun et al. 2014). A circular detection buffer of 0.2 unit radius was set around traps, based on the upper limit of empirical estimates (10 meters) of effective detection distance (Hofmeester et al. 2017) and adjusted proportionally to our landscape units (assuming 1 unit = 50 m). The array was set in the center of the simulation landscape, leaving a 60-unit buffer from the boundaries to minimize edge effects (Figure 3.2). Detections

consisted of only trajectories (of each timestep (i.e., $[\mu_{t-1}, \mu_t]$) that overlapped with the 10m buffer around traps, representing our detection dataset. At each trap, cell values of the resource landscape (at original resolution) covered by the circular trap buffer were extracted and the mean of those values (scaled to zero-mean and unit-variance, then discretized to the nearest 0.5 to speed up computation) was recorded as the trap covariate. The R packages `raster` (Hijmans and van Etten 2021) and `sp` (Bivrand et al. 2013; Pebesma et al. 2021) were used for the spatial data calculations.

The detection dataset was converted into a detection (or capture) history format (binary) with the function `spatialDetectionHistory` from the R package `camtrapR` (Niedballa et al. 2016). The detection histories, representing 30 days, were split evenly into five occasions ($T = 5$). There was minimal information loss in collapsing daily detections into binary data, given our sparse datasets (Table 3.2; Table B.1). The six-day occasion length also ensured that the average number of traps visited per individual per occasion was not too low, as the transience model estimates an activity center every occasion.

Table 3.2: Summary of detection histories for 100 replicates with an occasion length of six days, which translates to five occasions ($T = 5$). Values represent the mean and standard deviation (in brackets).

Survey summary	Females	Males
Number of independent detections	70.7 (8.6)	66.6 (8.2)
Number of individuals detected	29.8 (2.8)	23.2 (2.0)
Number of individuals detected once	10.2 (2.6)	5.8 (2.2)
Average detections per detected individual	2.4 (0.2)	3.3 (0.4)
Traps visited	52.3 (4.7)	50.1 (5.0)
Average traps visited per detected individual	1.9 (0.2)	2.4 (0.3)
Average traps visited per individual per occasion	0.48 (0.05)	0.58 (0.08)

3.2.2.3 Effect of wide-ranging individuals

While resident individuals' space use patterns broadly conformed to SCR's notion of an activity center, or an area that is clearly defined and stable (throughout the sampling duration), space use of transient individuals strongly violated this

assumption. Moreover, the assumption that σ_{det} (and consequently, area of use $A_{0.95}$) is normally distributed around the mean was also violated by the long right-tailed skew caused by the transient individuals. Thus, we tested the effect of transient individuals on SCR parameter estimation with datasets for the following scenarios: (A) all individuals ($N_{F/M} = 60/40$); (B) top 10% widest-ranging individuals from each sex removed ($N_{F/M} = 54/46$); and (C) top 20% widest-ranging individuals from each sex removed ($N_{F/M} = 48/42$). The resulting datasets show that the distribution of $A_{0.95}$ approaches a normal distribution with the removal of transients (Figure B.1). Widest-ranging transients were determined with hourly-sampled $A_{0.95}$ from the movement data (Section 3.2.1.5).

3.2.2.4 Model fitting

We fitted sex-specific capture histories to all five models (Table 3.3) because females and males have specific characteristics in terms of range of movement, abundance and density, and resultant detection probabilities. Additionally, sex-specific analyses facilitated comparison between SCR models as the RSF and transience models (as formulated by the authors) did not allow for individual-specific parameters.

Table 3.3: The full list of models fitted to simulated detection data.

Index	Model	Description
	Basic	
basic0	Null	$p_0 \sim 1$, $\sigma_{\text{det}} \sim 1$, $D \sim 1$
basic1	Covariate	$p_0 \sim z$, $\sigma_{\text{det}} \sim 1$, $D \sim z$
	RSF	
rsf0	Null	$p_0 \sim z$, $\sigma_{\text{det}} \sim 1$, $D \sim 1$
rsf1	Covariate	$p_0 \sim z$, $\sigma_{\text{det}} \sim 1$, $D \sim z$
	Transience	
transience0	Null	$p_0 \sim 1$, $\sigma_{\text{det}} \sim 1$, $D \sim 1$, $s \sim t$
–	Covariate	Not available

We fitted the generated capture histories to the basic SCR model with the R package `secr` (Efford 2021). We fitted the RSF likelihood model using the original code from Royle et al. (2013b). The Bayesian Markovian transience

model, fitted using R package `nimble` (Valpine et al. 2017) to optimize computational efficiency, sampled four Markov chains of 110,000 Markov Chain Monte Carlo (MCMC) iterations (first 10,000 discarded as burn-in) for a total of 400,000 posterior samples. We assessed convergence using the Gelman-Rubin diagnostic ($\hat{R}(N) \leq 1.1$) for all parameters and by visual inspection of parameter trace-plots (Gelman and Rubin 1992).

3.2.2.5 Model evaluation

We evaluated model performance based on mean estimates of total abundance $\hat{N}$ and scale parameter $\hat{\sigma}_{\text{det}}$ in terms of relative bias [RB], precision (coefficient of variation [CV]), and the coverage of the 95% confidence or credible intervals (for the likelihood and Bayesian models respectively) of true N and σ_{det}. In the evaluation of performance in $\hat{\sigma}_{\text{det}}$, we compared the derived 95% area used from the basic SCR model only ($\hat{A}_{0.95} = \pi r_{0.95}^2$, where $r_{0.95} = \hat{\sigma}_{\text{det}}\sqrt{5.99}$, see Royle et al. 2014b , section 5.4) with the empirically derived space use areas $A_{0.95}$ (both the hourly- and daily-sampled KDE estimates of $A_{0.95}$) from the simulated movement data (population mean). Since deriving $\hat{A}_{0.95}$ from $\hat{\sigma}_{\text{det}}$ in the RSF and transience models is not straightforward and tools are not readily available, we did not perform the evaluation for these models and instead limited our comparison solely to $\hat{\sigma}_{\text{det}}$. Additionally, we recorded and plotted estimates of resource effect size on density (D) (basic1, rsf1), baseline encounter probability (p_0) (basic1) and space use probability (α_2) (rsf0, rsf1), with the expectation of a positive effect of resources on all these parameters.

3.3 Results

The basic and RSF models converged for all datasets and across scenarios and sexes. The transience model converged for all datasets except in two instances (one female replicate of scenario A and C respectively), based on convergence of the abundance N parameter ($\hat{R}(N) \leq 1.1$).

3.3.1 Abundance estimation

Under scenarios A (full dataset) and B (top 10% of transients removed), all models produced unbiased $\hat{N}$ (within ±0.05 RB(N); Table 3.4; Figure 3.3). The explicit inclusion of the resource covariate governing variation in baseline detection probability (p_0) and spatial variation in density (D) did not improve performance metrics (RB, CV, coverage) for the basic model for any scenario or sex. In the female population, slight positive bias in $\hat{N}$ arose with the removal of 20% of the widest-ranging individuals in scenario C (top 20% of transients removed; RB($\hat{N}$)= 0.06–0.10) across all models, except for the RSF covariate model, which still produced an unbiased estimate (RB($\hat{N}$) = 0.02).

Coverage for $\hat{N}$ was nominal or conservative ($\geq$ 0.95) in all models, scenarios and populations except for the rsf for scenarios B and C in both female and male populations ($\geq$ 0.90; Table 3.4).

Overall, precision in $\hat{N}$ was similar between female and male populations across all models and scenarios (CV($\hat{N}$) = 0.13–0.18; Table 3.4). Loss of precision only marginally increased with widest-ranging individuals removed in scenario B and C across all models (CV($\hat{N}$) difference = +0–0.05).

Table 3.4: Average relative bias (RB), coefficient of variation (CV), coverage of total abundance $\hat{N}$ across 100 replicate datasets for all fitted SCR models in three scenarios. (A) all individuals ($N_{\mathrm{F/M}}$ = 60/40, (B) top 10% widest-ranging individuals from each sex removed ($N_{\mathrm{F/M}}$ = 54/46) and (C) top 20% widest-ranging individuals from each sex removed ($N_{\mathrm{F/M}}$ = 48/42).

Scenario	Model	Females			Males		
		RB	*CV*	*Coverage*	*RB*	*CV*	*Coverage*
A			$N = 60$			$N = 40$	
	Basic						
	Null	0.01	0.13	1.00	0.01	0.14	0.98
	Covariate	0.02	0.13	1.00	0.02	0.14	0.98
	RSF						
	Null	-0.01	0.13	0.97	-0.007	0.14	0.95
	Covariate	-0.002	0.13	0.97	-0.005	0.14	0.95
	Transience						
	Null	0.009	0.13	0.97	0.003	0.14	0.97

Scenario	Model	Females			Males		
B			$N = 54$			$N = 36$	
	Basic						
	Null	0.05	0.15	1.00	0.03	0.15	0.98
	Covariate	0.03	0.15	1.00	0.03	0.14	0.98
	RSF						
	Null	0.05	0.18	0.94	0.03	0.16	0.94
	Covariate	0.008	0.15	0.98	0.0002	0.14	0.96
	Transience						
	Null	0.04	0.14	0.97	0.03	0.14	0.97
C			$N = 48$			$N = 32$	
	Basic						
	Null	0.07	0.16	1.00	0.04	0.16	0.99
	Covariate	0.06	0.16	1.00	0.03	0.17	0.99
	RSF						
	Null	0.10	0.18	0.91	0.06	0.18	0.95
	Covariate	0.02	0.16	0.98	-0.001	0.17	0.96
	Transience						
	Null	0.06	0.15	0.98	0.04	0.16	0.98

3.3.2 Estimation of movement processes

Scale parameter estimates $\hat{\sigma}_{\text{det}}$ from all models decreased with the removal of the widest-ranging individuals from scenario A to C (Figure 3.4 a; Table B.1). Within each sex and scenario, $\hat{\sigma}_{\text{det}}$ from the basic and RSF models were comparable, but was always smaller by 16–24% for the transience model.

In the basic models (basic0, basic1), relative bias in area used $\hat{A}_{0.95}$ calculated from $\hat{\sigma}_{\text{det}}$ was highly dependent on the method chosen to derive the 'true' area used ($A_{0.95}$; Figure 3.4 b; Table B.2). Against hourly estimates of true $A_{0.95}$ (population mean), $\hat{A}_{0.95}$ tended to be overestimated across all scenarios (RB($\hat{A}_{0.95}$) between 0.41–0.53) and coverage was less-than-nominal (0.33–0.70). Against the daily estimates of true $A_{0.95}$, which were larger, the overestimation of $\hat{A}_{0.95}$ was much smaller across all scenarios for the basic models (RB($\hat{A}_{0.95}$) = 0.07–0.13) and coverage was generally better, albeit less-than-nominal (0.57–0.85). The removal of widest-ranging individuals only led to marginal reductions in $A_{0.95}$(hourly and daily) bias from scenario A to C (20% removed) in both the female and male

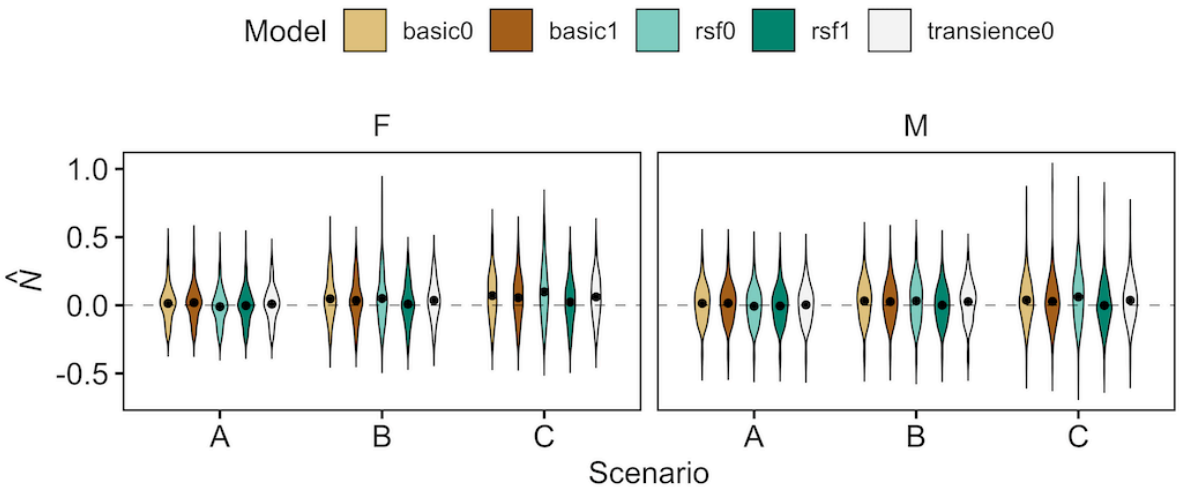

Figure 3.3: Relative bias of estimated total abundance, $\hat{N}$, for all fitted SCR models. Violin plots (F: females; M: males) represent the distribution of relative bias from 100 replicate datasets (black point representing the overall mean) of three scenarios: (A) all individuals ($N_{\mathrm{F/M}} = 60/40$), (B) top 10% widest-ranging individuals from each sex removed ($N_{\mathrm{F/M}} = 54/46$) and (C) top 20% widest-ranging individuals from each sex removed ($N_{\mathrm{F/M}} = 48/42$).

populations (RB($\hat{A}_{0.95}$)A-C difference = 0.01–0.11; Table B.1). $\hat{A}_{0.95}$(hourly and daily) was more precise in the female compared to the male population (Figure 3.4 b; Table B.1) in scenario A. Marginal gains in precision were observed with the removal of transients across the basic models for males (CV($\hat{A}_{0.95}$) = A: 0.41, B: 0.35, C: 0.29) but not for females (CV($\hat{A}_{0.95}$) = A: 0.29, B: 0.35, C:0.30).

In the transience model, mixing of the inter-occasion scale parameter estimate $\hat{\sigma}$ was challenging for many replicates. While $\hat{R}(\hat{\sigma}) \leq 1.1$ for 90% and 96% of female and male replicates respectively suggested adequate mixing (for scenario A), this was not consistent with visual inspections of trace-plots (44% female and 23% male replicates were poorly mixed; see Figure B.1). Intra-occasion scale parameter estimates $\hat{\sigma}_{\mathrm{det}}$ were similar to $\hat{\sigma}$ across scenarios in both females ($\hat{\sigma}_{\mathrm{det}}/\hat{\sigma}$ = A: 13.8/9.7, B: 10.9/8.6, C: 9.9/7.2) and males ($\hat{\sigma}_{\mathrm{det}}/\hat{\sigma}$ = A: 15.6/14.6, B: 12.8/13.1, C: 11.9/11.2).

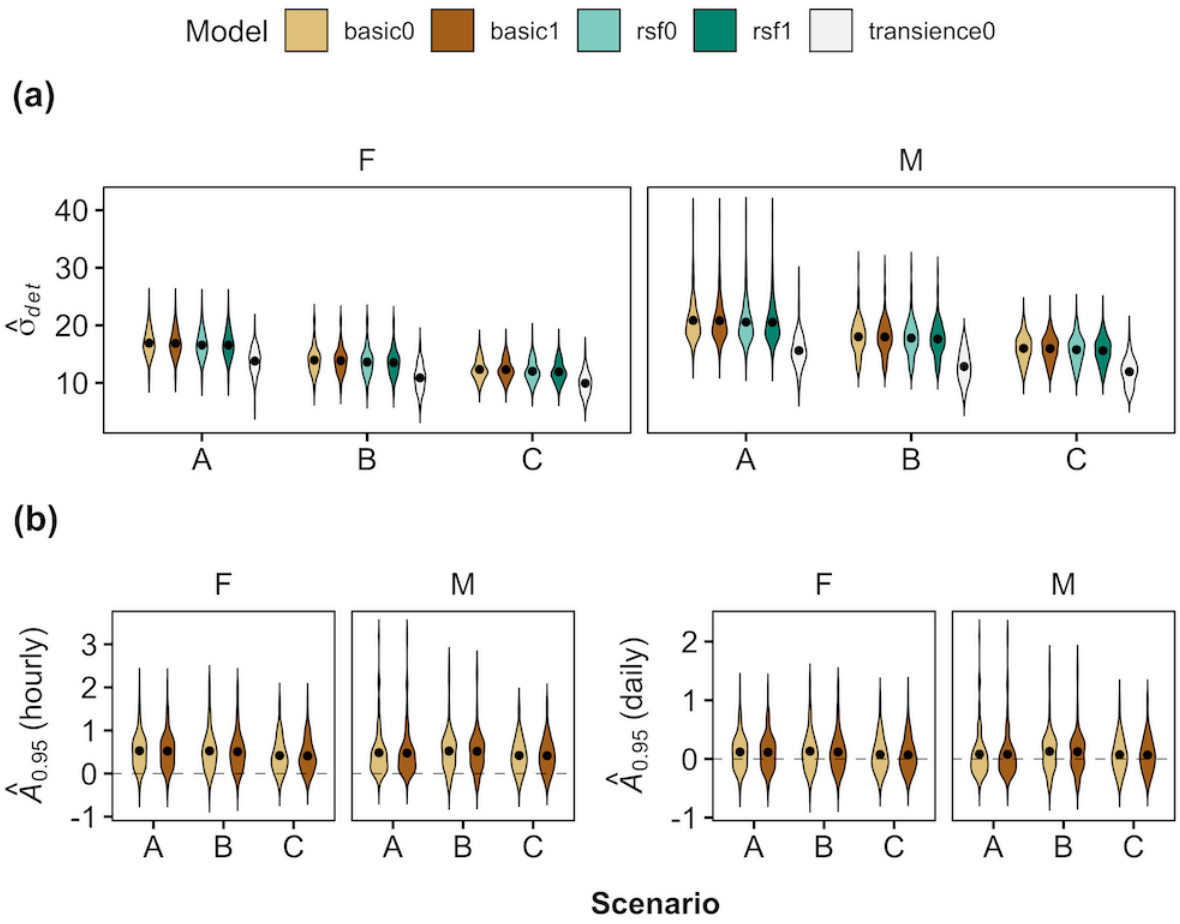

Figure 3.4: (a) Scale parameter estimates $\hat{\sigma}_{\text{det}}$ for all fitted SCR models and (b) relative bias of 95% area used $\hat{A}_{0.95}$ (derived from $\hat{\sigma}_{\text{det}}$) for all the basic SCR models only. Since deriving $\hat{A}_{0.95}$ from $\hat{\sigma}_{\text{det}}$ in the RSF and transience models is not straightforward and tools are not readily available (Royle et al. 2013, 2016), these models were omitted from the evaluation of $\hat{A}_{0.95}$. Violin plots (F: females; M: males) represent the distribution of relative bias from 100 replicate datasets (with the black point representing the overall mean) of three scenarios: A) all individuals ($N_{\text{F/M}} = 60/40$), B) top 10% widest-ranging individuals from each sex removed ($N_{\text{F/M}} = 54/46$) and C) top 20% widest-ranging individuals from each sex removed ($N_{\text{F/M}} = 48/42$).

3.3.3 Estimation of resource effects

Overall, the covariate models captured the positive effect of spatial variation in resources on density, but not its finer-scale positive effect on baseline detection probability (basic1) and space use probability (rsf0 and rsf1) (Figure 3.5). The inhomogeneous density models (basic1 and rsf1) produced similar overall positive estimates of resource effect size on density for both females and males (Figure 3.5). With the removal of transients (which tended to inhabit low resource areas), the

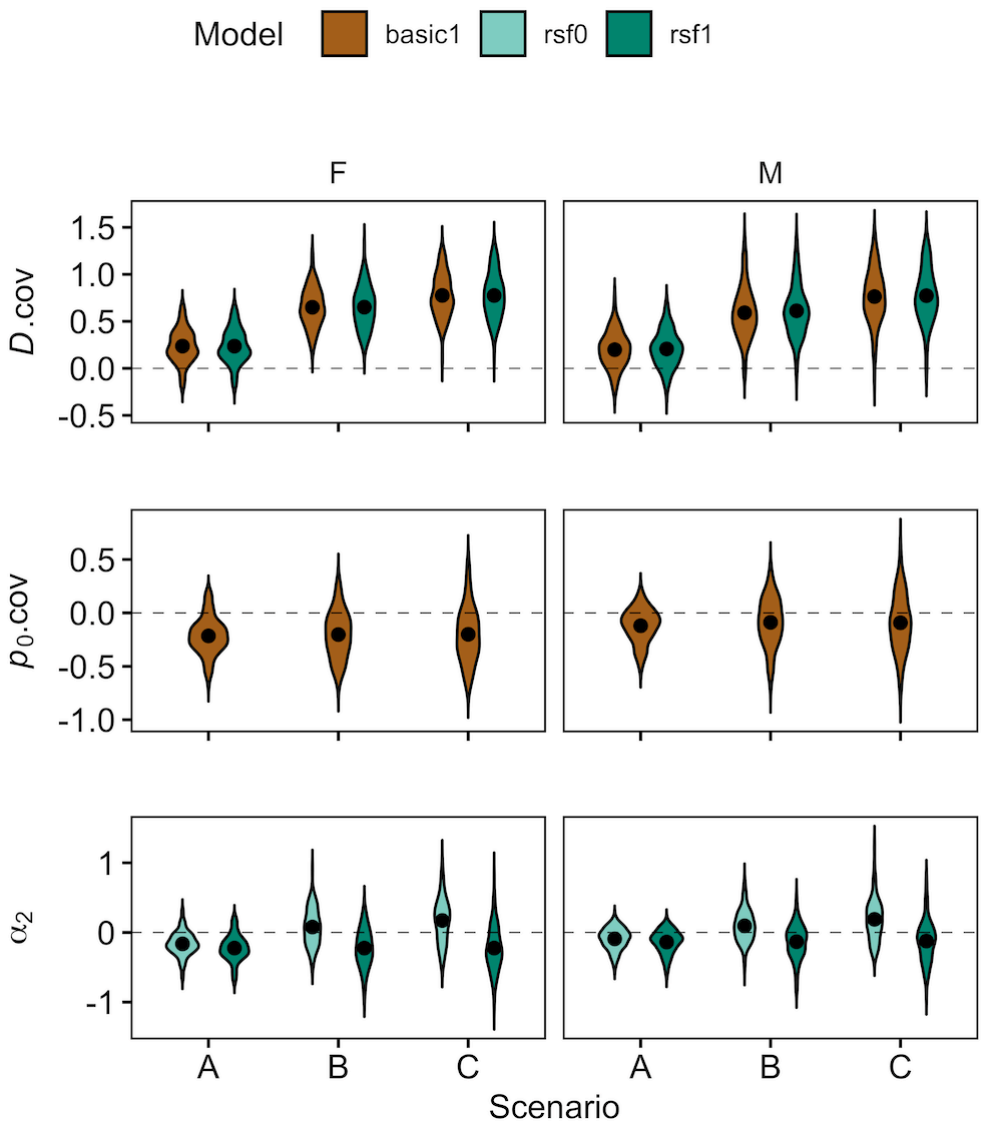

Figure 3.5: Effect size estimates of the resource covariate on D, p_0 and $p(\alpha_2)$ for basic and rsf SCR models. Violin plots (F: females; M: males) represent the distribution of effect size estimates from 100 replicate datasets (with the black point representing the overall mean) of three scenarios: A) all individuals ($N_{\mathrm{F/M}} = 60/40$), B) top 10% widest-ranging individuals from each sex removed ($N_{\mathrm{F/M}} = 54/46$) and C) top 20% widest-ranging individuals from each sex removed ($N_{\mathrm{F/M}} = 48/42$).

positive effect size of resources on density increased ($\mathrm{A}_{F/M}$: 0.23/0.20, B: 0.65/0.60, C: 0.77/0.77). The proportion of replicates with negative effect estimates on density also grew smaller with the removal of widest-ranging individuals ($\mathrm{basic1}_{F/M}$ = A: 0.08/0.14, B: 0/0.02, C: 0/0.01; $\mathrm{rsf1}_{F/M}$ = A: 0.08/0.13, B: 0/0.01, C: 0/0.01).

The expected positive effect of resource on detectability was not captured by

the covariate models (basic1, rsf0 and rsf1). Mean resource effect on baseline encounter probability (p_0) was weakly negative and did not change with the removal of widest-ranging individuals in the female (A: -0.22, B: -0.20, C: -0.20) and male populations (A: -0.12, B: -0.09, C: -0.09; Figure 3.5). Interestingly, mean resource effect on relative probability of use (α_2) grew from weakly negative to more positive across the scenarios in both female and male populations with the RSF model (homogenous density; ($A_{F/M}$: -0.16/-0.09, B: 0.08/0.10, C: 0.17/0.19), but did not change in the RSF-covariate model (inhomogeneous density; ($A_{F/M}$: -0.22/-0.14, B: -0.22/-0.13, C: -0.22/-0.12; Figure 3.5).

3.4 Discussion

SCR models have undergone numerous advancements since their development. However, most model evaluations continue to generate SCR data under the same analytical model (i.e., which make the same assumptions about space use), making it difficult to diagnose how models perform when applied to real data that can violate SCR model assumptions in multiple and subtle ways. Our study departs from the conventional evaluation approach by generating SCR data using mechanistic individual-based simulations of movement trajectories and investigating the consequences of assumption violations that emerge from realistic animal movement behavior on the inferences derived from a suite of commonly used single-session SCR models. While our findings largely confirm previous investigations about the robustness of the abundance estimator, inferences obtained from parameters related to movement and space use was limited.

Estimates of abundance from the basic SCR model were found to be robust to multiple violations of our SCR dataset, corroborating previous findings; namely: (i) non-circular home-range shapes (Efford 2019); (ii) individual heterogeneity in space use area (Efford and Mowat 2014) and (iii) movement patterns (i.e., resident vs. transient behavior, Royle et al. 2016); (iv) dynamic activity centers (Royle et al. 2016); (v) non-independent individuals' movements (Bischof et al.

2020a); and spatial variation in density (Dupont et al. 2021). The estimates were robust for both the female and male populations, which were characterized by different population densities and movement characteristics. Accounting for spatial heterogeneity in density, detectability and space use, and dynamic activity centers in the covariate and extension models did not improve performance metrics of $\hat{N}$. Moreover, the removal of widest-ranging individuals (that potentially strongly violated the basic model's activity center assumption) did not improve performance, but in fact marginally worsened it, likely because of sparser datasets. Even though the accuracy of $\hat{N}$ was highly sensitive to the realization of each replicate (biases of up to 45% were recorded in basic0, scenario A, female and male; Figure 3.3), coverage of the true abundance was consistently nominal or conservative (≥ 0.95).

Although abundance estimators from the basic model have been generally robust to different types of violations, considerable bias can be induced when violations of assumptions are substantial (Sutherland et al. 2015, Bischof et al. 2020a). While difficult to compare with existing studies due to the mechanistic simulation framework we have used, we suspect the degree of assumption violation in our datasets was low. For example, when spatial heterogeneity in resource selection is unaccounted for, it was shown to cause up to -20% bias in $\hat{N}$ due to unmodelled heterogeneity in detection probability (Royle et al. 2013b). It suggests that our movement simulations and trap placement resulted in minimal individual heterogeneity in detection (i.e., resource effect on space use, α_2, was negligible even with the removal of transient individuals that primarily inhabited low resource areas; Figure 3.5), or that heterogeneity was not spatially clustered (Moqanaki et al. 2021), which, if substantial, would have otherwise biased $\hat{N}$.

The smaller scale parameter σ_{det} estimates from the transience model compared to the other models tested demonstrated that σ_{det} tends to absorb additional variability in movement (e.g., transience of the activity center, Royle et al. 2016). As such, unless the basic model's restrictive assumptions about space use are met, home-range size cannot be directly inferred from σ_{det}. Extensions to the basic model (e.g., RSF and transience) have improved representations of animal space

use, but tools to derive home-range area from these models have yet been developed. In development and evaluation of such methods in the future, it will be crucial to determine what 'true' home-range area is in the first place. True home range size referenced in SCR studies are often calculated using conventional methods (e.g., KDE and MCP, Royle et al. 2011, Bischof et al. 2020b, Harmsen 2020) that do not account for temporally autocorrelated location data and hence yield different results at different sampling durations and frequencies (Noonan et al. 2019). As demonstrated with our KDE estimates of $A_{0.95}$ (Section 3.2.1.5), higher sampling frequencies tend to yield smaller space use measures, which are more reflective of an occurrence distribution (i.e., where an animal was located during the observation period) than a home-range (i.e., probability distribution of possible locations of an animal, Fleming et al. 2015). In striving to integrate more complex movement processes into SCR models (McClintock et al. 2022), it is thus also important to consider what the detection/movement process represents (i.e., a home-range or an occurrence distribution).

We found that convergence of the transience model, and especially the inter-occasion scale parameter σ, was difficult to attain with our datasets. This was primarily due to data sparsity as we found that convergence was easier to attain with datasets generated with double the trap density ($\hat{\sigma} \leq 1.1$ for all datasets from both sexes in scenario A; see Table B.4 and Figure B.3). Estimating transience (or dynamic activity centers) is known to be challenging (Gardner et al. 2018, Milleret et al. 2020), as it appears that the model requires large detection datasets (i.e., large number of individuals, occasions, traps). Another possible reason for the poor convergence of σ is that the model assumed complete transience (i.e., all individuals have non-stationary ACs) on populations that were predominantly residents. Interestingly, it also appears that the transient individuals in our populations were violating the assumption that AC movement distances are normally distributed (Equation 3.2.3), as the true distribution has a long tail towards large movements (Figure 3.6). The similarity in σ_{det} and $\hat{\sigma}$ estimates could also indicate that differentiating the intra (σ_{det})- and inter(σ)-occasion scale parameters was challenging,

when both parameters are comparable across the whole population. Ultimately, the number (and length) of occasions was arbitrary as there was no clear distinction of intra- and inter-occasion movement in our simulated populations, as often the case in reality. While we could have used the partial transience model (which has a parameter ϕ that governs the proportion of individuals with non-stationary ACs) instead, initial runs on several replicates showed that both σ and ϕ could not converge. This was likely a result of the sparse datasets and the small proportion of transients in the populations. Our results demonstrate that, especially for sparse SCR datasets, fitting transience models can be challenging in practice.

The SCR covariate models (basic1, rsf0, rsf1) could capture the positive effect of resource quality on density estimates but did not capture the positive effect of resource quality on space use (or detection probability). The fact that the removal of transient individuals strengthened the positive effect of resource on density is likely due to their different habitat preferences as a result of territorial exclusion and limited resources (Whittington-Jones et al. 2011, Mitchell et al. 2015, Hinton 2016). It would be useful to model heterogeneity in individual behavior, especially when individual covariate explaining such variation cannot be measured (Cubaynes 2010). In our case, categorizing resident and transient individuals would not be possible solely from the SCR dataset.

The failure to capture resource's positive effect on space use/detection was not a result of the sparseness of our datasets as similar effect sizes were returned with double the trap density (see Table B.4 and Figure B.3). We found that the lack of relationship between resource and space use was likely a result of aggregating the detection data into binary occasions (Figure 3.7). The relationship was dampened even when considering daily occasion, indicating that the individuals' attraction to resources was only visible at very fine spatio-temporal scales. Moreover, the dampened resource effect could have further reduced the level of individual heterogeneity in detection, and did not induce bias in $\hat{N}$ that may have otherwise be observed with stronger resource selection effects (Royle et al. 2013b, 2014c). This further strengthens the need to consider and develop SCR models

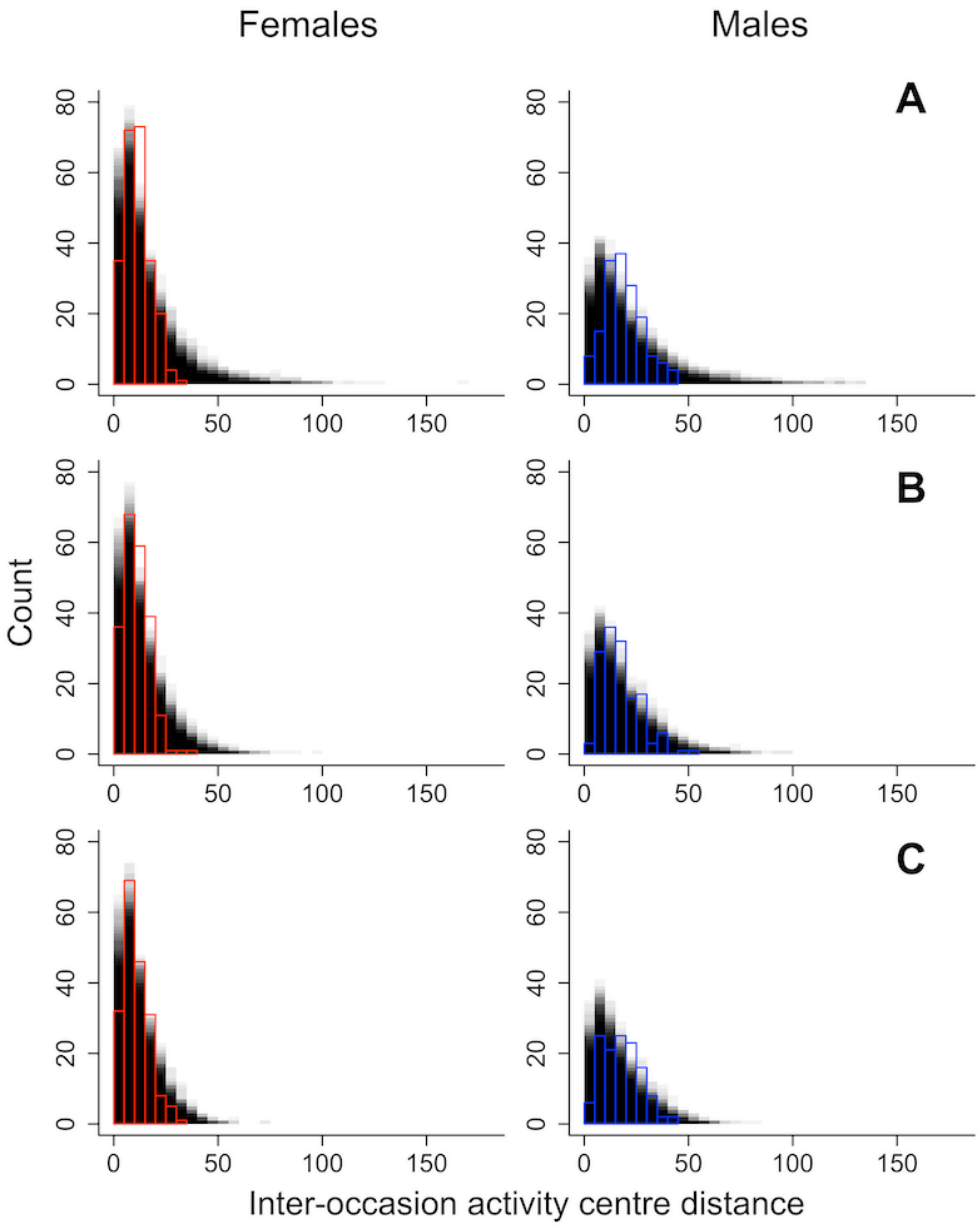

Figure 3.6: The realized ('true') and predicted distribution of inter-occasion activity center distances for scenario A (all individuals), B (10% of the widest-ranging individuals removed) and C (20% of the widest-ranging individuals removed) for the female and male populations. Each panel shows 100 overlaid replicate-specific distributions (represented as histograms with translucent black fill) and the predicted distribution simulated from the mean $\hat{\sigma}$ obtained from the transience SCR model across replicates (represented by the colored-border histograms). True activity centers were the centroids of the 95% kernel density estimate for each of the five occasions ($T = 5$) per individual.

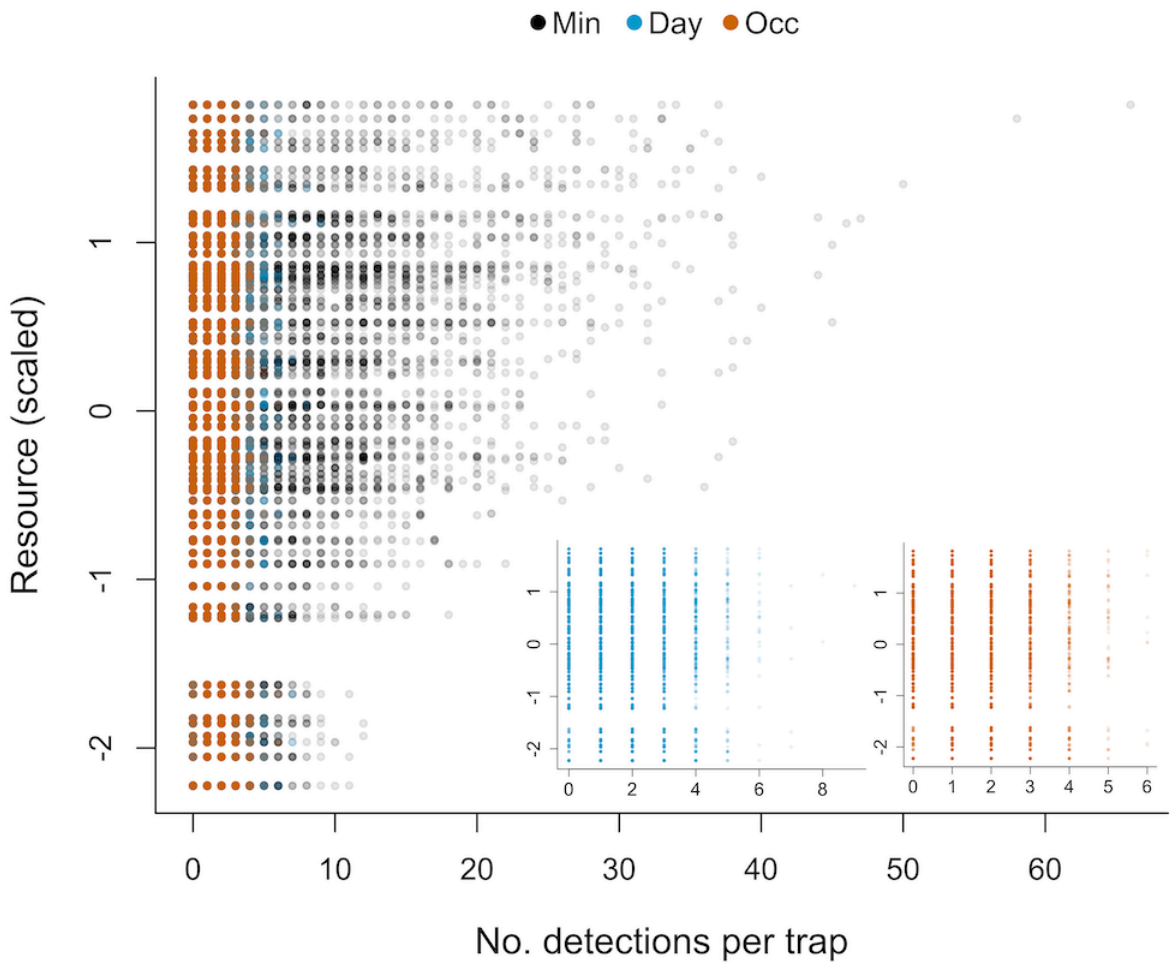

Figure 3.7: Number of detections per trap at different time resolutions (Min: minute; Day: day, Occ: occasion) and the corresponding scaled resource values per trap. Points with transparent fill represent traps from all 100 replicates. Inner plots show an expanded view of the data collapsed to the daily (left) and occasion level (right).

(e.g., continuous-time, Distiller et al. 2020, complex movement, McClintock et al. 2022) that explicitly integrate movement processes to account for spatio-temporal dependence in detections.

Implications and future work

The simulation approach here lays the groundwork for understanding SCR model performance under a range of increasingly realistic situations under controlled

conditions. As evaluations using real-life experiments are challenging to conduct (Fleming et al. 2021), our movement simulation model opens the door for users to test the robustness of SCR models to realistic SCR datasets according to the specificity of their systems and characteristics of the studied species (through appropriate parameterization; Table 3.1). We found the basic SCR model was sufficient to obtain robust abundance estimates under a specific set of conditions. However, investigating if this still holds for other realistically simulated populations, such as one with a stronger resource selection effect (i.e., to induce individual detection heterogeneity), open populations (e.g., Gardner et al. 2018, Glennie et al. 2019), and associations between individuals (Bischof et al. 2020a), as well as the influence of trap placement in a heterogeneous landscape, is warranted.

More importantly, our evaluation framework exposes the limitations of ecological and movement-related inferences made by established SCR models, offering several important insights into how inference about specific mechanisms in SCR models can be improved. For example, the covariate SCR models (basic and RSF) could only reveal the larger scale effect of resources on density, while the finer third-order effect (of resource on space use, detection probability) may require finer-scale data (Linden et al. 2018) and/or appropriate model specification to accurately reveal. Articles in this Special Feature offer potential solutions, such as allowing data supplementation with telemetry data within an SCR framework that integrates habitat-driven movement (Gardner et al. 2022). But when processes only operate at very fine temporal scales (e.g., minute or hour) and data supplementation with telemetry data is not possible, it may be necessary for integrated movement SCR models to move towards continuous-time formulations that allow for all detection data to be used (e.g., Distiller et al. 2020, also see continuous-time formulation outlined by McClintock et al. 2022).

The integration of explicit movement model parameters (e.g., σ, resource selection coefficients) into the SCR framework would capture the interaction between animal movement and its landscape (i.e., habitat-driven movement, Gardner et al.

2022, McClintock et al. 2022). However, we caution that while movement inferences certainly improve with integrated movement models, it may be challenging to fit with sparse detection datasets, as often is the case with SCR surveys. As we have demonstrated with data simulated independently of the SCR model, the transience model struggled to accurately capture inter-occasion movement σ (in our simulated data) with a normally distributed Markovian movement model. In this regard, testing a variety of distributions for σ (e.g., right-skewed, multimodal, etc.) is warranted in future investigations of integrated movement SCR models. The integration of telemetry data also presents a promising solution (Gardner et al. 2022), and could be tested using our simulation framework, as true individual locations (i.e., similar to telemetry data) are readily available.

The integration of SCR and animal movement models to expand the scope of ecological inference by addressing the relationships between population, movement and landscape ecology, holds much promise. In addition to integrating habitat drivers of movement into the SCR framework (Gardner et al. 2022), we encourage development of approaches that incorporate elements from our movement simulation model, such as multiple movement behavior states (McClintock et al. 2022) and interactions between individuals (e.g., territoriality, Reich and Gardner 2014, McLaughlin and Bar 2021). It should be noted, however, that quantifying memory processes is much less plausible as it remains challenging to disentangle the influence of resources from that of site familiarity (i.e., memory), even with telemetry data (Van Moorter et al. 2013). Nevertheless, the use of fine-scale mechanistic individual-based movement simulations offers a rich framework from which to further develop and test the ability to quantify additional movement processes within the SCR framework.

4

Performance of camera trap-based density estimators for unmarked populations

Statement of Authorship

Publication title	Performance of camera trap-based density estimators for unmarked populations
Publication status	Unpublished and Unsubmitted work written in manuscript style
Publication details	
Data and code	https://github.com/merylltheng/unmarked_eval

Principal Author

Name of principal author	Meryl Theng
Contribution to paper	Conceptualised and designed the study, performed all simulations and analysis, wrote the paper.
Overall percentage	90%
Certification	This paper reports on original research I conducted during the period of my Higher Degree by Research candidature and is not subject to any obligations or contractual agreements with a third party that would constrain its inclusion in this thesis. I am the primary author of this paper.

Date	12 March 2023

Co-author Contributions

By signing the Statement of Authorship, each author certifies that: (i) the candidate's stated contribution to the publication is accurate (as detailed above); (ii) permission is granted for the candidate in include the publication in the thesis; and (iii) the sum of all co-author contributions is equal to 100% less the candidate's stated contribution.

Name of Co-author 1	Pablo Palencia
Contribution to Paper	Supported conceptualisation, study design, analysis and writing.
Signature	
Date	12 March 2023
Name of Co-author 2	Phillip Cassey
Contribution to Paper	Supported writing. Provided supervisory support.
Signature	
Date	12 March 2023
Name of Co-author 3	Steven Delean
Contribution to Paper	Supported analysis and writing. Provided supervisory support.
Signature	
Date	12 March 2023

Abstract. Estimating density when animals are not individually identifiable (i.e., unmarked populations) has continued to be a key challenge and frontier in wildlife management. Camera traps have emerged as a popular tool to monitor multiple animal species at relatively low cost, for which several statistical methods have been developed to estimate density of unmarked populations. However, we are only just beginning to understand which methods can provide accurate estimates, and under what conditions the methods are robust. Here, we focused on assessing three such methods: Random Encounter Model (REM), Random Encounter and Staying Time (REST) and Camera Trap Distance Sampling (CTDS). We evaluated the methods under a wide range of simulated conditions that varied in population densities, movement rates (i.e., speed and home-range size), group aggregation, and trap effort. CTDS and REST generated density estimates that were robust for both solitary and group-living animals, if population densities were not too low (2–20 km^{-2}) and trap effort was substantial (100 traps). However, REM overestimated density across all simulated scenarios, which arose from underestimation of the day-range parameter (i.e., because faster movement sequences were disproportionately undetected) and underestimation of the detection radius parameter (i.e., from poor detection model fits to the data, worsening under large group scenarios). While all methods tested demonstrate potential in terms of reliable density estimation of unmarked populations, we caution that density estimates are prone to bias without careful consideration in the measurement and parameterisation of model-specific parameters.

4.1 Introduction

Obtaining reliable population size estimates is a fundamental task in wildlife conservation and population management. However, estimating population size has

traditionally been costly and laborious to undertake (i.e., capturing, and identifying or individually marking animals). In recent decades, remotely-triggered camera traps have emerged as a low-cost and minimally invasive tool allowing for continuous surveillance of multiple species in a wide range of habitats (Rovero & Zimmerman, 2016). As a result, camera traps have been widely adopted in population monitoring, and large database projects are increasingly popular (e.g., WildlifeInsights: https://www.wildlifeinsights.org/, Amazonia Camtrap: Antunes et al. 2022). Camera traps are used for diverse purposes including obtaining measures of species richness, beta diversity, occupancy and behaviour (Burton et al. 2015). However, camera trap studies estimating population density have largely been limited to individually identifiable animals (Gilbert et al. 2021), which precludes its use on the majority of animal species that possess no natural markings (i.e., unmarked). As such, methods that can reliably generate density estimates for unmarked species from camera trap-based data would have a broad applicability.

To address the demand for camera trap-based density estimation without the need for individual identification, a broad suite of novel analytical approaches have been developed. They include: the Random Encounter Model (Rowcliffe et al. 2008), Random Encounter and Staying Time (Nakashima et al. 2017), Spatial Count (Chandler and Royle 2013), Distance Sampling based on camera traps (Howe et al. 2017), Time to Event Model (Moeller et al. 2018), and more recently, the Time-In-Front-of-Camera method (Becker et al. 2022). Unlike well-established Spatial-Capture Recapture methods estimating population size in marked species (Royle et al. 2014b), there is currently no equivalent for unmarked animals. While empirical application of unmarked density estimation methods has been increasing, we are only just starting to understand the conditions required for these methods to produce reliable estimates (Gilbert et al. 2021). Several, mostly field-based (Rovero and Marshall 2009, Zero et al. 2013, Cusack et al. 2015, Caravaggi et al. 2016, Doran-Myers et al. 2021, Palencia et al. 2021a, Pettigrew et al. 2021) and a handful of simulation-based studies (Hayashi and Iijima 2022, Santini et al. 2022), have compared and evaluated the performance of multiple methods but results have

been mixed. Often, results demonstrating biased estimator performance appeared to be a result of deficient or inappropriate procedures used to estimate model-specific parameters (Nakashima 2022, Palencia et al. 2022). Thus, it has been challenging to identify the true weaknesses of these methods and to offer constructive priorities for further model development. Evaluation of these methods with a focus on appropriately estimating model parameters can help address the current gap. Furthermore, conducting the evaluation within a simulation framework would allow us to diagnose how and why models fail to perform, minimising performance issues related to inappropriate measurement and estimation of model parameters.

In this chapter, we focused on three unmarked population density estimation methods that can be applied to studies with comparable sampling designs: Random Encounter Model (REM), Random Encounter and Staying Time (REST), Camera-Trap Distance Sampling (CTDS). Their sampling design does not require spatial correlation in captures (i.e., an individual does not need to have probability of being captured in more than one camera) like in capture-recapture related models. This allows any spacing or arrangement of cameras to be used, and hence, a wide range of species can be sampled in a single survey. The three methods also share mathematical similarities that afford comparsions under common conditions. In addition to using standard encounter history data, these methods require estimation of the camera's effective detection zone (or field of view, FOV) of the camera trap and the movement rates (e.g., REM: speed, REST: staying time) of observed animals, along with other similarities in design assumptions (Table 4.1).

Specifically, we sought to determine how population density, animal behaviour (movement and social) and camera trap effort (i.e., number of cameras) affect the performance of REM, REST and CTDS density estimates. We measure bias, precision and coverage of density estimates to quantify the performance of these methods. Further, we quantified the bias in specific model parameter estimates to diagnose the potential sources of bias in density estimation.

Table 4.1: Assumptions of three unmarked density estimation methods evaluated in this study: Random Encounter Model (REM), Random Encounter and Staying Time (REST) and Camera Trap Distance Sampling (CTDS). Adapted from Palencia et al. (2021a).

Assumptions	REM	REST	CTDS
Cameras random relative to animals	X	X	X
Animal movement and behaviour not affected by camera trap	X	X	X
Closed population	X	X	X
Certain detection at specific area within detection zone	X	X	X
Animals at 0 distance perfectly detected	X		X
Animals are detected at their initial locations	X		X
Observations are independent events	X	X	X
Measurements are accurate	X	X	X

4.2 Methods

4.2.1 Movement simulation model used for solitary and group-living animal populations

4.2.1.1 Solitary animals

Animal movement was simulated as a discrete-time, biased, correlated random walk (BCRW). Solitary animals had fixed centres of attraction (i.e., activity centres), which were randomly distributed across the background landscape within a minimum distance apart from each other (proportional to population density). Step-lengths between point locations were drawn from a gamma distribution and turning angles at each step from a von Mises distribution. Step-length at timestep t was the average of the step-length of the previous timestep (l_{t-1}) and a draw from a gamma distribution with a mean and variance specific to each population scenario (λ_t), giving $l_t = \frac{l_{t-1}+\lambda_t}{2}$. Turning angle at timestep t was sampled from the following von Mises distribution,

$$\phi_t \sim \text{vM}(\Phi_t, \kappa_{\text{scenario}}), \tag{4.1.1}$$

with a concentration parameter specific to each population scenario κ_{scenario}, and expected movement direction,

$$\Phi_t = \omega\phi_{t-1} + (1-\omega)\mu, \tag{4.1.2}$$

which comprised a weighted average of the strength of bias in the previous movement direction ϕ_{t-1} and the bias in the direction of the solitary individual's fixed activity centre μ for $\omega \in [0, 1]$ (McClintock et al. 2012).

4.2.1.2 Group-living animals

In the group-living animal model simulations, group members made movement decisions relative to moving group-specific centroids (Langrock et al. 2014). Group centroid movement was modelled like solitary animal movement (as described above). Individual movement was simulated as a two-state random walk, comprising a BRW component (state 1) biased toward the current group centroid's location μ_t, and a CRW component (state 2) correlated to the direction of the previous step. Thus, turning angle at timestep t in state s is given by,

$$\phi_{t,s} \sim \text{vM}(\Phi_{t,s}, \kappa_{scenario,s}), \tag{4.1.3}$$

$$\Phi_{t,s} = \begin{cases} \mu_t & s_t = 1 \\ 0 & s_t = 2 \end{cases}, \tag{4.1.4}$$

where s_t represents state at time t with $s_t = 1$ indicating a BRW and $s_t = 2$ indicating a CRW, and $\kappa_{\text{scenario},s}$ is the scenario- and state-specific concentration parameter. The transition probabilities between states are given by the matrix,

$$\Gamma = \begin{pmatrix} 0.95 & 0.05 \\ 0.3 & 0.7 \end{pmatrix}, \tag{4.1.5}$$

such that individuals spend most of the time following the centroid (state 1), but occasionally move independently from the group (state 2). Step-length was first derived at the group-level, similar to that of solitary animal movement described above (i.e., l_t drawn from a gamma distribution now represented the group's mean step-length). Each group member's step-length was then drawn from a normal

distribution with mean l_t and standard deviation of $l_t/10$, representing correlation in their speeds.

We treated the duration of a timestep as 5 minutes and first ran the simulations for a total of 5,400 timesteps (excluding a 108 timestep burn-in to eliminate initial conditions), which corresponds to 50 days assuming 9 hours of activity per day. Animals moved within a square landscape of 10 × 10 km. To keep the population density constant, individuals leaving the landscape were set to appear on the opposite side.

4.2.2 Population scenarios

We simulated solitary animal populations at three levels of population density (*high*, *medium*, *low*), with corresponding movement rates (speed and home-range size; Table 4.2) based on reported values for real species (Table C.1 and C.2). We further simulated group-living animals for the *medium* and *high* density populations at two levels of group aggregation (with similar individual speeds as the solitary scenario; Figure 4.1). We did not simulate a group-living scenario for the *low* density population because the population parameters were reflective of solitary carnivores. Parameter values used in each population scenario can be found in Table C.3.

Table 4.2: Animal population scenarios simulated to test unmarked abundance estimators, and the respective realised movement rates and home-range size.

Density (km^{-2})	Behaviour	Group size	Movement speed (m/s)	Home-range size (km^2)
High (20)			0.16	
	Solitary	1		0.12
	$Group_{20}$	20		
	$Group_{100}$	100		
Medium (2)			0.33	
	Solitary	1		1.4
	$Group_5$	5		
	$Group_{25}$	25		
Low (0.1)			0.60	
	Solitary	1		17.0

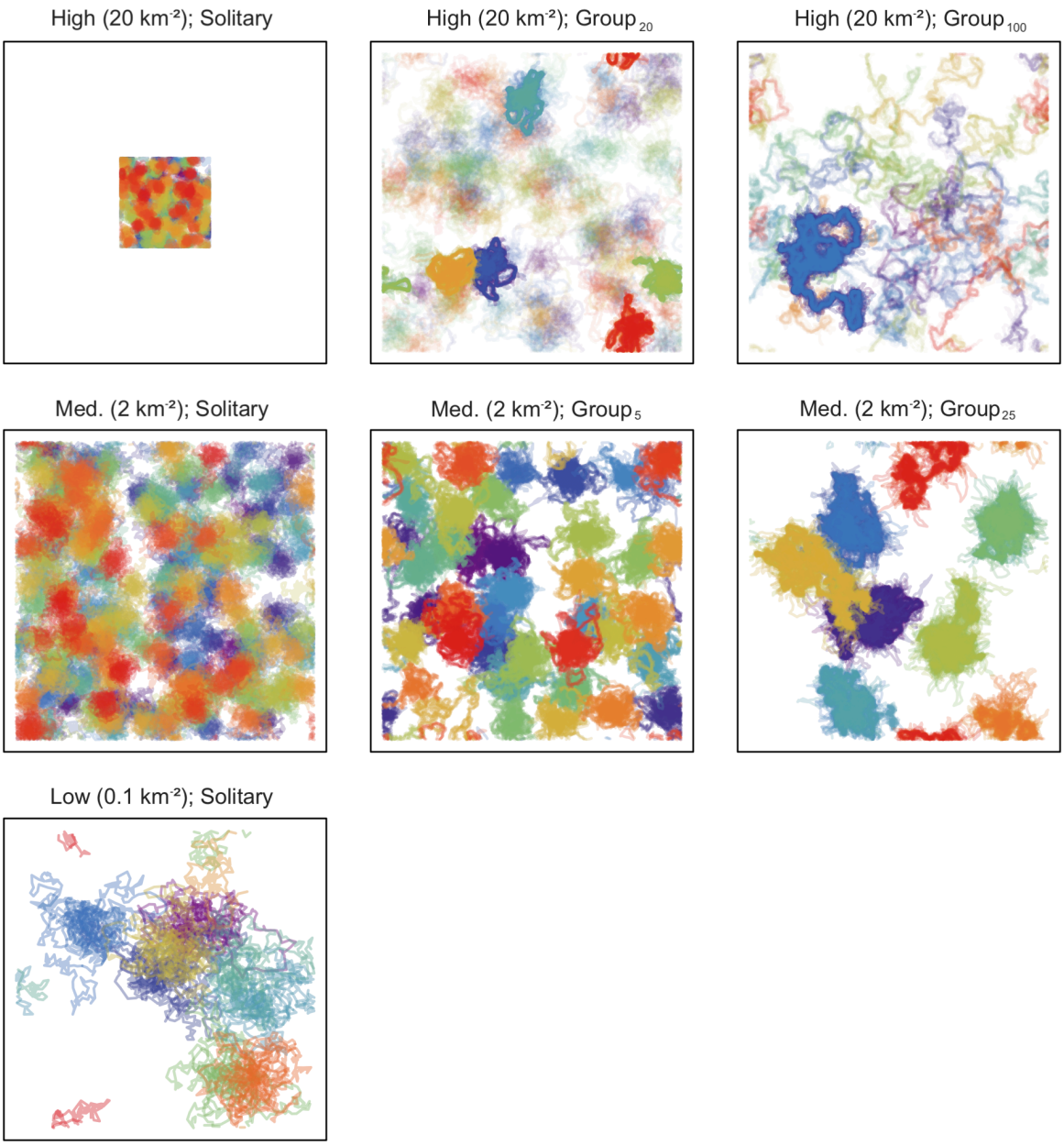

Figure 4.1: Examples of simulated movements of multiple population density (High, Medium, Low) and group aggregation (Solitary; Group$_x$, where x is the number of animals per group) scenarios on a 10 × 10 km landscape. Colours represent unique individuals. For the high-density examples, only trajectories of a subset of individuals were plotted - sol: individuals within a 3 × 3 km subset of the entire landscape; group$_{20}$: all 20 members of five groups highlighted, with two representative members for each of the other groups in the background (faded); group$_{100}$: all 100 members of one group highlighted, with 10 representative members for each of the other groups in the background (faded). Otherwise, the trajectories of all individuals in 10 days are presented.

4.2.3 Detection simulations

The sampling design for detecting simulated animals was a regular square grid of J camera traps (CT; $J = 25$ or 100) covering the 100 km^2 landscape. Each CT's field of view (FOV) was a circular segment of 10 m radius and 40° angle, radiating out from the CT location towards a random direction. When an animal's trajectory overlapped with a CT's FOV, detections were sampled sequentially at every 1-s interval of the overlapped trajectory according to the hazard-rate decay function, $p = 1-\exp(-(\alpha/d)^\gamma$ (following Equation 1b in Rowcliffe et al. 2011), where p is the detection probability at animal distance from the camera d, α is the width of the function and γ is the shape. Hazard logistic parameters used were $\alpha = 3$, $\gamma = 6$. If a detection occurred, the following two 1 second intervals were automatically recorded as 'bursts', consistent with the recording of CT images (Figure 4.2).

4.2.4 Density estimation

The three unmarked estimators of interest (REM, REST, CTDS) share parameters and design considerations. Central to these methods is relating population density D to the number of animal encounters y, survey effort ξ and model-specific detection zone and animal movement parameters (see Figure 4.2). To estimate the latter two parameters, it was necessary to record the position of each image-captured animal in the detection zone. We treated individuals as the unit of observation in group encounters, because group encounters can bias density estimates (Hayashi and Iijima 2022). Note that since no angular decay or animal inactivity was applied to our simulations, angle of FOV θ was fixed at 40° and activity level (i.e., proportion of time animal spends active) was fixed at 1.

4.2.4.1 REM

The Random Encounter Model (Rowcliffe et al. 2008) specifies the relationship between density D, encounter rate (i.e., number of encounters per unit time, y/ξ, where ξ is survey effort), animal speed v, and the dimensions of the CT detection zone comprising radius r and angle θ:

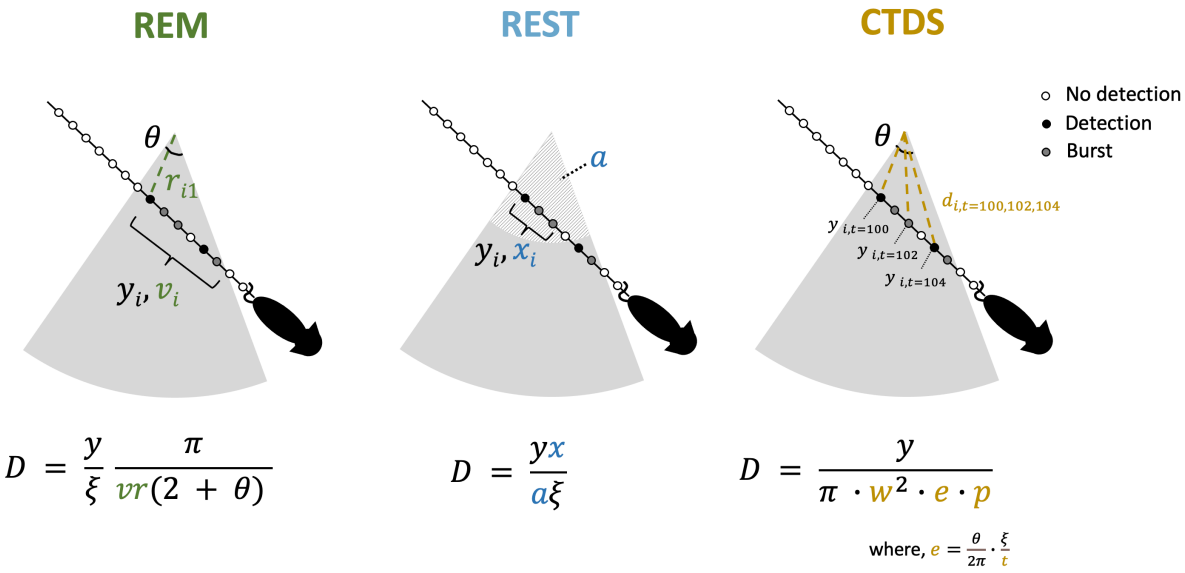

Figure 4.2: Conceptual diagram of measurements taken in a camera-trap (CT) detection for each method (REM: Random Encounter Model; REST: Random Encounter and Staying Time; CTDS: Camera-Trap Distance Sampling). The 1 s intervals (of a 5 min movement trajectory) that overlapped with the CT field of view (FOV; grey segment) were sequentially sampled for detections using a hazard-rate detection function that decayed with distance from the CT. Points along the trajectory indicate the sampling intervals, with black points representing a detection and the following two points (grey fill) are automatically recorded 'bursts', and points with white fill indicate non-detection. A single encounter either constituted detection(s) belonging to the same i-th movement sequence, y_i (i.e., of an individual entering and exiting the camera's FOV for REM or perfect detection area a for REST), or a single detection made at every specified time interval, y_{it} (e.g., say every 2 s, $t = 0, 2, 4..$; for CTDS). Within each concounter (y_i or y_{it}), measurements specific to each model are taken (coloured notation) to estimate density D: animal's speed/day-range v, detection radius r (i.e., distance to first detection of the encounter), staying time x, perfect detection area a, and distance(s) d (used to estimate probability of obtaining an image of an animal that is within truncation distance w and angle *theta* in front of the CT).

$$D = \frac{y}{\xi} \frac{\pi}{vr(2+\theta)}. \tag{4.2.1}$$

A unique encounter was defined as an individual entering and exiting the camera's FOV. We collapsed detections from consecutive movement tracks within the FOV (i.e., of the same individual but where there may be multiple changes in movement direction) into a single encounter, making the assumption that the individual could be traced from FOV entry to exit. Speed was calculated as the sum of distance traveled between sampled images, divided by the time difference

(in seconds) between the first and last image. The mean and standard error of all speed observations v were then estimated by the best fitted sized-biased model (log-normal, Weibull, gamma) to account for over-representation of faster speeds (Rowcliffe et al. 2016). To estimate detection radius r, we recorded the distance (from the CT) of the animal when it first triggered the CT (r_{i1}; i.e., the first 'image' of an encounter sequence) and then applied a distance sampling approach using a default hazard-rate function with no adjustment terms. To harmonise units across all parameters, camera time was measured in days and speed was converted to distance covered per day (i.e., day-range).

The encounter histories by trap j, y_j, and parameter estimates (mean and variance) formed the input data into the model. REM analysis was carried out with the `camtools` R package (https://github.com/MarcusRowcliffe/camtools) using a bootstrap method to produce variance estimates for density.

4.2.4.2 REST

The random encounter and staying time (REST) model is an extension of the REM model, which estimates density as a function of encounter rate y and staying time x in a predetermined detection zone a (i.e., the amount of time an animal is present in the zone) and survey effort ξ (Nakashima et al. 2017),

$$D = \frac{yx}{a\xi}. \tag{4.2.2}$$

The model assumes that animals entering the detection zone are detected with certainty (i.e., focal area a), which in our case was the area of the FOV segment where detection was perfect (0–2.2 m). Staying time was measured as the number of 1-s records of the individual inside the focal area. Records where the animals were outside of the focal area were discarded.

We fitted the REST model under a Bayesian framework (adapted from Amburgey et al. 2021). The number of encounters at trap j was modelled as negative binomial random variables, $y_j \sim \text{NegBin}(p_j, \sigma)$, with size parameter σ and mean encounter rate μ_j (giving probability $p_j = \sigma/(\sigma + \mu_j)$). Staying time for encounter

i was modelled as exponentially distributed random values with mean λ, giving $x_i \sim \text{Exp}(\lambda)$. We used vague priors where $\lambda \sim \text{Uniform}(0, 5)$, $\sigma \sim \text{Uniform}(0, 10)$ and $D \sim \text{Gamma}(0.1, 0.1)$. We ran the model with the R package `nimble` (Valpine et al. 2017), using four chains of 110,000 iterations with the first 10,000 discarded as burn-in. We assessed model convergence using the improved Markov Chain Monte Carlo convergence diagnostic ($0.99 < \hat{R} < 1.01$; Effective Sample Size $>$ 400) for the density parameter D (Vehtari et al. 2021).

4.2.4.3 CTDS

Camera-Trap Distance Sampling (CTDS) is a point transect distance sampling approach, which treats cameras as stationary 'observers' (Howe et al. 2017). Essentially, it models proportion of time animals are available for detection to estimate density. The number of times a CT can potentially detect an animal is discretised according to the specified time interval as T_k/t (see below). Thus, density D is a function of the total encounters y and the animals' availability for detection,

$$D = \frac{y}{\pi \cdot w^2 \cdot e \cdot p}, \tag{4.2.3}$$

where $e = \theta/2\pi \cdot \xi/t$ consists the sampling effort and detection zone (t is the specified time interval between sampled 'images', θ is the detection zone angle, ξ is the survey effort), w is the truncation distance beyond which any recorded distances are discarded (10m), p is the estimated detection probability of an animal within distance w from the CT, estimated from a detection function fitted to animal distances from the CT (Buckland et al. 2001). Finally, we subset our sampled image data at 2 s intervals ($t = 2$). Finally, we followed the detection model fitting and selection procedure, and used a nonparametric bootstrap to produce variance estimates for density/abundance (as described in Howe et al. 2018).

4.2.5 Model evaluation

We evaluated model performance based on mean estimates of density $\hat{D}$ in terms of relative bias (RB) from true values, precision (coefficient of variation; CV), and the

coverage of the 95% confidence or credible intervals (for likelihood and Bayesian estimates respectively) of true D. Precision was evaluated against a benchmark CV of ≤ 0.2, which is often considered the gold-standard target for population monitoring (Pollock and Hines 1990).

4.3 Results

In terms of bias, CTDS performed the best amongst the three methods, returning unbiased estimates across almost all simulated scenarios ($\text{RB}(\hat{D}) \leq 0.10$; Figure 4.3). Bias was only observed in the medium-density group_{25} and low-density solitary scenario under low effort ($\text{RB}(\hat{D}) = 0.16$, 0.19 respectively). REST also performed well, generating unbiased estimates under most scenarios. Positive bias was observed under low effort under the medium-density group_{25} scenario ($\text{RB}(\hat{D}) = 0.35$) and to a small extent in the medium-density solitary and high-density group_{20} scenario ($\text{RB}(\hat{D}) = 0.11$ for both). REM overestimated D under all scenarios and group aggregation worsened the positive bias in $\hat{D}$ in the high-density populations (solitary: 0.20, group_{20}: 0.44; group_{100}: 0.85). Compared to low trap effort ($J = 25$), high trap effort ($J = 100$) saw reduced variability of point estimates across replicates. However, there was minimal difference in mean $\text{RB}(\hat{D})$ (across replicates) between the two effort levels across scenarios, except for the medium-density group_{25} scenario, which saw a marked increase in density estimates under low effort.

Estimates were generally precise (i.e., meeting benchmark of $\text{CV}(\hat{D}) \leq 0.20$; Figure 4.4) in the high-density scenarios, even at low trap effort, except under REST. In the medium-density scenarios, precision generally met the benchmark CV at high trap effort, but not at low trap effort. In the low-density scenario, high trap effort was not enough to achieve the benchmark CV under any method. The increase of group aggregation saw higher precision in the high-density scenario. However, it led to lower precision in the medium-density scenario. Between methods, REST produced the least precise estimates.

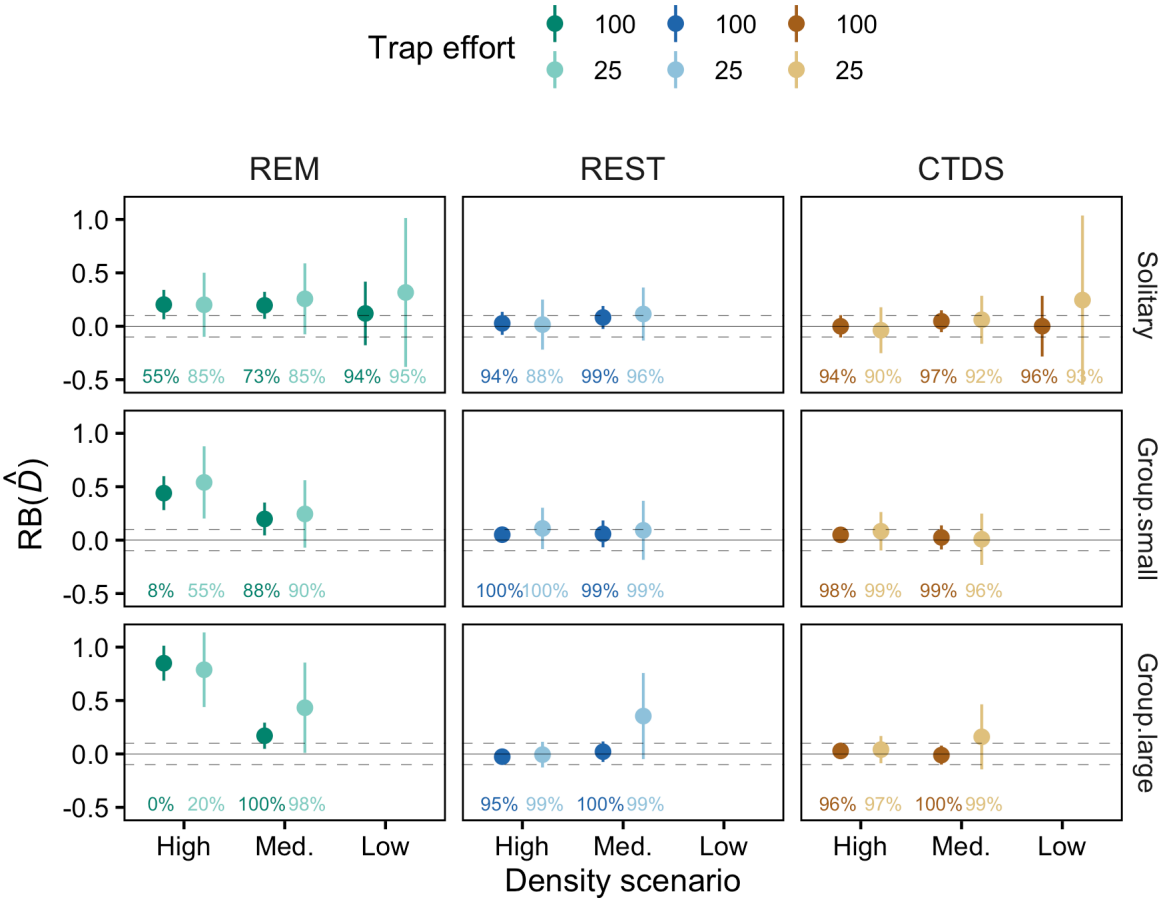

Figure 4.3: Relative bias (RB) of density estimates $\hat{D}$ for all fitted unmarked density estimation methods (REM: random encounter model; REST: random encounter and staying time; CTDS: camera-trap distance sampling). Error plots represent the 95% distribution of RB from 100 replicate datasets (points representing the overall mean) of multiple population density (High: 20 km^{-2}; Medium: 2 km^{-2}; Low: 0.1 km^{-2}), group aggregation (Solitary; Group.small: 20 and 5 animals/group for high and medium density respectively; Group.large: 100 and 25 animals/group for high and medium density respectively) and trap effort (100 and 25 traps) scenarios. The solid horizontal line represents no bias in estimates, with the dashed horizontal lines representing an allowable amount of bias (±0.10). Percentage values at the base of each error bar represent coverage of the 95% confidence intervals of the true density.

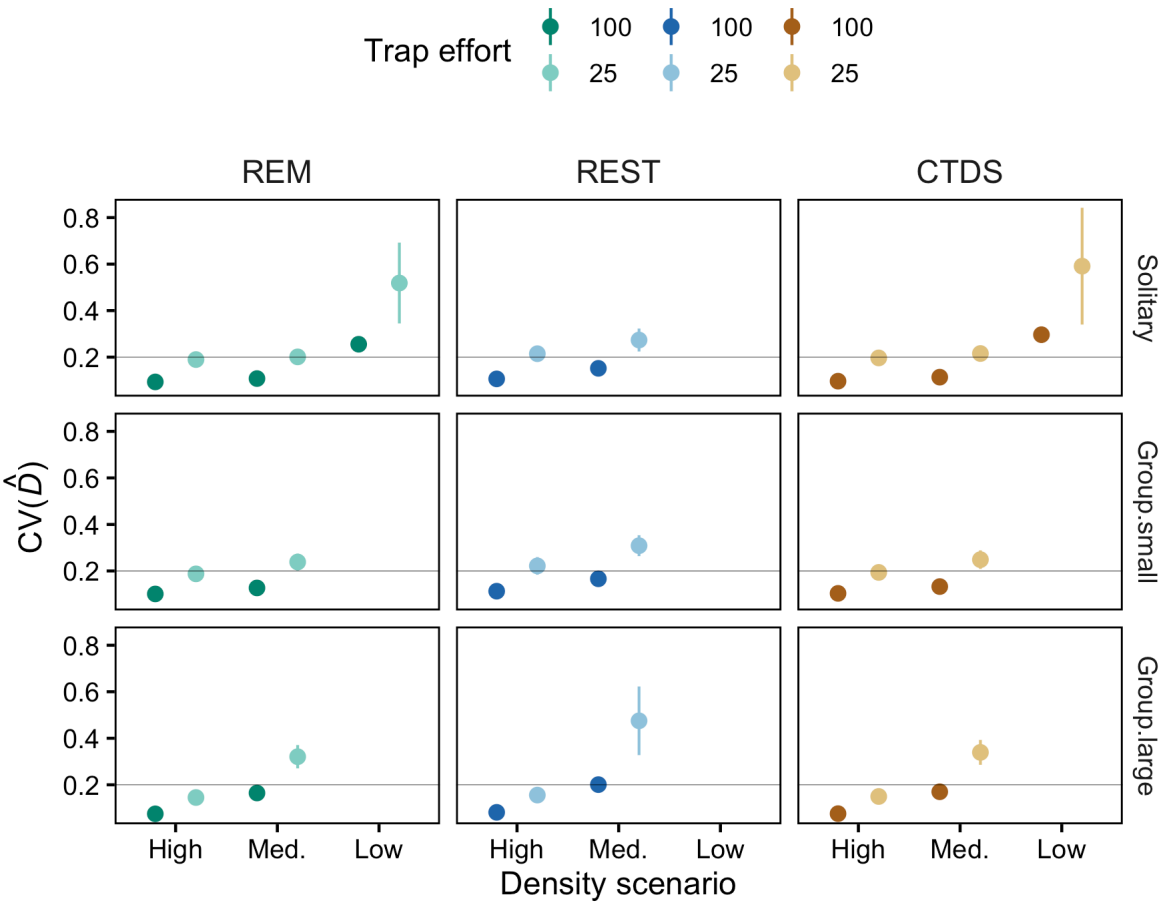

Figure 4.4: Coefficient of variation (CV) of density estimates $\hat{D}$ for all fitted unmarked density estimation methods (REM: random encounter model; REST: random encounter and staying time; CTDS: camera-trap distance sampling). Error plots represent the 95% distribution of CV from 100 replicate datasets (points representing the overall mean) of multiple population density (High: 20 km^{-2}; Medium: 2 km^{-2}; Low: 0.1 km^{-2}), group aggregation (Solitary; Group.small: 20 and 5 animals/group for high and medium density respectively; Group.large: 100 and 25 animals/group for high and medium density respectively) and trap effort (100 and 25 traps) scenarios. The solid horizontal line represents a benchmark level of precision (CV $\leq$ 0.2).

Confidence interval coverage tended to be poor when density estimates were both biased and precise (REST across all scenarios, REM in the high-density group_{100} scenario; Figure 4.3).

REM and CTDS converged for almost all datasets (98-100%) across all scenarios, except for the low-density low trap effort scenario (92% and 78% respectively). Note that in low-density populations where REM converged, sample size was very small ($y < 38$). REST converged for 99-100% of the replicates in the high-density populations, had lower convergence rates in the medium-density populations (83-95%) and failed to converge for almost all replicates of the low-density populations (high effort = 3%; low effort = 1%).

REM bias

To investigate the source of bias in REM's density estimates $\hat{D}$, we conducted a post-hoc analysis comparing the results (i.e., imperfect detection) to that under perfect detection for the solitary scenarios only. Under perfect detection, all animal movement was detected within the specified FOV (i.e., $r = 10$m) and exact measurements of animal speeds (day-range) were taken. Bias in $\hat{D}$ disappeared under perfect detection (Figure 4.5).

Underestimates in day-range were found, which were marginally greater the faster the animals moved in each population density scenario (High(slower): -6—-4%, Medium: -7—-5%, Low(faster): -9%; Figure 4.6 a). Underestimating day-range will cause overestimates in density because both parameters are inversely related. However, this only partially explained the positive bias in $\hat{D}$ (i.e., unexplained bias). The unexplained bias appeared to be greater the slower the population was (Table 4.3).

In parameters where bias could not be determined (i.e., radius r and encounter rate y), we only compared parameter estimates between scenarios. Radius estimates $\hat{r}$ (i.e., imperfect detection) appeared to decrease at higher levels of group aggregation under the high-density scenario but were similar under all medium-density scenarios (Figure 4.6 b). Under the solitary scenarios, faster populations

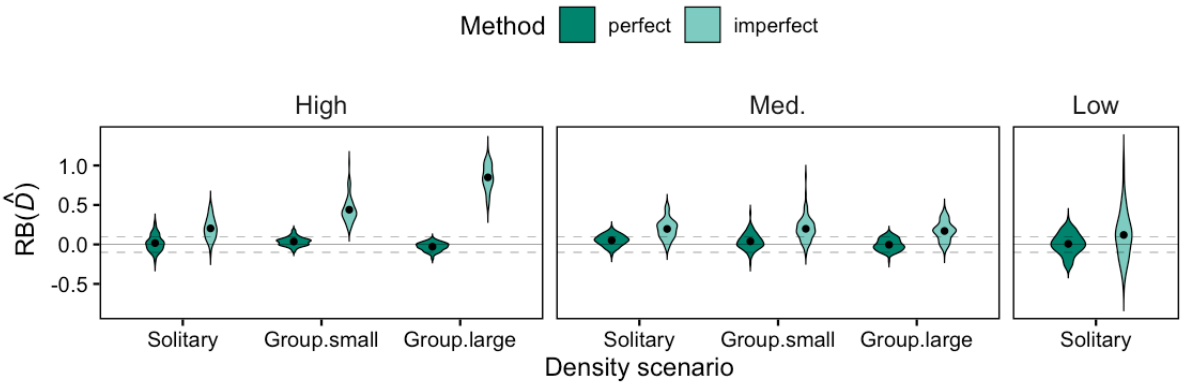

Figure 4.5: Comparison of relative bias of estimated density $\hat{D}$ derived under perfect and imperfect detection for the random encounter model (REM). Violin plots represent the distribution of relative bias from 100 replicate datasets (points representing the overall mean) of multiple population density (High: 20 km^{-2}; Medium: 2 km^{-2}; Low: 0.1 km^{-2}) and group aggregation (Solitary; Group.small: 20 and 5 animals/group for high and medium density respectively; Group.large: 100 and 25 animals/group for high and medium density respectively) scenarios. The solid horizontal line represents no bias in estimates, with the dashed horizontal lines representing an allowable amount of bias (±0.10). Note that we only compared estimates under high effort (100 traps).

had lower $\hat{r}$ (Table 4.3). Trends in encounter rates appeared similar between perfect and imperfect detection scenarios, except for the high-density group$_{100}$ scenario, which was proportionally greater under imperfect detection than perfect detection (Figure 4.6 c and d).

Table 4.3: Summary of parameter estimate bias for each population density scenario (High: 20 km^{-2}; Medium: 2 km^{-2}; Low: 0.1 km^{-2}; solitary only) under the random encounter model (REM). RB: relative bias; D: density; v: day-range (or speed); r: radius. Note that an additional population scenario (Med.*) was simulated to isolate the effect of speed on density estimates. †RB($\hat{D}$) under perfect detection.

	High (v=0.16m/s; D=20 km^{-2})	Med. (v=0.33m/s; D=2 km^{-2})	Med.* (v=0.60m/s; D=2 km^{-2})	Low (v=0.60m/s; D=0.1 km^{-2})
RB($\hat{D}$)	+20.3%	+19.6%	+7.7%	+12.6%
RB($\hat{v}$)	-3.7%	-4.5%	-7.7%	-8.9%
Baseline bias†	+1.7%	+5.1%	+1.0%	+0.7%
Unexplained bias	+14.9%	+10.0%	+1%	+3%
$\hat{r}$	4.4 m	3.9 m	3.7m	3.7m

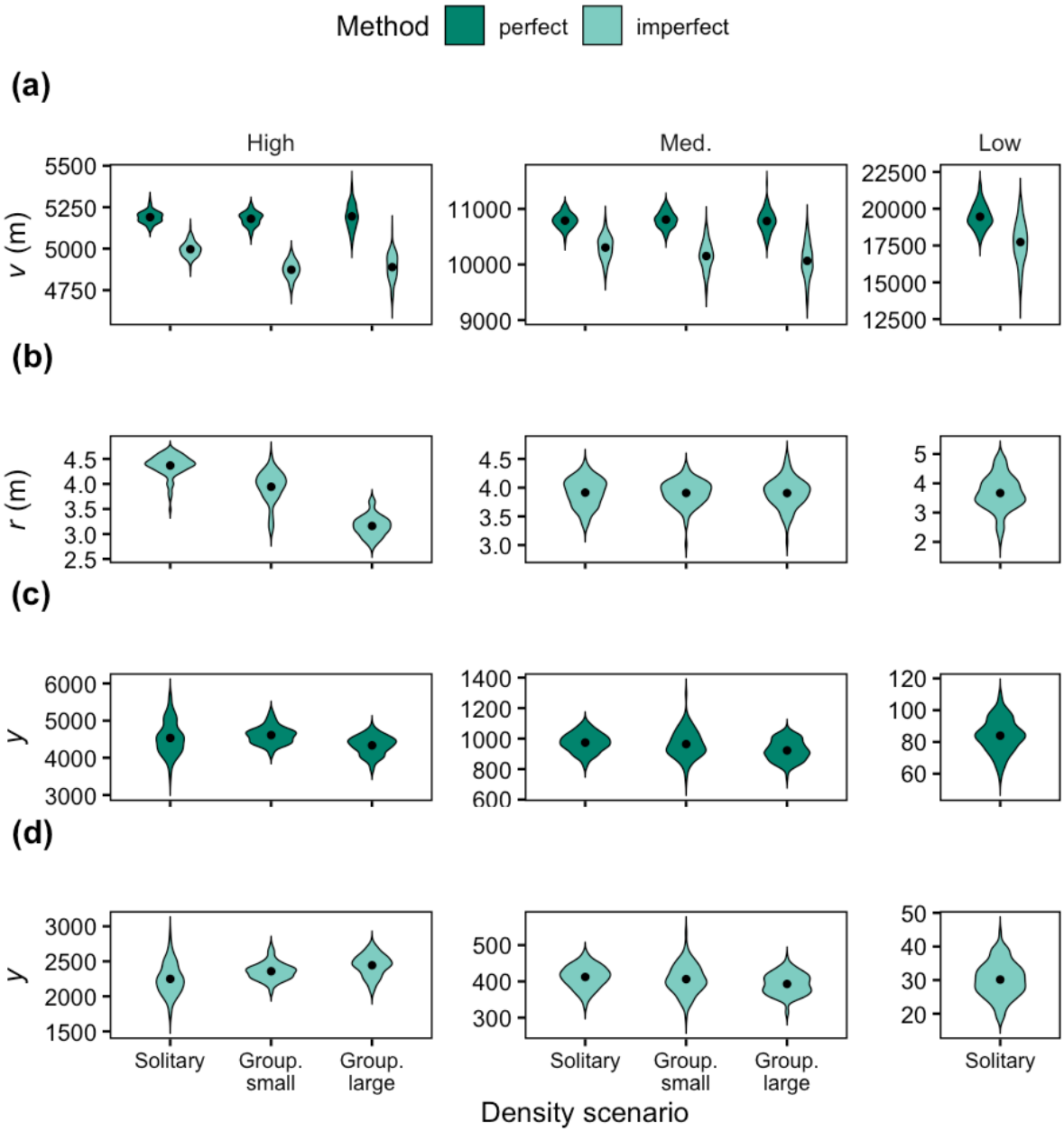

Figure 4.6: Comparison of random encounter model (REM) parameter estimates (v: day-range, r: radius, y: encounter rate) under perfect and imperfect detection. Violin plots represent the distribution of parameter estimates from 100 replicate datasets (points representing the overall mean) of multiple population density (High: 20 km^{-2}; Medium: 2 km^{-2}; Low: 0.1 km^{-2}) and group aggregation (Solitary; Group.small: 20 and 5 animals/group for high and medium density respectively; Group.large: 100 and 25 animals/group for high and medium density respectively) scenarios. Note that only we only compared estimates under high effort (100 traps).

4.4 Discussion

4.4.1 CTDS and REST reliable for both solitary and group animals

Generally, CTDS and REST reliably estimated density in both solitary and group animal populations. Density estimates from both methods were robust to varying levels of group aggregation (5–100/group). This represents the first study of CTDS performance under simulations of group association and the second for REST, which found a similar result (Hayashi and Iijima 2022). For low-density populations ($D = 0.1$ km^{-2}), it appears that only CTDS can provide unbiased point estimates and near-benchmark precision of 0.2 (CV($\hat{D}$) $\approx$ 0.3). However, our results suggest this takes ambitious effort of at least 100 cameras, similar to findings from an empirical study (Cappelle et al. 2021). Nonetheless, our results reinforce the wide applicability of CTDS to provide robust density estimates for multiple species (Howe et al. 2017, Cappelle et al. 2019, Palencia et al. 2021a). It is important to note that a drawback of CTDS is that image/video-processing is time-consuming, which may become prohibitive in cases where there are a large number of encounters (e.g., resulting from high-density populations or high camera trap effort). Consequently, the method will be more practical in situations where population density is not too high (Palencia et al. 2021a). Otherwise, REST could be used instead because of a comparatively low number of encounters that need to be processed (i.e., most detections outside the small focal area are discarded).

4.4.2 Biased density estimation in REM

4.4.2.1 Negative bias in day-range estimates

In REM, density is a derived parameter from encounter rate, speed (i.e., day-range), radius and angle (see Equation 4.2.1). Thus, positive bias in $\hat{D}$ was associated with biases in model parameter estimates and this was confirmed in our post-hoc analysis.

The first source of bias, the underestimation of day-range, was attributed to faster movement sequences having a lower probability of being detected (i.e., at least one trigger) compared to slower sequences at distances where detection was imperfect. This difference in probability can be explained by the way we point sampled for detections along a movement sequence — faster sequences had a smaller number of sampling intervals that were distanced further apart (due to the effect of time) compared to slower sequences. Hence, the comparative undersampling of fast sequences translated to underestimates in day-range, which were estimated from detected sequences. Undersampling of fast movements tends to be associated with device trigger speeds approaching or greater than 1 s (Rowcliffe et al. 2016). However, the interaction effect between animal speed and declining detection probability with distance may also lead to undersamples of fast movement (Palencia et al. 2021b). Thus, future work could test the prevalence of such a phenomenon in the field and evaluate if current methods to estimate day-range (i.e., speed) are adequate.

4.4.2.2 Poor detection model fits to radius data

We suspect that the remaining bias in $\hat{D}$ was associated with radius estimation. Detection model fits to the radius data (i.e., position on first capture) tended to be poor because the data distribution did not match that expected from our simulated hazard-rate detection function and could not be appropriately fitted with a hazard-rate function (Figure 4.7). In *solitary* animal scenarios, fits tended to be worse the slower the population was, corresponding to the greater unexplained bias in density (*high* (slower): +15%, *medium*: +10 %, *low*(faster): +3%; Table 4.3). This appeared to be a consequence of how we simulated detections, where first captures of slow movement sequences tended to crowd near the edge of the FOV where detection probability was high, meaning the detection zone approached to being the circumference rather than the area of the FOV (Figure C.3). In such cases, fitting the radial detection function is inappropriate and tended to underestimate radius, leading to an overestimate in density. Detection model fits worsened even further

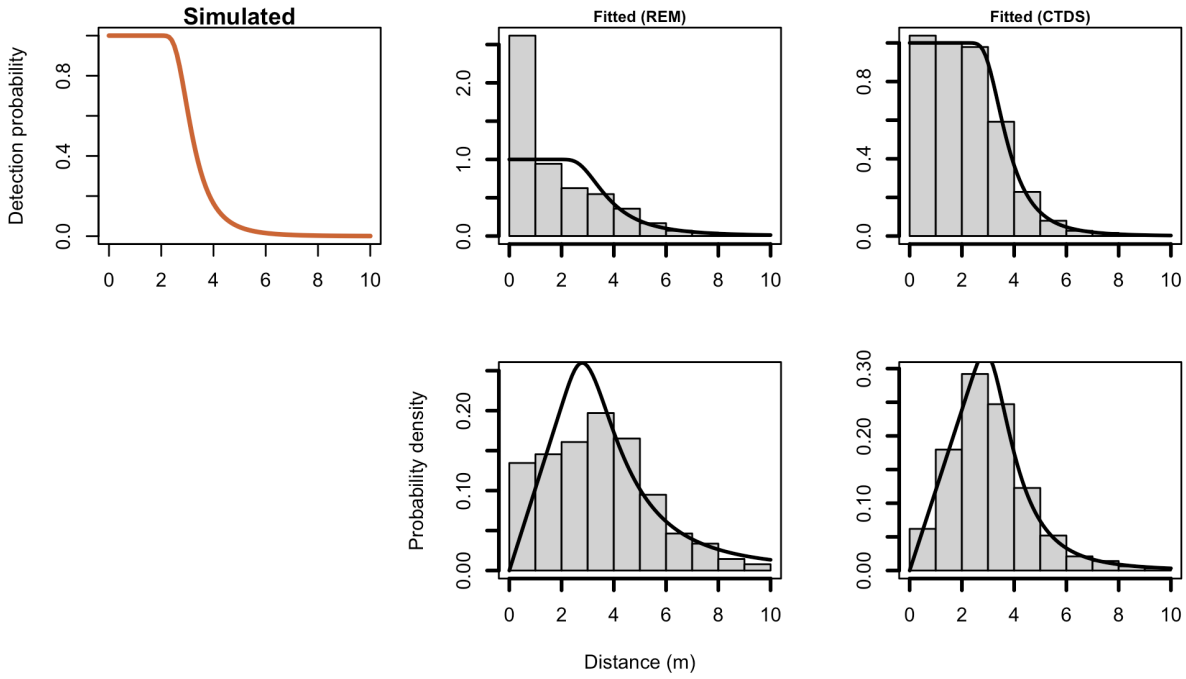

Figure 4.7: Fitted detection probability and probability density curves (black lines) to REM and CTDS data (histograms with 1m distance bins) from one medium-density, solitary population. Here, we used a hazard-rate model with no adjustments. The left-most panel shows the simulated hazard-rate detection function.

in the high-density *group* scenarios, as group animal detections (i.e., animals simultaneously captured with the animal that triggered the camera) inflated encounters at further distances (i.e., where detection probability < 1; Figure C.1). As such, we expected higher radius estimates $\hat{r}$ in group animal populations, but the poor fits instead caused $\hat{r}$ to decrease at higher levels of group aggregation (Figure 4.6 b), causing greater positive bias in $\hat{D}$. We did not encounter the same poor detection model fits with estimating the equivalent effective detection radius (EDR) under CTDS. Unlike in REM, we could achieve much better detection model fits to the CTDS distance data (for all scenarios) because the data generating process for CTDS was similar to how we simulated detections (i.e., every snapshot/record made at every 2 s interval; Figure 4.7 and C.1).

The bias in REM density estimates resulted from poor fit of an inappropriate detection model because the data generating process for the fitted data did not match it. We investigated if following standard distance sampling model-fitting and selection procedure (fitting multiple candidate detection models, Buckland et al.

2001) improved model fits and radius estimates. Despite the general improvement in fits from the selected model (i.e., lower AIC values compared to default hazard-rate model), radius estimates were instead smaller, which worsened positive bias in density estimates across all scenarios (Figure C.5 and C.6). These results may indicate that improved detection model fit to the data does not necessarily translate to accurate radius estimates because a better fit does not mean accurate representation of the underlying detection process. While our results were at least partially consequential of how we simulated our data, it emphasises the danger of naive model fitting and selection without careful consideration of the underlying data generating process. In contrast to our findings, Rowcliffe et al. (2011) found minimal bias using the distance-based approach, arguing that though it does not match the underlying detection process modelled in REM, it approximates it. We are unsure of the extent to which either the results of Rowcliffe et al. (2011) or our presented results are limited to our respective data generating processes and how representative they are of empirical systems. Though, some empirical examples indicate variability in distributions of animal position data (Figure C.4). Thus, we encourage further investigation into the efficacy of implementing current point distance-based approaches on detection zone estimation (for REM and CTDS, also to estimate focal area for REST in the field, Palencia et al. 2021a), as current approaches may require more flexibility to accommodate variability.

4.4.3 Substantial trap effort required for adequate precision

Our results suggest that low trap effort (≤ 25 cameras) generates insufficient data to reliably estimate density due to the lack of precision under most situations. While bias under low trap effort was not worse than that under high trap effort (except for medium-density, group_{25}), precision was generally generally higher than the benchmark of CV ≤ 0.2 (i.e., the gold-standard target for population monitoring, Pollock and Hines 1990) unless population density was high ($D = 20$ km^{-2} in our case; under REM and CTDS). High trap effort appears necessary to

meet the benchmark precision in moderate to low density populations (D = 0.1–2 km^{-2}), but in very low-density populations ($D < 0.1$ km^{-2}) even an ambitious trap effort of 100 CTs was not enough to provide achieve benchmark precision even under the best-performing method (CTDS). Another source of poorer precision was the high trap-level heterogeneity (i.e., variance greater than mean) in the medium-density populations' encounter data, which increased with greater levels of group aggregation in the medium-density scenarios (Table C.4). Interestingly, trap encounter rate variance in the largest group scenario (100 animals per group; high-density population) was relatively low because the random-walk movement we simulated (i.e., mimicking nomadic behaviour of large groups) was within a closed landscape, causing encounters to be more homogeneous over time. However, it could be argued that such a scenario is empirically unlikely. Wild populations are often spatially aggregated (e.g., due to group association, habitat use), and the greater the degree of aggregation, the higher the variance in encounter rate and the greater the trap effort required to achieve precise estimates (Palencia et al. 2022). Palencia et al. (2022) found that a minimum of 60 sampling locations was required for highly aggregated populations to achieve a precision of CV ≤ 0.2 in REM. Here, we show that even more trap locations may be required depending on the estimation method used (e.g., REST requires more because of relatively small encounter rates) and the density of the study population (D < 2 km^{-2}; Figure 4.3), at levels which are unrealistic for resource-limited monitoring programs. Thus, we do not recommend density estimation unless one or more of the following is guaranteed: (i) investment of substantial trap effort ($\gg$ 25 sampling locations), (ii) population density is expected to be high (e.g., D > 10 km^{-2} across a 10 km^2 area with an effort of 100 CTs), *or* (iii) spatial aggregation in populations is low (e.g., survey during seasons when individuals are more homogeneously distributed). However, we acknowledge that CVs in the range 20-40% can be acceptable in real-world applications, in which case these recommendations can be relaxed. In any case, pre-survey power analyses should be conducted to determine trap effort needed for a target CV. Further, we suggest future research into optimal survey design to improve precision of density

estimates (e.g., rotating camera traps across multiple locations), and the effect of trap effort (in terms of both density and duration) on density estimation (bias, precision, coverage) in highly aggregated populations. Lastly, it is also important to note that high precision may mean poor coverage (95%-CI) of true density, if the point estimate is biased (e.g., high-density, $J = 100$ scenarios; Figure 4.3).

4.4.4 Assumptions and caveats

CTDS and REST returned unbiased estimates under our simulated conditions that assumed perfect knowledge of the FOV angle and focal area (respectively), which are potential sources of bias if inaccurately parameterized. Furthermore, we assumed that detection probability was uniform with respect to angle from the centre of the FOV. Departures from the uniformity assumption can arise from an insufficiently fast CT trigger speed and a decay in sensor sensitivity approaching the periphery of the FOV (Rowcliffe et al. 2011, Rovero and Zimmermann 2016). If not accounted for (e.g., using the distance-based approach to estimate effective angular distance, Rowcliffe et al. 2011), density will be underestimated. Additionally, it is critical to note that almost all unmarked methods assume that detection probability is certain in a specific area within the camera's detection zone (i.e., REST: focal area; REM and CTDS: assumption of distance sampling analysis), and assumption violation causes underestimation of density (Rowcliffe et al. 2011, Nakashima et al. 2022). Thus, it is paramount that cameras have reliably rapid responses (<0.3 s), and where this is not possible a double-observer approach or left truncation should be considered (Howe et al. 2017, Nakashima et al. 2022).

Unbiased density estimates from unmarked methods is conditional on unbiased estimation of model-specific parameters (e.g., day-range, staying time, detection zone). Accurate parameter estimation requires full understanding of the analytical methods (Nakashima 2022), careful consideration of any underlying processes that potentially bias parameter estimates (e.g., camera trigger speed, detection model), and estimating parameters from only animal position data measured from the

camera trap data itself (speed, staying time, distance from camera). These requirements necessitate substantial investment of resources, which may be a barrier to some practitioners. Unsurprisingly, incorrectly parameterising unmarked methods using information outside of the camera trap survey – such as reference values from telemetry data and camera trap technical specifications (e.g., Doran-Myers et al. 2021, Loonam et al. 2021) – to reduce effort and cost of collecting additional data, is not uncommon. However, this leads to biased density estimates (Corlatti et al. 2020, Palencia et al. 2022). Hence, use of unmarked density estimators should be avoided, unless the user is committed to meeting the aforementioned requirements of appropriate use. Future work may also consider how technological advances can reduce the labour of data collection and processing, such as automating measurements of animal positions from camera trap data (e.g., using "bounding box" classification, Norouzzadeh et al. 2018).

Our approach for simulating population scenarios was broadly based on reported values for real species and simple movement patterns (e.g., attraction towards a home-range centre). Qualitatively, we expect the trends observed in our results to be similar regardless of the specific parameters of the simulated population and detection process. However, the quantitative performance of density estimates is subject to variation outside of the specific set of conditions we have tested (e.g., survey duration, shape of simulated detection function, more complex animal movement). Furthermore, we did not consider a key assumption to many unmarked methods that is commonly violated in the field — random animal movement with respect to camera traps (we simulated animal movement independently from camera trap placement). Animals may react to camera traps or exhibit preferential habitat use, which can erode estimator performance. These issues can be mitigated by discarding records where animal reactions or resting behaviour are observed for the purpose of speed and staying time estimation (Cusack et al. 2015, Bessone et al. 2020). Practitioners should also avoid baiting cameras as it can cause severe positive bias in density estimates (Amburgey et al. 2021). Stratified sampling can be employed to avoid biased placement of cameras in heterogeneous landscapes

(Rowcliffe et al. 2008), though it can be challenging to fully achieve due to the small sampling area of each camera; since encounter rate is more strongly influenced by microsite conditions than by large-scale habitat characteristics that are usually used for stratification. Accounting for microsite conditions via the incorporation of covariates and allowing for inhomogenous density models could be considered in future model development (e.g., Wearn et al. 2022).

4.5 Conclusion

We provided one of the first assessments of unmarked density estimators under common conditions, in a simulation study. Our results imply that CTDS and REST can reliably estimate for both solitary and group-living animals, if population densities are not low ($D > 0.1$ km^{-2}), trap effort is substantial ($\gg 25$ cameras) and parameter estimates related to detection zone are accurate. REM is potentially reliable under the same circumstances, but model parameter estimates (i.e., day-range and detection radius) are prone to bias without careful consideration in the parameterisation process. While unmarked density estimation requires substantial investment of effort, it provides the gold-standard of population monitoring — density — rather than occupancy or relative abundance. Improving the cost-effectiveness of unmarked methods should be a priority for future research, such as (i) automating measurements (of animal position) from camera trap images/videos, (ii) optimising sampling design with a limited number of cameras, and (iii) establishing clear, easy-to-use analytical procedures. Given that most of these methods are still new and undergoing rapid development, we believe that their accessibility to practitioners will continue to improve.

5

General Discussion

In applying the new tools and approaches I have developed to simulate animal movement and camera-trap (CT)-like detection processes, I have shown that animal movement has a profound impact on inferences generated by both *marked* and *unmarked* abundance estimation methods. In this final chapter, I first discuss the importance of investigations at the interface of animal movement and population dynamics, and identify avenues for future research. I then review the core challenges to robust abundance estimation with a focus on CT applications, integrating the knowledge gained from my work with knowledge from existing literature. Based on my new insights into CT-based abundance estimation, I discuss potential solutions and future directions taking from latest developments in technology and methodologies.

5.1 Integrating movement and population dynamics

Ecologists have traditionally focused on demonstrating density-dependent relationships in population dynamics without necessarily specifying the mechanisms driving these relationships (Krebs 2020). Animal movement is a significant driver of these relationships that, if ignored, is associated with deficient ecological inference about

a study system (e.g., Roever et al. 2014, Abrahms et al. 2017, Keiter et al. 2017). For example, the effect of resources on spatial variation in density is often modulated by underlying processes, such as territorial behaviour – in that the estimated resource effect is weak at higher population densities due to territorial exclusion (i.e., leading to transient animals inhabiting low resource areas), but stronger at lower densities when competition for resources is lower (**Chapter 3**). Simply describing the correlative relationships between density and resources (e.g., inhomogenous density SCR models tested in **Chapter 3**) essentially assumes resource use to be a one-dimensional process and ignores numerous underlying mechanisms (e.g., memory-mediated resource use and territorial behaviour), which tends to result in weak inference about resource selection. Accounting for behaviour-specific movement in resource selection has been shown to strengthen inferences and failing to do so risks resulting in weak or incorrect inference — which has consequences for how key habitats are prioritised in conservation mangement (e.g., Roever et al. 2014, Abrahms et al. 2017). Misspecifying movement processes may also lead to inferences that are scale-dependent, and hence, not meaningful (see later section 'Limitations in ecological inference' for further discussion). Finally, ignoring movement processes underlying observed patterns often means that density-dependent relationships are not repeatable and form a weak basis for predictive science (Krebs 2020).

Studies at the interface of movement and population dynamics can help identify these deficiencies. While I did not explicitly integrate movement and population models – an endeavor that is quantitatively challenging (see McClintock et al. 2022), especially with more complex movement models (e.g., **Chapter 2**) – I have shown that exploration of this interface can expose current limitations in population-level inference and pinpoint areas for future development. The approach used to evaluate population model inference in **Chapter 3** can be adopted to simulate further real-world complexities, such as trap-shyness and human disturbance (i.e., to model threat avoidance using the predator component of the

movement model, see Bracis et al. 2018b), and to explore the effect of ignoring these mechanisms on population inferences.

Ongoing efforts to integrate movement and SCR models (i.e., population dynamics such as abundance, survival, recruitment) explicitly into a single framework connecting individual-level data to population-level processes can help address current limitations in ecological inference. For example, McClintock et al. (2022) outlines an approach describing different point process models of space use for resident and transient individuals (i.e., third-order resource selection within a home-range), while scaling to a population-level utilisation distribution in a point process model describing spatial variation on density of centers of attraction (i.e., second-order resource selection of individual home-ranges). Beyond this specific example, integrated models can be used to examine the links between diverse movement behaviours (e.g., territoriality, transience, dispersal, group-living) and population dynamics (survival and recruitment rates), specify mechanisms underlying spatial variation in abundance and resource selection (e.g., Gardner et al. 2022), and connecting individual activity budgets to survival and reproduction. It also opens the door for continuous-time movement and SCR models (e.g., Borchers et al. 2014, Distiller et al. 2020), which would provide inferences that are scale-invariant and resolve issues related to integration of movement and SCR data possessing different spatiotemporal resolution (McClintock et al. 2022).

Exploring the movement and population interface also provides a glimpse into potential avenues for integrated formulations. Modelling the processes underlying spatial patterns not only improves ecological insight into the drivers of population dynamics, but it also offers the ability to predict responses to changes in the system, particularly at larger spatial and temporal scales where highly mobile animals and metapopulation structure are involved (e.g., Bischof et al. 2020b). For example, connecting the emergence of resident and transience behaviours with territorial space use and resource quality (e.g., movement simulations in **Chapter 3**) may be useful in forecasting dispersal patterns within open population SCR models. In the management of disease outbreak or population control (e.g., culling), specifying

resource competition (nonterritorial or territorial) underlying density-dependence could offer the ability to predict spatial organisation in responses to deaths in the population (e.g., Figure 2.3, Potts et al. 2013). Incorporating memory processes in studies of migratory populations may provide more accurate predictions on changes in spatial distribution (and abundance) as memory provides a clear signal directing migrants to their destination as opposed to simpler navigational processes (e.g., perception, Bracis and Mueller 2017).

While the potential benefits of integrated movement and population dynamics models are clear, it is likely that they will entail additional data (e.g., telemetry data) and model complexity (see McClintock et al. 2022 sec. 4.1.1 for a detailed discussion). The conceptual, technical and practical obstacles will have to be overcome for the full potential of integrated models to be realised. Moreover, it is important to note that such integrated formulations are likely not applicable to unmarked population data that it is not informative for estimation of demographic parameters beyond abundance or density (i.e., birth, mortality rates, immigration, and emigration rates) because individual-specific processes (e.g., survival, recruitment, dispersal, transience) cannot be determined (McClintock and Thomas 2020). If the goal is to understand the mechanisms (e.g., movement and vital rates) driving population dynamics, then marking individuals and/or tracking individual movements should be considered (e.g., Supp et al. 2021).

Individual animal movement underlies virtually all ecological processes occurring at the larger scale of populations. Thus, the consequences of ignoring the complexities of movement (e.g., behaviour) in studies of populations are hard to overlook, especially in a time of rapid environmental change and biodiversity loss (Schlägel et al. 2020). While explicit integration of complex movement processes into population models can be quantitatively challenging, it is important for ecologists to consider how movement behaviours influence the quality of population model inference (and its implications for prediction) at the very least.

5.2 The future of abundance estimation with camera-trap data

Despite the rapid increase in camera-trap (CT) applications over the last two decades, a small minority have been conducted with the goal of abundance estimation (representing just 5.5% of all applications as of 2018, Gilbert et al. 2021). Fortunately, recent advances in the statistical methods available to estimate population abundances from remotely recorded animal observations using new technologies have created vast opportunities for monitoring wildlife populations (Burton et al. 2015, Lahoz-Monfort and Magrath 2021). In the following section, I review four key prevailing obstacles limiting the uptake and proper implementation of CT-based abundance estimation methods. I discuss the potential solutions and future directions for each challenge, facilitated by emerging technologies and methodologies.

5.2.1 Challenges and potential solutions

5.2.1.1 Data demands

Meeting the data demands required for robust (i.e., accurate and precise) abundance estimation of animal populations is a resource-intensive exercise. Firstly, obtaining sufficient encounter data for abundance estimation usually requires a substantial amount of trap effort. Spatial capture-recapture (SCR) abundance estimates have proved to be robust to realistic animal movement simulations that violated multiple model assumptions (**Chapter 3**), but these findings were made under an effort of 100 traps (or detectors). Similarly, while SCR is generally a robust method to estimate abundance in marked animals unless violations to model assumptions are high, it is typically assumed under conditions with 64–144 traps (e.g., Royle et al. 2013b, Sun et al. 2014, Sutherland et al. 2015, Bischof et al. 2020a). Even under optimisation of design criteria, an effort of $\approx$ 100 traps is required in populations that exhibit strong spatial aggregation patterns (otherwise $\approx$ 49 appears to be the minimum) (Dupont et al. 2021). Furthermore, data demands grow as SCR methods incorporate increasingly complex movement

models (see McClintock et al. 2022 sec. 4.1.1 for a detailed discussion). Royle et al. (2014a) noted that most SCR data is sparse, producing only a few observations per individual (1–5), which is not sufficient to support complex movement processes without additional information such as telemetry data (e.g., Gardner et al. 2018). These trap effort requirements are certainly not limited to SCR methods (i.e., marked populations). Unmarked abundance estimators also require significant trap effort ($\gg$ 25 traps; demonstrated in **Chapter 4**) for accurate and precise estimates in most simulated scenarios, unless population density is expected to be high. It is also important to note that the realised spatial aggregation density patterns in the simulations (**Chapter 4**) were generally low. Under higher levels of spatial aggregation, at least 60 traps may be required for sufficient precision in abundance estimates (Palencia et al. 2022). Low precision has been reported as a weakness of REM when spatial aggregation is high, as it was shown to be lower than that of reference methods (SCR, distance sampling and drive counts) (Palencia et al. 2022). Further investigation to determine if this holds true for other unmarked abundance estimation methods is warranted.

Secondly, the ancillary data required for abundance estimation can be difficult to collect and process. Each encounter data point must be associated with individual identification information for *marked* methods, and accurate animal-to-camera position data (i.e., distance, and sometimes, angle) for *unmarked* methods. While easily acquired in simulations (**Chapter 3** and **4**), this additional information is manually derived from CT images (or videos), which tends to be a time-consuming process (Palencia et al. 2021a). For *marked* population data, individual identification from recorded images typically involves establishing a database of unique identities based on first captures and matching recaptured individuals with the database. Furthermore, complete identification usually requires simultaneous image capture of both flanks of an animal (markings are usually bilaterally asymmetric, McClintock et al. 2013) at least once, necessitating paired CT placement. This presents a challenge for projects with a limited number of CTs, though SCR

with partial identity models (SPIM) can be used to reduce the trap effort required (Augustine et al. 2018).

For *unmarked* population data, collecting animal-to-camera position information involves pre-survey calibration of distance markers at CT sites and post-survey measurement of distances (and other associated data, such as speed) from recorded images. Such information is usually not available for most existing CT data unless collected with the intent for application of these methods. Practitioners may resort to using reference values outside of the CT survey, such as telemetry data and camera technical specifications, but this is inappropriate and biases abundance estimates (Corlatti et al. 2020, Palencia et al. 2022). It is also important to note that while there may be tempting alternatives that bypass the additional data requirements and only require encounter data (i.e., unmarked SCR-derived approaches), performance of such methods suffers beyond a narrow range of conditions (e.g., trap spacing is too large or small relative to density and home-range overlap, non-independence between individuals, Chandler and Royle 2013, Ramsey et al. 2015, Sun et al. 2022).

Reducing the effort required for data collection and processing is a definite priority. In terms of trap effort, practitioners can find optimal designs using trap effort simulations and/or methods to optimise design criteria (e.g., Dupont et al. 2021 for SCR) tailored to the specificities of their study system. While optimal sampling design can be found with existing simulation studies for SCR (e.g., Sollmann 2012, Sun et al. 2014), it is lacking for unmarked methods. The code base I have developed in this thesis produces trap effort simulations for unmarked methods (**Chapter 4**; code packaged into easily parameterisable R functions). Future investigation into other array designs (e.g., clustered) and optimising trap placement in heterogeneous landscapes (i.e., to minimise biased placement) for unmarked methods under simulation conditions is merited.

While optimising trap placement is important, cost savings in terms of reducing trap effort are likely to be minimal because abundance estimation will ultimately be poor with sparse datasets. The true potential for time and cost savings lies in

the data management and processing component. Automating the data pipeline of handling, storing, and processing the massive amounts of data (into usable data for subsequent analysis) provide enormous cost-savings. The recent incorporation of AI capabilities (e.g., Conservation AI, MegaDetector, MLWIC2: Machine Learning for Wildlife Image Classification and WildlifeInsights) to classify images according to animal categories (down to the species level) has increased processing efficiencies considerably (e.g., by 500%, Fennell et al. 2022).

Unfortunately, these existing capabilities can only automate the process up to narrowing down the data to the species of interest. While it is currently not possible to identify individuals automatically (based on natural markings) and measure animal distances from images for abundance estimation, these solutions appear to be on the horizon with the rapid development of automation tools for CT data (Norouzzadeh et al. 2018). For example, there is ongoing development in automation technology for reidentification of individual animals (including unmarked animals) from CT images (and videos) using deep learning methods (see Schneider et al. 2019). Another very recent example already presents a fully automatic approach to estimate camera-to-animal distances (Johanns et al. 2022), which appears to work in a zoo setting but should be tested in field settings in the near-future. While these technologies are still in development, it should be noted that researchers can already use existing established tools to reduce manual labour (up to automatic classification of images to species, see review by Vélez et al. 2023).

5.2.1.2 Lack of a consistent analytical framework

Finding the appropriate approaches to use to parameterise the *unmarked* abundance estimation models (especially REM) remains a challenge because it requires piecing together multiple sources of information (and code), and there are multiple ways to estimate a single model parameter – e.g., REM's radius parameter estimated with the standard distance approach (Palencia et al. 2021a), with an augmented approach, (Rowcliffe et al. 2011), *or* with an approach for overdispersed data (Howe et al. 2018). Establishing the appropriate analytical procedures to use

may require repeated consultations with experts (in my experience), which suggests a current lack of clarity around model application. Thus, it is not surprising that many studies parameterise these models inappropriately with external data sources that lead to biased abundance estimates (e.g., Rovero and Marshall 2009, Zero et al. 2013, Cusack et al. 2015, Caravaggi et al. 2016, Doran-Myers et al. 2021, Loonam et al. 2021, Pettigrew et al. 2021). Resolving this issue is critical for unmarked methods because abundance estimates are very sensitive to model misspecifications (as seen in **Chapter 4**).

The lack of a consistent and consolidated approach to parameterisation of CT-based *unmarked* abundance estimators is understandable because the methods are relatively new, early in the development phase and model applications are few (though increasing, see Gilbert et al. 2021). To tackle this issue, it is first paramount that future work prioritise research transparency and reproducibility, such as making the code (for simulation and analysis) and data publicly available to facilitate model application and development (e.g., links to all code used in this thesis are provided in the Authorship Statements at the start of each data chapter). In cases where data cannot be made publicly available (e.g., threatened species), plots of the fitted distributions to the data (in parameter estimation) should be included in the publications (at least in the Appendices) because the quality of model fit has implications on the accuracy of unmarked abundance estimates (see following paragraphs). Additionally, efforts to consolidate existing literature to inform best practices though reviews (e.g., Palencia et al. 2022 for REM) and vignettes (e.g., CTDS: https://examples.distancesampling.org/Distance-cameratraps/camera-distill.html), and updating them as the methods evolve, would be immensely valuable to model users. Model developers may also consider setting up online forums for direct queries about model implementation (e.g., Google groups, Github discussion).

I suspect a large part of the reason why consistent approaches are lacking for these methods is that appropriate specification for accurate estimation of model parameters is difficult, requiring improvements in the methods themselves. Accurate estimation of parameters such as CT zone (distance and angle) and movement speed

can be challenging due to the variability that can arise with imperfect detection (as demonstrated in **Chapter 4**).

For detection zone estimation, appropriate specification of detection probability within the area of the detection zone can be difficult due to the wide variability that arises from the interaction of multiple factors, including – an animal's movement speed and body mass, and the CT device's trigger speed and sensitivity performance (i.e., to fast movements and smaller animals, Palencia et al. 2021b). Following procedures to optimise detection model fits to the data (e.g., binning data at irregular distance intervals, left or right truncation of data, see Howe et al. 2018) can be useful to improve abundance estimator accuracy. However, it is plausible that a good fit still cannot be obtained on atypically distributed animal position data even after optimisation procedures, but the prevalence of such problems is not known because the use of CT-based unmarked abundance estimators is still relatively new. Some empirical examples demonstrating the variability of observed distributions seen in animal position data (Figure C.4), suggest that point distance-based approaches to estimate detection zone (for REM and CTDS, also to estimate focal area for REST in the field, Palencia et al. 2021a) may need to be more flexible to accommodate such variability. This should be a priority in unmarked abundance estimation method development. Additionally, relaxing the restrictive assumption (of distance-based approaches) of certain detection within a specific area within the detection zone should be considered.

In terms of speed (or day-range) estimation (for REM), the recommended procedure down-weights faster speeds because they are more likely observed than slower speeds (Rowcliffe et al. 2016), but it does not account for the possibility that fast speeds have a lower probability of detection. The speed parameter can be underestimated (to a greater degree in fast populations; up to +10%) because the probability of cameras missing fast compared to slow sequences were higher under my simulated conditions (as shown in **Chapter 4**). Further investigation into the sensitivity of CTs to animal speeds is warranted to ensure appropriate specification for accurate estimation of this parameter, and consequently, unbiased

estimates of density. If it is indeed a problem, models will need to develop a way to account for missed fast movement sequences, potentially incorporating estimates of the camera's performance (i.e., trigger speed) into the model. Future applications are advised to follow recommendations to maximise device performance in the field, such as setting traps at shoulder height of the target species to maximise detection probability (see Palencia et al. 2021b). Additionally, improvements to device technology in terms of trigger speed and sensitivity should be a priority.

5.2.1.3 Technical barriers to entry

Applying these abundance estimation methods in practice may demand a level of statistical skill and computational power that poses obstacles for their practical use. Firstly, model users must fully understand the statistical concepts within the models (e.g., detection function fitting) to apply them to data appropriately. This is particularly critical in *unmarked* abundance methods because reliable abundance estimation is conditional on accurate estimates of associated parameters (Howe et al. 2017, Nakashima 2022, Palencia et al. 2022). While *marked* population abundance estimates from SCR appear generally robust to model misspecifications (as mentioned earlier), ecological and movement related inference at the finer scale (i.e., resource effects on space use, home-range size) requires the associated model process(es) to be specified appropriately (as demonstrated in **Chapter 3**). Appropriate model specification may involve customisation of model formulations, such as selecting the appropriate distribution or function to fit the data. Further, the increasing adoption of Bayesian modelling (MCMC: Markov chain Monte Carlo) approaches offers users new degrees of model customisation according to their data (e.g., prior distributions for parameters, incorporation of covariates and random effects) and a flexible framework to explore increasingly complex processes underlying population density patterns (e.g., McClintock et al. 2022). However, the flexibility afforded by MCMC approaches may present as a lack of structure to some practitoners.

Establishing a consistent analytical framework and associated reference resources, as discussed in the preceding section, would facilitate understanding and proper implementation of these methods. This type of framework is particularly needed for *unmarked* methods, which are early in development compared to the established class of SCR methods for marked animals (for which many resources are available; e.g., https://www.otago.ac.nz/density/SECRinR.html). Additionally, training workshops (both online and offline) can be conducted to equip practitioners with the necessary statistical skills and knowledge. Though specific workshops for the *unmarked* methods are not available (to my knowledge) — with the exception of CTDS — attending the regularly-run distance sampling workshops (https://workshops.distancesampling.org/) will be relevant for unmarked methods that use distance-based methods to estimate CT detection zone.

Secondly, model implementation may require substantial computational power (i.e., high performance computing) that present barriers to standard use. Due to their spatial component, SCR analysis tends to be considerably more computationally intensive compared to nonspatial CR and the nonspatial *unmarked* methods (e.g., methods used in **Chapter 4**). SCR models can become very computationally costly and intractable when large spatial scales, many individuals and/or activity centre movement are involved, particularly when using Bayesian MCMC estimation. Since MCMC sampling scales with the dimensions of extensive detection history data (i.e., detections/nondetections of every individual at every detector at every occasion), analyses for large study areas with many detectors (e.g., a regional network of cameras) can become very costly (Milleret et al. 2018). The need for data augmentation to account for completely unobserved individuals (i.e., requiring specification of $M \gg N$, Royle et al. 2007) and their state (presence in population) may be computationally prohibitive in large populations. Furthermore, modelling activity centre movement (e.g., transience model in **Chapter 3**) involves the updating of activity centre locations for every occasion, increasing the MCMC sampling dimensions even further.

Fortunately, technical solutions to reduce the runtime of computationally intensive SCR analysis are available. These techniques are mostly implemented in `nimble` (Valpine et al. 2017), which include vectorisation of model calculations to reduce model size, restricting detector calculations to the locality of each individual, and disabling unnecessary model calculations for never-detected individuals when using data augmentation (see Turek et al. 2021). The need for data augmentation in Bayesian SCR can even be bypassed altogether using a "semi-complete" data likelihood approach (Zhang et al. 2023), though it only applies to closed-population SCR models.

5.2.1.4 Limitations in ecological inference

There is currently tremendous potential for ecological inference with SCR models (marked animals) with the increasing relation of demographic rates (e.g., abundance, survival, recruitment) to animal movement, habitat use, landscape connectivity and behaviour (Royle et al. 2013a, McClintock et al. 2022). However, there are certain limitations in ecological inference with SCR methods, which are related to scale (see **Chapter 3**). The interpretation of resource effects on space use (or movement) appears to depend on the temporal scale of detection data (i.e., occasion length). While integration of telemetry data into the SCR-RSF model has been shown to improve inferences on spatial variability in space-use (third-order), it is also likely that interpretation varies with the scale of telemetry data used — scale dependence in ecological interpretation is a consequence of the arbitrary scale of telemetry locations (Bastille-Rousseau et al. 2018). As such, it may not be suitable to estimate meaningful responses to resources that vary across multiple scales. Similar issues may arise when inferring home-range size from the scale parameter alone. The influence of scale of data on ecological and movement inference within the SCR framework warrants further consideration and investigation, especially as SCR methods continue to advance in complexity. A mechanistic movement simulation approach (as used in **Chapter 3**) offers a rich framework to conduct such investigations. Continuous-time formulations of movement and SCR models

that are scale-invariant to time scale (Borchers et al. 2014, Distiller et al. 2020) present an intuitive solution to scale-dependence in ecological inference. However, the benefits of continuous time-models should be weighed against the associated difficulties in implementation as they require custom model-fitting algorithms that are computationally demanding (see McClintock et al. 2022).

Relative to SCR methods, *unmarked* abundance estimation methods, in their original formulations, generally possess limited ability for ecological inference beyond single measures of estimable model parameters (e.g., density, day-range, activity proportion). Ecological inference through incorporation of covariates was only explored recently for unmarked abundance estimators. Using a hierarchical Bayesian approach, Wearn et al. (2022) included covariates explaining heterogeneity (i.e., variation) in movement, detection zone sensitivity, and activity proportion within a multi-species REM. REST was also extended to allow spatial variation in density as a function of spatial covariates (e.g., habitat, elevation, Nakashima et al. 2020). While CTDS does not permit inference about spatial variation in density, it is possible with the standard distance sampling methods (Royle et al. 2004) that can be extended to CT based methods in the future.

5.2.2 Looking ahead: integrated solutions

Perhaps the most exciting future for abundance estimation of animal populations lies in the potential for integrated solutions that can address all four major challenges presented here (i.e., data and technical obstacles, limitations in ecological inference, and inconsistency in analytical approaches) in a single framework. Cloud-based AI platforms for CT data (e.g., Conservation AI, WildlifeInsights) are a promising area of development, with aims to provide (semi-)automated data workflows from input to analysis within a user-friendly environment. These platforms already offer a workflow for data storage, management, image processing (i.e., automatic metadata extraction, animal classification down to species) and data exploration (e.g., descriptive statistics, visualisation), with further plans for an analytics module to allow for occupancy modelling and point abundance estimation

(e.g., WildlifeInsights, Ahumada et al. 2020). It is not a leap to imagine that the next step would be to extend the existing architecture to allow for abundance estimation, which I envision would include the following (Figure 5.1):

i. the incorporation of future improvements to AI image processing technology to automatically extract information (i.e., individual identify, camera-to-animal distance);

ii. access to a curated set of abundance modelling tools (with model assumptions clearly stated), and implementation within a low-/no-code environment;

iii. allow for incorporation of auxiliary data such as covariate information (as list of values or spatial layer) and telemetry data (for some SCR extensions)

iv. AI-mediated 'fail-safe' features to detect and warn users if model fit to data is poor; and

v. provision of cloud computer power to run high-performance tasks.

These capabilities would dramatically lower existing technical barriers by reducing data processing time and allowing users with limited statistical and coding knowledge (and limited computer power) to run analyses within a standardised analytical framework set from best practices. These functionalities should be developed with collaboration between IT engineers, computer scientists (for machine learning tasks), statistical experts, camera-trap engineers, and potential end-users (e.g., from government or non-government organisations). It is worth looking to ongoing development of cloud-based solutions for species distribution modelling (SDMs) to support decision making (e.g., EcoCommons, BiosecurityCommons), as they provide great examples of the development process behind the unification of tools, models and infrastructure centred around the needs of current and future users.

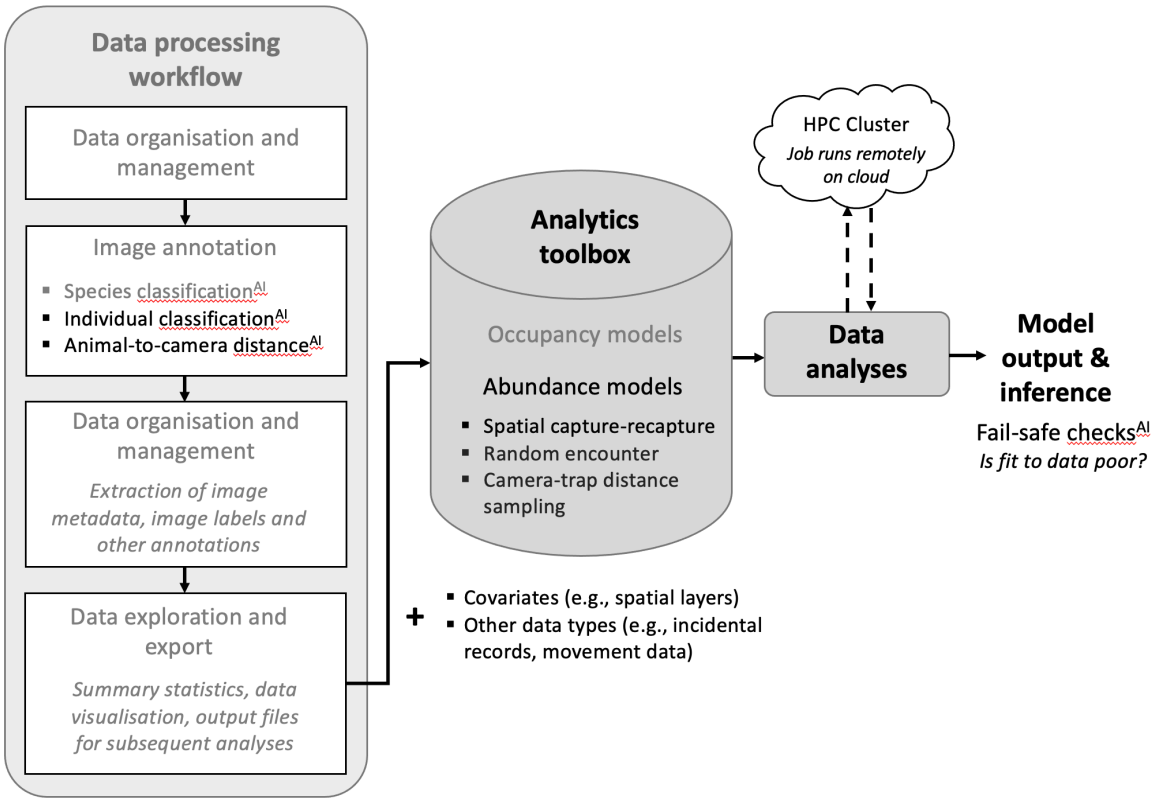

Figure 5.1: A conceptual diagram of the potential features for population abundance estimation (solid colours) that could be integrated with existing services (faded colours) provided by cloud-based platforms for camera-trap data (e.g., https://www.wildlifeinsights.org/). [AI]Artificial- intelligence-mediated features. HPC: High-performance computing.

5.2.3 Conclusion

I have highlighted some of the core challenges to CT-based abundance estimation for both *marked* and *unmarked* populations. Key recommendations to address these obstacles include: (i) using latest software to automate parts of the data processing workflow; (ii) promoting research documentation to ensure reproducibility; and (iii) investment in training material and workshops. Further model development is required for *unmarked* methods to improve reliability of abundance estimates, particularly in terms of estimating camera detection zone. The potential for huge labour-savings is on the horizon with rapid advancement in AI-driven image-processing technology and cloud-based integrated solutions. It is important that ongoing developments are made in collaboration with the statistical and

ecological community to optimise efficiency and utility to future users (Buckland et al. 2023) and to avoid misguided use (Lahoz-Monfort and Magrath 2021).

References

Abrahms, B., S. C. Sawyer, N. R. Jordan, J. W. McNutt, A. M. Wilson, and J. S. Brashares. 2017. Does wildlife resource selection accurately inform corridor conservation? Journal of Applied Ecology 54:412–422.

Ahumada, J. A., E. Fegraus, T. Birch, N. Flores, R. Kays, T. G. O'Brien, J. Palmer, S. Schuttler, J. Y. Zhao, W. Jetz, M. Kinnaird, S. Kulkarni, A. Lyet, D. Thau, M. Duong, R. Oliver, and A. Dancer. 2020. Wildlife insights: A platform to maximize the potential of camera trap and other passive sensor wildlife data for the planet. Environmental Conservation 47:1–6.

Allen, M. L., H. U. Wittmer, E. Setiawan, S. Jaffe, and A. J. Marshall. 2016. Scent marking in sunda clouded leopards (neofelis diardi): Novel observations close a key gap in understanding felid communication behaviours. Scientific Reports 6:35433.

Amburgey, S. M., A. A. Yackel Adams, B. Gardner, N. J. Hostetter, S. R. Siers, B. T. McClintock, and S. J. Converse. 2021. Evaluation of camera trap-based abundance estimators for unmarked populations. Ecol Appl 31:e02410.

Anile, S., B. Ragni, E. Randi, F. Mattucci, and F. Rovero. 2014. Wildcat population density on the etna volcano, italy: A comparison of density estimation methods. Journal of Zoology 293:252–261.

Antunes, A. C., A. Montanarin, D. M. Gräbin, E. C. dos Santos Monteiro, F. F. de Pinho, G. C. Alvarenga, J. Ahumada, R. B. Wallace, E. E. Ramalho, A. P. A. Barnett, A. Bager, A. M. C. Lopes, A. Keuroghlian, A. Giroux, A. M. Herrera, A. P. de Almeida Correa, A. Y. Meiga, A. T. de Almeida Jácomo, A. de Barros Barban, A. Antunes, A. G. de Almeida Coelho, A. R. Camilo, A. V. Nunes, A. C. dos Santos Maroclo Gomes, A. C. da Silva Zanzini, A. B. Castro, A. L. J. Desbiez, A. Figueiredo, B. de Thoisy, B. Gauzens, B. T. Oliveira, C. A. de Lima, C. A. Peres, C. C. Durigan, C. R. Brocardo, C. A. da Rosa, C. Zárate-Castañeda, C. M. Monteza-Moreno, C. Carnicer, C. T. Trinca, D. J. Polli, D. da Silva Ferraz, D. F. Lane, D. G. da Rocha, D. C. Barcelos, D. Auz, D. C. P. Rosa, D. A. Silva, D. V. Silvério, D. P. Eaton, E. Nakano-Oliveira, E. Venticinque, E. C. Junior, E. N. Mendonça, E. M. Vieira, E. Isasi-Catalá, E. Fischer, E. P. Castro, E. G. Oliveira, F. R. de Melo, F. de Lima Muniz, F. Rohe, F. B.

Baccaro, F. Michalski, F. P. Paim, F. Santos, F. Anaguano, F. B. L. Palmeira, F. da Silva Reis, F. H. Aguiar-Silva, G. de Avila Batista, G. Zapata-Ros, G. Forero-Medina, G. D. S. F. Neto, G. B. Alves, G. Ayala, G. H. P. Pedersoli, H. R. El Bizri, H. A. do Prado, H. B. Mozerle, H. C. M. Costa, I. J. Lima, J. Palacios, J. de Resende Assis, J. P. Boubli, J. P. Metzger, J. V. Teixeira, J. M. D. Miranda, J. Polisar, J. Salvador, K. Borges-Almeida, K. Didier, K. D. de Lima Pereira, K. Torralvo, K. Gajapersad, L. Silveira, L. U. Maioli, L. Maracahipes-Santos, L. Valenzuela, L. Benavalli, L. Fletcher, L. N. Paolucci, L. P. Zanzini, L. Z. da Silva, L. C. R. Rodrigues, M. Benchimol, M. A. Oliveira, M. Lima, M. B. da Silva, M. A. dos Santos Junior, M. Viscarra, M. Cohn-Haft, M. I. Abrahams, M. A. Benedetti, M. Marmontel, M. R. Hirt, N. M. Tôrres, O. F. C. Junior, P. Alvarez-Loayza, P. Jansen, P. R. Prist, P. M. Brando, P. B. Perônico, R. do Nascimento Leite, R. M. Rabelo, R. Sollmann, R. Beltrão-Mendes, R. A. F. Ferreira, R. Coutinho, R. da Costa Oliveira, R. Ilha, R. R. Hilário, R. A. P. Pires, R. Sampaio, R. da Silva Moreira, R. Botero-Arias, R. V. Martinez, R. A. de Albuquerque Nóbrega, R. F. Fadini, R. G. Morato, R. L. Carneiro, R. P. S. Almeida, R. M. Ramos, R. Schaub, R. Dornas, R. Cueva, S. Rolim, S. Laurindo, S. Espinosa, T. N. Fernandes, T. M. Sanaiotti, T. H. G. Alvim, T. T. Dornas, T. E. N. Piña, V. L. Caetano Andrade, W. T. V. Santiago, W. E. Magnusson, Z. Campos, and M. C. Ribeiro. 2022. AMAZONIA CAMTRAP: A data set of mammal, bird, and reptile species recorded with camera traps in the amazon forest. Ecology 103:e3738.

Aronsson, M., and J. Persson. 2018. Female breeding dispersal in wolverines, a solitary carnivore with high territorial fidelity. European Journal of Wildlife Research 64:7.

Auger-Méthé, M., K. Newman, D. Cole, F. Empacher, R. Gryba, A. A. King, V. Leos-Barajas, J. Mills Flemming, A. Nielsen, G. Petris, and L. Thomas. 2021. A guide to state–space modeling of ecological time series. Ecological Monographs 91:e01470.

Augustine, B. C., J. A. Royle, M. J. Kelly, C. B. Satter, R. S. Alonso, E. E. Boydston, and K. R. Crooks. 2018. Spatial capture–recapture with partial identity: An application to camera traps. The Annals of Applied Statistics 12:67–95.

Avgar, T., J. A. Baker, G. S. Brown, J. S. Hagens, A. M. Kittle, E. E. Mallon, M. T. McGreer, A. Mosser, S. G. Newmaster, B. R. Patterson, D. E. B. Reid, A. R. Rodgers, J. Shuter, G. M. Street, I. Thompson, M. J. Turetsky, P. A. Wiebe, and J. M. Fryxell. 2015. Space-use behaviour of woodland caribou based on a cognitive movement model. Journal of Animal Ecology 84:1059–1070.

Avgar, T., A. Mosser, G. S. Brown, and J. M. Fryxell. 2013. Environmental

and individual drivers of animal movement patterns across a wide geographical gradient. Journal of Animal Ecology 82:96–106.

Avgar, T., J. R. Potts, M. A. Lewis, and M. S. Boyce. 2016. Integrated step selection analysis: Bridging the gap between resource selection and animal movement. Methods in Ecology and Evolution 7:619–630.

Baker, P., S. Funk, S. Harris, and P. White. 2000. Flexible spatial organization of urban foxes, vulpes vulpes, before and during an outbreak of sarcoptic mange. Anim Behav 59:127–146.

Bastille-Rousseau, G., D. L. Murray, J. A. Schaefer, M. A. Lewis, S. P. Mahoney, and J. R. Potts. 2018. Spatial scales of habitat selection decisions: Implications for telemetry-based movement modelling. Ecography 41:437–443.

Bateman, A. W., M. A. Lewis, G. Gall, M. B. Manser, and T. H. Clutton-Brock. 2015. Territoriality and home-range dynamics in meerkats, suricata suricatta: A mechanistic modelling approach. Journal of Animal Ecology 84:260–271.

Becker, M., D. J. Huggard, M. Dickie, C. Warbington, J. Schieck, E. Herdman, R. Serrouya, and S. Boutin. 2022. Applying and testing a novel method to estimate animal density from motion-triggered cameras. Ecosphere 13:e4005.

Bessone, M., H. S. Kühl, G. Hohmann, I. Herbinger, K. P. N'Goran, P. Asanzi, P. B. Da Costa, V. Dérozier, E. D. B. Fotsing, B. I. Beka, M. D. Iyomi, I. B. Iyatshi, P. Kafando, M. A. Kambere, D. B. Moundzoho, M. L. K. Wanzalire, and B. Fruth. 2020. Drawn out of the shadows: Surveying secretive forest species with camera trap distance sampling. Journal of Applied Ecology 57:963–974.

Bianchi, N. A. G., Rita de Cassia AND Olifiers. 2016. Niche partitioning among mesocarnivores in a brazilian wetland. PLOS ONE 11:1–17.

Bischof, R., P. Dupont, C. Milleret, J. Chipperfield, and J. A. Royle. 2020a. Consequences of ignoring group association in spatial capture–recapture analysis. Wildlife Biology 2020.

Bischof, R., C. Milleret, P. Dupont, J. Chipperfield, M. Tourani, A. Ordiz, P. de Valpine, D. Turek, J. A. Royle, O. Gimenez, Øystein Flagstad, M. Åkesson, L. Svensson, H. Brøseth, and J. Kindberg. 2020b. Estimating and forecasting spatial population dynamics of apex predators using transnational genetic monitoring. Proceedings of the National Academy of Sciences 117:30531–30538.

Borchers, D. L., and M. G. Efford. 2008. Spatially explicit maximum likelihood methods for capture–recapture studies. Biometrics 64:377–385.

Borchers, D., G. Distiller, R. Foster, B. Harmsen, and L. Milazzo. 2014. Continuous-time spatially explicit capture–recapture models, with an application to a jaguar camera-trap survey. Methods in Ecology and Evolution 5:656–665.

Börger, L., B. D. Dalziel, and J. M. Fryxell. 2008. Are there general mechanisms of animal home range behaviour? A review and prospects for future research. Ecology Letters 11:637–650.

Bracis, C., K. L. Bildstein, and T. Mueller. 2018a. Revisitation analysis uncovers spatio-temporal patterns in animal movement data. Ecography 41:1801–1811.

Bracis, C., E. Gurarie, J. D. Rutter, and R. A. Goodwin. 2018b. Remembering the good and the bad: Memory-based mediation of the food–safety trade-off in dynamic landscapes. Theoretical Ecology 11:305–319.

Bracis, C., E. Gurarie, B. Van Moorter, and R. A. Goodwin. 2015. Memory effects on movement behavior in animal foraging. PLOS ONE 10:1–21.

Bracis, C., and T. Mueller. 2017. Memory, not just perception, plays an important role in terrestrial mammalian migration. Proceedings of the Royal Society B: Biological Sciences 284:20170449.

Bracis, C., and A. J. Wirsing. 2021. Prey foraging behavior after predator introduction is driven by resource knowledge and exploratory tendency. Frontiers in Ecology and Evolution 9.

Breitenmoser-Würsten, C., F. Zimmermann, A. Molinari-Jobin, P. Molinari, S. Capt, J.-M. Vandel, P. Stahl, and U. Breitenmoser. 2007. Spatial and social stability of a eurasian lynx population: An assessment of 10 years of observation in the jura mountains. Wildlife Biology 13:365–380.

Broadley, K., A. C. Burton, T. Avgar, and S. Boutin. 2019. Density-dependent space use affects interpretation of camera trap detection rates. Ecology and Evolution 9:14031–14041.

Buckland, S. T., D. R. Anderson, K. P. Burnham, and J. L. Laake. 1993. Distance sampling: Estimating abundance of biological populations. Chapman; Hall, London.

Buckland, S. T., D. R. Anderson, K. P. Burnham, J. L. Laake, D. L. Borchers, and L. Thomas. 2001. Introduction to distance sampling: Estimating abundance of biological populations. Book, Oxford University Press.

Buckland, S. T., D. L. Borchers, T. A. Marques, and R. M. Fewster. 2023. Wildlife population assessment: Changing priorities driven by technological advances. Journal of Statistical Theory and Practice 17:20.

Buckland, S. T., E. A. Rexstad, T. A. Marques, and C. S. Oedekoven. 2015. Distance sampling: Methods and applications. First edition. Springer Cham.

Burton, A. C., E. Neilson, D. Moreira, A. Ladle, R. Steenweg, J. T. Fisher, E. Bayne, and S. Boutin. 2015. REVIEW: Wildlife camera trapping: A review and recommendations for linking surveys to ecological processes. Journal of

Applied Ecology 52:675–685.

Cagnacci, F., L. Boitani, R. A. Powell, and M. S. Boyce. 2010. Animal ecology meets GPS-based radiotelemetry: A perfect storm of opportunities and challenges. Philosophical Transactions of the Royal Society B: Biological Sciences 365:2157–2162.

Cappelle, N., M.-L. Després-Einspenner, E. J. Howe, C. Boesch, and H. S. Kühl. 2019. Validating camera trap distance sampling for chimpanzees. American Journal of Primatology 81:e22962.

Cappelle, N., E. J. Howe, C. Boesch, and H. S. Kühl. 2021. Estimating animal abundance and effort–precision relationship with camera trap distance sampling. Ecosphere 12.

Caravaggi, A., M. Zaccaroni, F. Riga, S. C. Schai-Braun, J. T. A. Dick, W. I. Montgomery, and N. Reid. 2016. An invasive-native mammalian species replacement process captured by camera trap survey random encounter models. Remote Sensing in Ecology and Conservation 2:45–58.

Chandler, R. B., and J. A. Royle. 2013. Spatially explicit models for inference about density in unmarked or partially marked populations. The Annals of Applied Statistics 7:936–954.

Corlatti, L., S. Sivieri, B. Sudolska, S. Giacomelli, and L. Pedrotti. 2020. A field test of unconventional camera trap distance sampling to estimate abundance of marmot populations. Wildlife Biology 2020:1–11.

Cubaynes, R. A. C., Sarah And Pradel. 2010. Importance of accounting for detection heterogeneity when estimating abundance: The case of french wolves. Conservation Biology 24:621–626.

Cusack, J. J., A. Swanson, T. Coulson, C. Packer, C. Carbone, A. J. Dickman, M. Kosmala, C. Lintott, and J. M. Rowcliffe. 2015. Applying a random encounter model to estimate lion density from camera traps in serengeti national park, tanzania. The Journal of Wildlife Management 79:1014–1021.

Dey, S., R. Bischof, P. P. A. Dupont, and C. Milleret. 2022. Does the punishment fit the crime? Consequences and diagnosis of misspecified detection functions in bayesian spatial capture–recapture modeling. Ecology and Evolution 12:e8600.

Distiller, G. B., D. L. Borchers, R. J. Foster, and B. J. Harmsen. 2020. Using continuous-time spatial capture–recapture models to make inference about animal activity patterns. Ecology and Evolution 10:e6822.

Doran-Myers, D., A. J. Kenney, C. J. Krebs, C. T. Lamb, A. K. Menzies, D. Murray, E. K. Studd, J. Whittington, and S. Boutin. 2021. Density estimates for canada lynx vary among estimation methods. Ecosphere 12:e03774.

Dupont, G., J. A. Royle, M. A. Nawaz, and C. Sutherland. 2021. Optimal sampling design for spatial capture–recapture. Ecology 102:e03262.

Efford, M. 2004. Density estimation in live-trapping studies. Oikos 106:598–610.

Efford, M. G. 2019. Non-circular home ranges and the estimation of population density. Ecology 100:e02580.

Efford, M. G., and G. Mowat. 2014. Compensatory heterogeneity in spatially explicit capture–recapture data. Ecology 95:1341–1348.

Elith, J., J. R. Leathwick, and T. Hastie. 2008. A working guide to boosted regression trees. Journal of Animal Ecology 77:802–813.

Ellison, N., B. J. Hatchwell, S. J. Biddiscombe, C. J. Napper, and J. R. Potts. 2020. Mechanistic home range analysis reveals drivers of space use patterns for a non-territorial passerine. Journal of Animal Ecology 89:2763–2776.

Fagan, W. F., M. A. Lewis, M. Auger-Méthé, T. Avgar, S. Benhamou, G. Breed, L. LaDage, U. E. Schlägel, W. Tang, Y. P. Papastamatiou, J. Forester, and T. Mueller. 2013. Spatial memory and animal movement. Ecol Lett 16:1316–1329.

Fennell, M., C. Beirne, and A. C. Burton. 2022. Use of object detection in camera trap image identification: Assessing a method to rapidly and accurately classify human and animal detections for research and application in recreation ecology. Global Ecology and Conservation 35:e02104.

Fleming, C. H., W. F. Fagan, T. Mueller, K. A. Olson, P. Leimgruber, and J. M. Calabrese. 2015. Rigorous home range estimation with movement data: A new autocorrelated kernel density estimator. Ecology 96:1182–1188.

Fleming, J., E. H. C. Grant, S. C. Sterrett, and C. Sutherland. 2021. Experimental evaluation of spatial capture–recapture study design. Ecological Applications 31:e02419.

Frank, S. C., M. Leclerc, F. Pelletier, F. Rosell, Jon. E. Swenson, R. Bischof, J. Kindberg, H. G. Eiken, S. B. Hagen, and A. Zedrosser. 2018. Sociodemographic factors modulate the spatial response of brown bears to vacancies created by hunting. Journal of Animal Ecology 87:247–258.

Fuller, A. K., C. S. Sutherland, J. A. Royle, and M. P. Hare. 2016. Estimating population density and connectivity of american mink using spatial capture–recapture. Ecological Applications 26:1125–1135.

Gardner, B., B. T. McClintock, S. J. Converse, and N. J. Hostetter. 2022. Integrated animal movement and spatial capture–recapture models: Simulation, implementation, and inference. Ecology 103:e3771.

Gardner, B., J. A. Royle, and M. T. Wegan. 2009. Hierarchical models for

estimating density from DNA mark–recapture studies. Ecology 90:1106–1115.

Gardner, B., R. Sollmann, N. S. Kumar, D. Jathanna, and K. U. Karanth. 2018. State space and movement specification in open population spatial capture–recapture models. Ecology and Evolution 8:10336–10344.

Gelman, A., and D. B. Rubin. 1992. Inference from Iterative Simulation Using Multiple Sequences. Statistical Science 7:457–472.

Gerber, B. D., and R. R. Parmenter. 2015. Spatial capture–recapture model performance with known small-mammal densities. Ecological Applications 25:695–705.

Gilbert, N. A., J. D. J. Clare, J. L. Stenglein, and B. Zuckerberg. 2021. Abundance estimation of unmarked animals based on camera-trap data. Conservation Biology 35:88–100.

Giuggioli, L., J. R. Potts, and S. Harris. 2011. Animal interactions and the emergence of territoriality. PLoS Comput Biol 7:e1002008.

Giuggioli, L., J. R. Potts, D. I. Rubenstein, and S. A. Levin. 2013. Stigmergy, collective actions, and animal social spacing. Proc Natl Acad Sci U S A 110:16904–16909.

Glennie, R., D. L. Borchers, M. Murchie, B. J. Harmsen, and R. J. Foster. 2019. Open population maximum likelihood spatial capture-recapture. Biometrics 75:1345–1355.

Goldberg, T. A. N., Joshua F. AND Tempa. 2015. Examining temporal sample scale and model choice with spatial capture-recapture models in the common leopard panthera pardus. PLOS ONE 10:1–19.

Grimm, V., and S. F. Railsback. 2005. Individual-based modeling and ecology: STU - Student edition. Princeton University Press.

Grimm, V., and S. F. Railsback. 2012. Pattern-oriented modelling: A 'multi-scope' for predictive systems ecology. Philos Trans R Soc Lond B Biol Sci 367:298–310.

Gurarie, E., C. Bracis, M. Delgado, T. D. Meckley, I. Kojola, and C. M. Wagner. 2016. What is the animal doing? Tools for exploring behavioural structure in animal movements. Journal of Animal Ecology 85:69–84.

Harmsen, R. J. A. Q., Bart J. AND Foster. 2020. Spatially explicit capture recapture density estimates: Robustness, accuracy and precision in a long-term study of jaguars (panthera onca). PLOS ONE 15:1–19.

Hayashi, K., and H. Iijima. 2022. Density estimation of non-independent unmarked animals from camera traps. Ecological Modelling 472.

Hinton, C. A. K., Joseph W. AND Proctor. 2016. Space use and habitat selection

by resident and transient red wolves (canis rufus). PLOS ONE 11:1–17.

Hodgens, P. 2019. Felixer versus felis: Innovative engagement of kangaroo island landholders in feral cat control activities. A report for the felixer versus felis project. Natural Resources Kangaroo Island, Kingscote.

Hofmeester, T. R., J. M. Rowcliffe, P. A. Jansen, R. Williams, and N. Kelly. 2017. A simple method for estimating the effective detection distance of camera traps. Remote Sensing in Ecology and Conservation 3:81–89.

Holmes, R. T., P. P. Marra, and T. W. Sherry. 1996. Habitat-specific demography of breeding black-throated blue warblers (dendroica caerulescens): Implications for population dynamics. Journal of Animal Ecology 65:183–195.

Hooten, M. B., D. S. Johnson, B. T. McClintock, and J. M. Morales. 2017. Animal movement: Statistical models for telemetry data. 1st edition. CRC Press.

Hooten, M. B., H. R. Scharf, and J. M. Morales. 2019. Running on empty: Recharge dynamics from animal movement data. Ecology Letters 22:377–389.

Horne, J. S., E. O. Garton, S. M. Krone, and J. S. Lewis. 2007. Analyzing animal movements using brownian bridges. Ecology 88:2354–2363.

Howe, E. J., S. T. Buckland, M. DesprésEinspenner, H. S. Kühl, and J. Matthiopoulos. 2017. Distance sampling with camera traps. Methods in Ecology and Evolution 8:1558–1565.

Howe, E. J., S. T. Buckland, M. DesprésEinspenner, H. S. Kühl, and J. Matthiopoulos. 2018. Model selection with overdispersed distance sampling data. Methods in Ecology and Evolution 10:38–47.

Jimenez, J., R. Chandler, J. Tobajas, E. Descalzo, R. Mateo, and P. Ferreras. 2019. Generalized spatial mark–resight models with incomplete identification: An application to red fox density estimates. Ecology and Evolution 9:4739–4748.

Johanns, P., T. Haucke, and V. Steinhage. 2022. Automated distance estimation for wildlife camera trapping. Ecological Informatics 70:101734.

Kacelnik, A. 1984. Central place foraging in starlings (sturnus vulgaris). I. Patch residence time. Journal of Animal Ecology 53:283–299.

Karanth, K. U., J. D. Nichols, N. S. Kumar, and J. E. Hines. 2006. Assessing tiger population dynamics using photographic capture–recapture sampling. Ecology 87:2925–2937.

Kays, R., M. C. Crofoot, W. Jetz, and M. Wikelski. 2015. Terrestrial animal tracking as an eye on life and planet. Science 348:aaa2478.

Keiter, D. A., A. J. Davis, O. E. Rhodes, F. L. Cunningham, J. C. Kilgo, K. M. Pepin, and J. C. Beasley. 2017. Effects of scale of movement, detection

probability, and true population density on common methods of estimating population density. Scientific Reports 7:9446.

Krebs, C. J. 2020. How to ask meaningful ecological questions. Pages 3–16 Population ecology in practice. Wiley-Blackwell.

Lahoz-Monfort, J. J., and M. J. L. Magrath. 2021. A Comprehensive Overview of Technologies for Species and Habitat Monitoring and Conservation. BioScience 71:1038–1062.

Lampa, J.-B. A. G., Simone AND Mihoub. 2015. Non-invasive genetic mark-recapture as a means to study population sizes and marking behaviour of the elusive eurasian otter (lutra lutra). PLOS ONE 10:1–20.

Langrock, R., J. G. C. Hopcraft, P. G. Blackwell, V. Goodall, R. King, M. Niu, T. A. Patterson, M. W. Pedersen, A. Skarin, R. S. Schick, and N. Yoccoz. 2014. Modelling group dynamic animal movement. Methods in Ecology and Evolution 5:190–199.

Lewis, M. A., and J. D. Murray. 1993. Modelling territoriality and wolf–deer interactions. Nature 366:738–740.

Linden, D. W., A. P. K. Sirén, and P. J. Pekins. 2018. Integrating telemetry data into spatial capture–recapture modifies inferences on multi-scale resource selection. Ecosphere 9:e02203.

Loonam, K. E., D. E. Ausband, P. M. Lukacs, M. S. Mitchell, and H. S. Robinson. 2021. Estimating abundance of an unmarked, low-density species using cameras. The Journal of Wildlife Management 85:87–96.

Luo, G., W. Wei, Q. Dai, and J. Ran. 2020. Density estimation of unmarked populations using camera traps in heterogeneous space. Wildlife Society Bulletin 44:173–181.

Macdonald, D. W. 1980. Patterns of scent marking wilh urine and faeces amongst carnivore.

Mahoney, P. J., and J. K. Young. 2017. Uncovering behavioural states from animal activity and site fidelity patterns. Methods in Ecology and Evolution 8:174–183.

Manly, B. F. J., L. L. McDonald, D. L. Thomas, T. L. McDonald, and E. W. P. 2007. Resource selection by animals: Statistical design and analysis for field studies. Springer Dordrecht.

Mares, M. A., M. D. Watson, and T. E. Lacher. 1976. Home range perturbations in tamias striatus. Food supply as a determinant of home range and density. Oecologia 25:1–12.

McClintock, B. T., B. Abrahms, R. B. Chandler, P. B. Conn, S. J. Converse,

R. L. Emmet, B. Gardner, N. J. Hostetter, and D. S. Johnson. 2022. An integrated path for spatial capture–recapture and animal movement modeling. Ecology 103:e3473.

McClintock, B. T., P. B. Conn, R. S. Alonso, and K. R. Crooks. 2013. Integrated modeling of bilateral photo-identification data in mark–recapture analyses. Ecology 94:1464–1471.

McClintock, B. T., R. King, L. Thomas, J. Matthiopoulos, B. J. McConnell, and J. M. Morales. 2012. A general discrete-time modeling framework for animal movement using multistate random walks. Ecological Monographs 82:335–349.

McClintock, B. T., and T. Michelot. 2018. momentuHMM: R package for generalized hidden markov models of animal movement. Methods in Ecology and Evolution 9:1518–1530.

McClintock, B. T., and L. Thomas. 2020. Estimating abundance or occupancy from unmarked populations. Pages 49–98 Population ecology in practice. Wiley-Blackwell.

McLaughlin, P., and H. Bar. 2021. A spatial capture–recapture model with attractions between individuals. Environmetrics 32:e2653.

Mcloughlin, P. D., and S. H. Ferguson. 2000. A hierarchical pattern of limiting factors helps explain variation in home range size. Écoscience 7:123–130.

Mech, L. D., and L. Boitani. 2010. Wolves: Behavior, ecology, and conservation. University of Chicago Press.

Merkle, J. A., J. R. Potts, and D. Fortin. 2017. Energy benefits and emergent space use patterns of an empirically parameterized model of memory-based patch selection. Oikos 126.

Milleret, C., P. Dupont, H. Brøseth, J. Kindberg, J. A. Royle, and R. Bischof. 2018. Using partial aggregation in spatial capture recapture. Methods in Ecology and Evolution 9:1896–1907.

Milleret, C., P. Dupont, J. Chipperfield, D. Turek, H. Brøseth, O. Gimenez, P. de Valpine, and R. Bischof. 2020. Estimating abundance with interruptions in data collection using open population spatial capture–recapture models. Ecosphere 11:e03172.

Mitchell, N., M. W. Strohbach, R. Pratt, W. C. Finn, and E. G. Strauss. 2015. Space use by resident and transient coyotes in an urban–rural landscape mosaic. Wildlife Research 42:461–469.

Moeller, A. K., P. M. Lukacs, and J. S. Horne. 2018. Three novel methods to estimate abundance of unmarked animals using remote cameras. Ecosphere 9:e02331.

Mohamed, A., R. Sollmann, H. Bernard, L. N. Ambu, P. Lagan, S. Mannan, H. Hofer, and A. Wilting. 2013. Density and habitat use of the leopard cat (Prionailurus bengalensis) in three commercial forest reserves in Sabah, Malaysian Borneo. Journal of Mammalogy 94:82–89.

Moorcroft, P. R., M. A. Lewis, and R. L. Crabtree. 1999. Home range analysis using a mechanistic home range model. Ecology 80:1656–1665.

Moorcroft, P. R., M. A. Lewis, and R. L. Crabtree. 2006. Mechanistic home range models capture spatial patterns and dynamics of coyote territories in yellowstone. Proc Biol Sci 273:1651–1659.

Moqanaki, E. M., C. Milleret, M. Tourani, P. Dupont, and R. Bischof. 2021. Consequences of ignoring variable and spatially autocorrelated detection probability in spatial capture-recapture. Landscape Ecology 36:2879–2895.

Morales, J. M., P. R. Moorcroft, J. Matthiopoulos, J. L. Frair, J. G. Kie, R. A. Powell, E. H. Merrill, and D. T. Haydon. 2010. Building the bridge between animal movement and population dynamics. Philos Trans R Soc Lond B Biol Sci 365:2289–2301.

Morin, D. J., M. J. Kelly, and L. P. Waits. 2016. Monitoring coyote population dynamics with fecal DNA and spatial capture–recapture. The Journal of Wildlife Management 80:824–836.

Mueller, T., and W. F. Fagan. 2008. Search and navigation in dynamic environments – from individual behaviors to population distributions. Oikos 117:654–664.

Nakashima, Y. 2022. Guidelines for evaluating density estimation models for unmarked populations - santini et al. (2022). Basic and Applied Ecology.

Nakashima, Y., K. Fukasawa, H. Samejima, and P. Stephens. 2017. Estimating animal density without individual recognition using information derivable exclusively from camera traps. Journal of Applied Ecology 55:735–744.

Nakashima, Y., S. Hongo, and E. F. Akomo-Okoue. 2020. Landscape-scale estimation of forest ungulate density and biomass using camera traps: Applying the REST model. Biological Conservation 241:108381.

Nakashima, Y., S. Hongo, K. Mizuno, G. Yajima, and Z. C. B. Dzefck. 2022. Double-observer approach with camera traps can correct imperfect detection and improve the accuracy of density estimation of unmarked animal populations. Scientific Reports 12:2011.

Nathan, R., W. M. Getz, E. Revilla, M. Holyoak, R. Kadmon, D. Saltz, and P. E. Smouse. 2008. A movement ecology paradigm for unifying organismal movement research. Proceedings of the National Academy of Sciences

105:19052–19059.

Neilson, E. W., T. Avgar, A. C. Burton, K. Broadley, and S. Boutin. 2018. Animal movement affects interpretation of occupancy models from camera-trap surveys of unmarked animals. Ecosphere 9:e02092.

Niedballa, J., R. Sollmann, A. Courtiol, and A. Wilting. 2016. camtrapR: An r package for efficient camera trap data management. Methods in Ecology and Evolution 7:1457–1462.

Nield, A. P., R. Nathan, N. J. Enright, P. G. Ladd, and G. L. W. Perry. 2020. The spatial complexity of seed movement: Animal-generated seed dispersal patterns in fragmented landscapes revealed by animal movement models. Journal of Ecology 108:687–701.

Noonan, M. J., M. A. Tucker, C. H. Fleming, T. S. Akre, S. C. Alberts, A. H. Ali, J. Altmann, P. C. Antunes, J. L. Belant, D. Beyer, N. Blaum, K. Böhning-Gaese, L. Cullen Jr., R. C. de Paula, J. Dekker, J. Drescher-Lehman, N. Farwig, C. Fichtel, C. Fischer, A. T. Ford, J. R. Goheen, R. Janssen, F. Jeltsch, M. Kauffman, P. M. Kappeler, F. Koch, S. LaPoint, A. C. Markham, E. P. Medici, R. G. Morato, R. Nathan, L. G. R. Oliveira-Santos, K. A. Olson, B. D. Patterson, A. Paviolo, E. E. Ramalho, S. Rösner, D. G. Schabo, N. Selva, A. Sergiel, M. Xavier da Silva, O. Spiegel, P. Thompson, W. Ullmann, F. Ziba, T. Zwijacz-Kozica, W. F. Fagan, T. Mueller, and J. M. Calabrese. 2019. A comprehensive analysis of autocorrelation and bias in home range estimation. Ecological Monographs 89:e01344.

Norouzzadeh, M. S., A. Nguyen, M. Kosmala, A. Swanson, M. S. Palmer, C. Packer, and J. Clune. 2018. Automatically identifying, counting, and describing wild animals in camera-trap images with deep learning. Proceedings of the National Academy of Sciences 115:E5716–E5725.

Noss, R. F., H. B. Quigley, M. G. Hornocker, T. Merrill, and P. C. Paquet. 1996. Conservation biology and carnivore conservation in the rocky mountains. Conservation Biology 10:949–963.

Oliveira-Santos, L. G. R., J. D. Forester, U. Piovezan, W. M. Tomas, and F. A. S. Fernandez. 2016. Incorporating animal spatial memory in step selection functions. Journal of Animal Ecology 85:516–524.

Otis, D. L., K. P. Burnham, G. C. White, and D. R. Anderson. 1978. Statistical inference from capture data on closed animal populations. Wildlife Monographs:3–135.

Palencia, P., P. Barroso, J. Vicente, T. R. Hofmeester, J. Ferreres, P. Acevedo, M. Rowcliffe, and A. Caravaggi. 2022. Random encounter model is a reliable

method for estimating population density of multiple species using camera traps. Remote Sensing in Ecology and Conservation.

Palencia, P., J. M. Rowcliffe, J. Vicente, and P. Acevedo. 2021a. Assessing the camera trap methodologies used to estimate density of unmarked populations. Journal of Applied Ecology 58:1583–1592.

Palencia, P., J. Vicente, R. C. Soriguer, and P. Acevedo. 2021b. Towards a best-practices guide for camera trapping: Assessing differences among camera trap models and settings under field conditions. Journal of Zoology 316:197–208.

Palomares, F. 1994. Site fidelity and effects of body mass on home-range size of egyptian mongooses. Canadian Journal of Zoology 72:465–469.

Péron, G. 2019. The time frame of home-range studies: From function to utilization. Biological Reviews 94:1974–1982.

Pettigrew, P., D. Sigouin, and M.-H. St-Laurent. 2021. Testing the precision and sensitivity of density estimates obtained with a camera-trap method revealed limitations and opportunities. Ecology and Evolution 11:7879–7889.

Pitt, W. C., P. W. Box, and Frederick. F. Knowlton. 2003. An individual-based model of canid populations: Modelling territoriality and social structure. Ecological Modelling 166:109–121.

Polansky, L., W. Kilian, and G. Wittemyer. 2015. Elucidating the significance of spatial memory on movement decisions by african savannah elephants using state–space models. Proceedings of the Royal Society B: Biological Sciences 282:20143042.

Pollock, J. A. B., KH And Nichols, and J. Hines. 1990. Statistical-inference for capture-recapture experiments. Pages 1–97 Wildlife Monographs.

Potts, J. R., S. Harris, and L. Giuggioli. 2013. Quantifying behavioral changes in territorial animals caused by sudden population declines. The American Naturalist 182:E73–E82.

Potts, J. R., and M. A. Lewis. 2014. How do animal territories form and change? Lessons from 20 years of mechanistic modelling. Proceedings of the Royal Society B: Biological Sciences 281:20140231.

Potts, J. R., and M. A. Lewis. 2016. How memory of direct animal interactions can lead to territorial pattern formation. Journal of The Royal Society Interface 13:20160059.

Potts, J. R., K. Mokross, and M. A. Lewis. 2014. A unifying framework for quantifying the nature of animal interactions. Journal of The Royal Society Interface 11:20140333.

Potts, S. A. G., Jonathan R. AND Harris. 2012. Territorial dynamics and stable home range formation for central place foragers. PLOS ONE 7:1–11.

Powell, R. A., and M. S. Mitchell. 2012. What is a home range? Journal of Mammalogy 93:948–958.

Prowse, T. A. A., C. J. A. Bradshaw, S. Delean, P. Cassey, R. C. Lacy, K. Wells, M. E. Aiello-Lammens, H. R. Akçakaya, and B. W. Brook. 2016. An efficient protocol for the global sensitivity analysis of stochastic ecological models. Ecosphere 7:e01238.

Ramsey, D. S. L., P. A. Caley, and A. Robley. 2015. Estimating population density from presence–absence data using a spatially explicit model. The Journal of Wildlife Management 79:491–499.

Ranc, N., P. R. Moorcroft, F. Ossi, and F. Cagnacci. 2021. Experimental evidence of memory-based foraging decisions in a large wild mammal. Proceedings of the National Academy of Sciences 118:e2014856118.

Reich, B. J., and B. Gardner. 2014. A spatial capture-recapture model for territorial species. Environmetrics 25:630–637.

Reppucci, J., B. Gardner, and M. Lucherini. 2011. Estimating detection and density of the Andean cat in the high Andes. Journal of Mammalogy 92:140–147.

Richardson, T. O., L. Giuggioli, N. R. Franks, and A. B. Sendova-Franks. 2017. Measuring site fidelity and spatial segregation within animal societies. Methods in Ecology and Evolution 8:965–975.

Riotte-Lambert, L., S. Benhamou, C. Bonenfant, and S. Chamaillé-Jammes. 2017. Spatial memory shapes density dependence in population dynamics. Proc Biol Sci 284.

Riotte-Lambert, L., S. Benhamou, and S. Chamaillé-Jammes. 2015. How memory-based movement leads to nonterritorial spatial segregation. Am Nat 185:E103–16.

Roever, C. L., H. L. Beyer, M. J. Chase, and R. J. van Aarde. 2014. The pitfalls of ignoring behaviour when quantifying habitat selection. Diversity and Distributions 20:322–333.

Rovero, F., and A. R. Marshall. 2009. Camera trapping photographic rate as an index of density in forest ungulates. Journal of Applied Ecology 46:1011–1017.

Rovero, F., and F. Zimmermann. 2016. Camera trapping for wildlife research. Pelagic Publishing.

Rowcliffe, J. M., C. Carbone, P. A. Jansen, R. Kays, and B. Kranstauber. 2011. Quantifying the sensitivity of camera traps: An adapted distance sampling

approach. Methods in Ecology and Evolution 2:464–476.

Rowcliffe, J. M., J. Field, S. T. Turvey, and C. Carbone. 2008. Estimating animal density using camera traps without the need for individual recognition. Journal of Applied Ecology 45:1228–1236.

Rowcliffe, J. M., P. A. Jansen, R. Kays, B. Kranstauber, C. Carbone, and N. Pettorelli. 2016. Wildlife speed cameras: Measuring animal travel speed and day range using camera traps. Remote Sensing in Ecology and Conservation 2:84–94.

Royle, J. A., R. B. Chandler, K. D. Gazenski, and T. A. Graves. 2013a. Spatial capture–recapture models for jointly estimating population density and landscape connectivity. Ecology 94:287–294.

Royle, J. A., R. B. Chandler, R. Sollmann, and B. Gardner. 2014a. Spatial capture-recapture. Academic Press, Boston.

Royle, J. A., R. B. Chandler, R. Sollmann, and B. Gardner, editors. 2014b. Spatial capture-recapture. Academic Press, Boston.

Royle, J. A., R. B. Chandler, C. C. Sun, and A. K. Fuller. 2013b. Integrating resource selection information with spatial capture–recapture. Methods in Ecology and Evolution 4:520–530.

Royle, J. A., R. B. Chandler, C. C. Sun, and A. K. Fuller. 2014c. Reply to efford on "integrating resource selection information with spatial capture–recapture". Methods in Ecology and Evolution 5:603–605.

Royle, J. A., D. K. Dawson, and S. Bates. 2004. Modeling abundance effects in distance sampling. Ecology 85:1591–1597.

Royle, J. A., R. M. Dorazio, and W. A. Link. 2007. Analysis of multinomial models with unknown index using data augmentation. Journal of Computational and Graphical Statistics 16:67–85.

Royle, J. A., A. K. Fuller, and C. Sutherland. 2016. Spatial capture–recapture models allowing markovian transience or dispersal. Population Ecology 58:53–62.

Royle, J. A., A. K. Fuller, and C. Sutherland. 2018. Unifying population and landscape ecology with spatial capture-recapture. ECOGRAPHY 41:444–456.

Royle, J. A., A. J. Magoun, B. Gardner, P. Valkenburg, and R. E. Lowell. 2011. Density estimation in a wolverine population using spatial capture–recapture models. The Journal of Wildlife Management 75:604–611.

Royle, J. A., and K. V. Young. 2008. A hierarchical model for spatial capture-recapture data. Ecology 89:2281–2289.

Sálek, M., L. Drahnková, and E. Tkadlec. 2015. Changes in home range sizes and

population densities of carnivore species along the natural to urban habitat gradient. Mammal Review 45:1–14.

Santangeli, A., H. Hakkarainen, T. Laaksonen, and E. Korpimäki. 2012. Home range size is determined by habitat composition but feeding rate by food availability in male tengmalm's owls. Animal Behaviour 83:1115–1123.

Santini, G., M. Abolaffio, F. Ossi, B. Franzetti, F. Cagnacci, and S. Focardi. 2022. Population assessment without individual identification using camera-traps: A comparison of four methods. Basic and Applied Ecology 61:68–81.

Schlägel, U. E., V. Grimm, N. Blaum, P. Colangeli, M. Dammhahn, J. A. Eccard, S. L. Hausmann, A. Herde, H. Hofer, J. Joshi, S. Kramer-Schadt, M. Litwin, S. D. Lozada-Gobilard, M. E. H. Müller, T. Müller, R. Nathan, J. S. Petermann, K. Pirhofer-Walzl, V. Radchuk, M. C. Rillig, M. Roeleke, M. Schäfer, C. Scherer, G. Schiro, C. Scholz, L. Teckentrup, R. Tiedemann, W. Ullmann, C. C. Voigt, G. Weithoff, and F. Jeltsch. 2020. Movement-mediated community assembly and coexistence. Biological Reviews 95:1073–1096.

Schneider, S., G. W. Taylor, S. Linquist, and S. C. Kremer. 2019. Past, present and future approaches using computer vision for animal re-identification from camera trap data. Methods in Ecology and Evolution 10:461–470.

Schoepf, I., G. Schmohl, B. König, N. Pillay, and C. Schradin. 2015. Manipulation of population density and food availability affects home range sizes of african striped mouse females. Animal Behaviour 99:53–60.

Schradin, C., G. Schmohl, H. G. Rödel, I. Schoepf, S. M. Treffler, J. Brenner, M. Bleeker, M. Schubert, B. König, and N. Pillay. 2010. Female home range size is regulated by resource distribution and intraspecific competition: A long-term field study. Animal Behaviour 79:195–203.

Sciaini, M., M. Fritsch, C. Scherer, and C. E. Simpkins. 2018. NLMR and landscapetools: An integrated environment for simulating and modifying neutral landscape models in r. Methods in Ecology and Evolution 9:2240–2248.

Seber, G. A. F. 1982. The estimation of animal abundance and related parameters. Macmillan Publishing Company.

Sollmann, B. A. B., Rahel AND Gardner. 2012. How does spatial study design influence density estimates from spatial capture-recapture models? PLOS ONE 7:1–8.

Spencer, W. D. 2012. Home ranges and the value of spatial information. Journal of Mammalogy 93:929–947.

Spitz, D. B., M. Hebblewhite, and T. R. Stephenson. 2017. "MigrateR": Extending model-driven methods for classifying and quantifying animal movement behav-

ior. Ecography 40:788–799.

Steenweg, R., M. Hebblewhite, J. Whittington, P. Lukacs, and K. McKelvey. 2018. Sampling scales define occupancy and underlying occupancy–abundance relationships in animals. Ecology 99:172–183.

Sun, C. C., A. K. Fuller, and J. A. Royle. 2014. Trap configuration and spacing influences parameter estimates in spatial capture-recapture models. PLOS ONE 9:1–9.

Sun, C., J. M. Burgar, J. T. Fisher, and A. C. Burton. 2022. A cautionary tale comparing spatial count and partial identity models for estimating densities of threatened and unmarked populations. Global Ecology and Conservation 38:e02268.

Supp, S. R., G. Bohrer, J. Fieberg, and F. A. La Sorte. 2021. Estimating the movements of terrestrial animal populations using broad-scale occurrence data. Movement Ecology 9:60.

Sutherland, C., A. K. Fuller, and J. A. Royle. 2015. Modelling non-euclidean movement and landscape connectivity in highly structured ecological networks. Methods in Ecology and Evolution 6:169–177.

Tao, Y., L. Börger, and A. Hastings. 2016. Dynamic range size analysis of territorial animals: An optimality approach. The American Naturalist 188:460–474.

Theng, M., C. Milleret, C. Bracis, P. Cassey, and S. Delean. 2022. Confronting spatial capture–recapture models with realistic animal movement simulations. Ecology 103:e3676.

Thurfjell, H., S. Ciuti, and M. S. Boyce. 2014. Applications of step-selection functions in ecology and conservation. Movement Ecology 2:4.

Turek, D., C. Milleret, T. Ergon, H. Brøseth, P. Dupont, R. Bischof, and P. de Valpine. 2021. Efficient estimation of large-scale spatial capture–recapture models. Ecosphere 12:e03385.

Valpine, P. de, D. Turek, C. J. Paciorek, C. Anderson-Bergman, D. T. Lang, and R. Bodik. 2017. Programming with models: Writing statistical algorithms for general model structures with NIMBLE. Journal of Computational and Graphical Statistics 26:403–413.

Van Moorter, B., D. Visscher, S. Benhamou, L. Börger, M. S. Boyce, and J.-M. Gaillard. 2009. Memory keeps you at home: A mechanistic model for home range emergence. Oikos 118:641–652.

Van Moorter, B., D. Visscher, I. Herfindal, M. Basille, and A. Mysterud. 2013. Inferring behavioural mechanisms in habitat selection studies getting the null-hypothesis right for functional and familiarity responses. Ecography 36:323–

330.

Vehtari, A., A. Gelman, D. Simpson, B. Carpenter, and P.-C. Bürkner. 2021. Rank-normalization, folding, and localization: An improved R for assessing convergence of MCMC (with discussion). Bayesian Analysis 16.

Vélez, J., W. McShea, H. Shamon, P. J. Castiblanco-Camacho, M. A. Tabak, C. Chalmers, P. Fergus, and J. Fieberg. 2023. An evaluation of platforms for processing camera-trap data using artificial intelligence. Methods in Ecology and Evolution n/a.

Wearn, O. R., T. E. M. Bell, A. Bolitho, J. Durrant, J. K. Haysom, S. Nijhawan, J. Thorley, and J. M. Rowcliffe. 2022. Estimating animal density for a community of species using information obtained only from camera-traps. Methods in Ecology and Evolution 13:2248–2261.

Whittington-Jones, B. M., D. M. Parker, R. T. F. Bernard, and H. T. Davies-Mostert. 2011. Habitat Selection by Transient African Wild Dogs (Lycaon pictus) in Northern KwaZulu-Natal, South Africa: Implications for Range Expansion. South African Journal of Wildlife Research 44:135–147.

Williams, B. K., J. D. Nichols, and M. J. Conroy. 2002. Analysis and management of animal populations: Modeling, estimation and decision making. Academic Press, San Diego, CA.

Zero, V. H., S. R. Sundaresan, T. G. O'Brien, and M. F. Kinnaird. 2013. Monitoring an endangered savannah ungulate, grevy's zebra equus grevyi: Choosing a method for estimating population densities 47:410–419.

Zhang, W., J. D. Chipperfield, J. B. Illian, P. Dupont, C. Milleret, P. de Valpine, and R. Bischof. 2023. A flexible and efficient bayesian implementation of point process models for spatial capture–recapture data. Ecology 104:e3887.

A

Supplementary information: Chapter 2

Text A.1: Description of the empirical data and parameterisation of the simulation landscape

We used data from 11 GPS-tagged adult female and male feral cats from a 2019 feral cat control study conducted in Kangaroo Island (South Australia) by the Department for Environment and Water South Australia (obtained with permission; Figure A.3). Location data for all individuals started on the same date (13 February 2019), and fixes were taken every 15 minutes between 6 pm – 6 am (active period) up until mortality from poison or collars falling off.

As we aimed to relate simulated data to the real dataset, we used a simulation resource landscape representative of the 4 × 6 km study area (spatial extent of [763421, 767421] to [6029884, 6035884]; UTM zone 53H). One spatial unit of our simulation landscape was equivalent to 10 m. Resource values were derived by calculating the $1–(\log_2+1)$ scaled Euclidean distance from three environmental variables hypothesised to be of importance to cats – water courses, vegetation and buildings (J. Smith, personal communication, 2 March 2021) – expressing non-linear preference for areas nearer these resources compared to areas further from them. Environmental layers were obtained from https://data.environment.sa.gov.au/.

The number of simulated individuals was kept constant at 30, loosely based on the estimated density of cats in the study area (Berris et al. 2019). Since territorial

behaviour (i.e., conspecific avoidance) was mostly exhibited within the same sex (Figure A.3), we attempted to parameterise our simulations to a single sex. This translated to a density of 1.25 km^{-2} in our simulation landscape, which is slightly less than half of the empirical density estimate of 2.98 km^{-2}.

Each simulation was run for 21,600 timesteps with a prior burn-in of 5,040 timesteps. We treated the output as equivalent to 30 days (i.e., one timestep as one minute on a 12-hour activity day).

Text A.2: Sensitivity analysis details

Parameters of interest. Since we were interested in the physical properties of emergent movement patterns, we selected parameters that were hypothesised to be of significant influence: resource regeneration rate, searching speed, feeding speed, short-term memory decay rate, long-term memory decay rate, memory expectation, scent deposition rate, scent decay rate and scent response spatial scale. Length parameters (searching and feeding speed), resource regeneration and consumption rates were hypothesised to directly influence distance metrics (step-length, step-length distribution skewness, daily distance covered). We selected two memory parameters, the short- and long-term decay rate, that were predicted to affect the exploratory tendencies of individuals via repulsion (from recently visited areas) and attraction (to long-term memory of resource quality) respectively. As the role of scent was postulated to play an important role in mediating UD area and degree of UD overlap, we selected three of five scent parameters for the SA (scent deposition and decay rate, scent response strength).

Summary statistics. Summary statistics for each replicate simulation were calculated from data subsampled at 15-minute intervals (one timestep = one minute) to match the temporal resolution of the cat data and were calculated as follows:

- **Step-length** was measured as the Euclidean distance between consecutive steps, and the median of all individuals' median step-length was taken as the summary statistic for the replicate.
- **Step-length distribution skewness** was the replicate median skewness measure across all individuals' step-length distributions.
- **Daily distance** was measured as the sum of all step-lengths within each 12-hour bloc (treated as one day), and the median of all individuals' median daily distance covered was taken as the summary statistic for the replicate.
- **UD area** was the replicate median of individuals' 95% kernel density estimate of utilisation distribution (UD) area.

- **UD size skewness** was the skewness measure across individuals' UD area.
- **UD overlap** was the median across individuals' maximum pairwise (proportional) overlap in UD.

For the first three summary statistics, we first converted the data to an `ltraj` object (of R package `adehabitatLT`), which automatically calculates the Euclidean distance between each consecutive step for each individual. UD area was calculated using the kernel density estimator function kernelUD in the R package `adehabitatHR`. For UD overlap, we calculated each individual's pairwise proportional overlap in HR with every other individual, which was taken as the overlapped area (using function `gIntersection` and `gArea` of R package `rgeos`) divided by the pair's merged UD area (using function `gUnion` and `gArea` of R package `rgeos`). Since most individual pairs are not adjacent and hence do not overlap, we prevent the effect of zero-inflation by taking the maximum value for each individual (i.e., the conspecific that it overlaps with the most). We used a proportional measure of UD overlap rather than an absolute measure to account for the confounding effect of varying UD sizes.

Text A.3: BRT model fitting and selection

To optimise sampling within a high dimensional parameter space, we drew 1,000 Latin hypercube (LH) samples of parameter combinations uniformly distributed over ranges given by Table 2.1 with the function `randomLHS` in the R package `lhs`. LH sampling implements an equal-area subdivision of the sample space and then samples randomly within each subdivision (McKay et al. 1979). We ran movement simulations for 1,000 LH samples, one sample (replicate) per parameter combination. We traded-off more replicate runs per sample to more extensively sample across parameter space as it more accurately captures the input-output relationship of the simulation model (Prowse et al. 2016).

The influence of input parameters on each respective output metric (i.e., response) was estimated with boosted regression trees (BRT) to account for complex, non-linear relationships and parameter interactions (Elith et al. 2008; Prowse et al. 2016). We fitted multiple models for each response by varying the BRT interaction depth (or tree complexity) permitted. We fitted BRT models with the R package `dismo` using the function `gbm.step` with a learning rate of 0.01, a bag fraction of 0.75, and a tree complexity of 1–9, and optimised the number of fitted trees based on five-fold cross-validation (CV). We assumed Gaussian errors for all the response variables. We selected the least complex model (lowest interaction depth) within one standard error of the best model (lowest CV deviance) (see Section 7.10 in Hastie et al. 2013). If CV deviance for a response was less than 0.01 at tree complexity (tc) of 1, we automatically selected this model.

We calculated the relative influence of each input parameter, calculated as the number of times the parameter is selected for splitting a tree, weighted by the improvement resulting from that split, averaged over all trees. It was then scaled to sum to 100, with higher numbers indicating stronger influence on the output metric. We then constructed partial dependency plots to visualise the relationship between each input parameter and output metric. In models with a tc > 1, we measured the interaction strength for top pairwise interactions between input parameters, with values near zero representing negligible interactions.

Text A.4: Parameter calibration details

Coarse-tuning. We started the calibration process by first determining an optimised parameter set with which to achieve the target values for the six summary statistics simultaneously. Their respective BRT models were used to predict and optimise output to target statistics, using the base R function `optim`. Optimisation was initialised with appropriate starting values determined by the SA rather than random values because of convergence issues (e.g., local maxima, step-like predictions did not fit method's smooth functions). We eventually prioritised optimisation to UD statistics (area, area skewness, overlap) because the step-length and daily distance statistics' respective upper ranges (output from the SA) had little and no overlap with the target (i.e., empirical) values (did not emerge from the range of input values). We then ran 10 simulations with this parameter set.

Manual fine-tuning. Since the simulation output's concordance with UD statistics and spatio-temporal patterns was low, subjective decisions had to be made as we proceeded with a manual calibration. Here, we added two criteria (cumulative UD size and spatial distribution of locations) to supplement the reductive measure of UD size, which alone could not capture the complex spatio-temporal properties of animal trajectories. We visually compared these patterns (and did not include them in the SA) because we were unable to derive a quantitative metric (e.g., individual cumulative UD curves were unique, and no one function fit closely to individual curves). UD overlap was also evaluated visually because the empirical measure was based only on a subset of the individuals occurring in the area. Thus, our target criteria for the manual-tuning procedure consisted: UD area, UD area skew, UD overlap, cumulative UD area and spatial distribution of locations.

We evaluated the output's concordance with the five target criteria and manually adjusted the parameter set based on that information. This process was iterated until no further improvement was found (i.e., improving one metric made another worse). We then ran 10 simulations using our final set of parameters and compared the outcomes with the empirical data.

Table A.1: Comparison of output metrics from empirical data, predictions from boosted regression tree (BRT) models and simulations (i.e., realised data). The mean (within one standard deviations) of all 10 simulations is presented.

Metric	Empirical	Prediction	Realised (simulations)
Step-length (km)	0.07	0.05	0.06 ± 0.003
Step-length skewness	2.2	1.8	1.6 ± 0.06
Daily distance covered (km)	4.8	3.0	3.4 ± 0.17
UD area (km^2)	1.9	1.8	1.9 ± 0.28
UD area skewness	1.8	1.6	1.4 ± 0.72

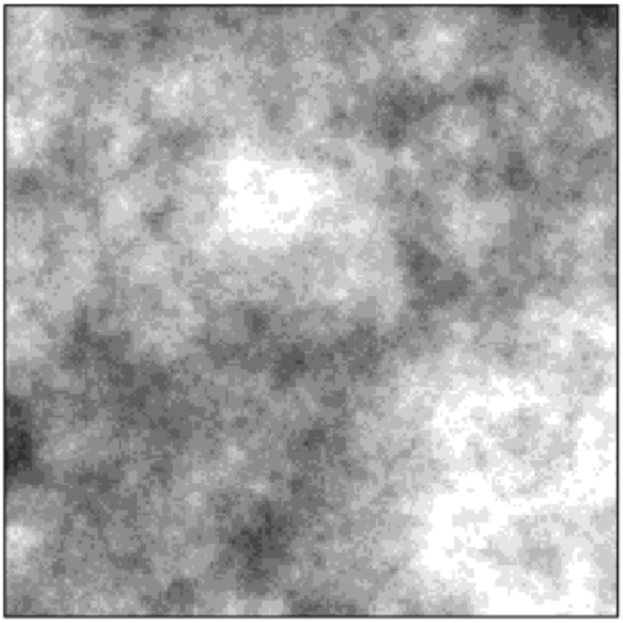

Figure A.1: The 200 by 200 pixel heterogenous resource landscape used in movement simulations for the theoretical examples. Colour indicates resource quality from none (white) to low (light grey) to high (dark grey).

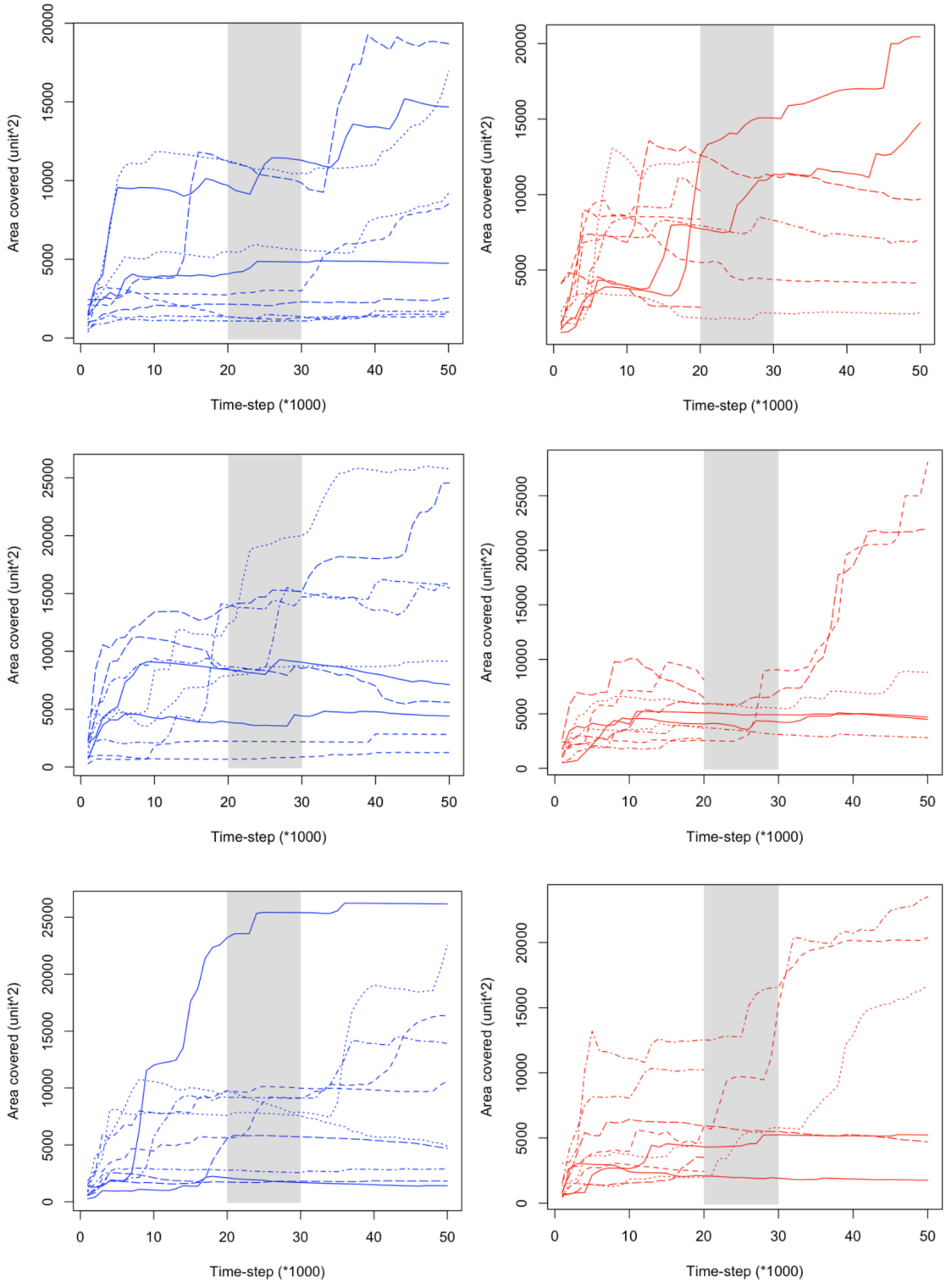

Figure A.2: Cumulative area covered over time in population manipulation simulations from three realisations in the null scenario (left panel; no removal of individuals) and the treatment scenario (right panel; removal of four individuals). Each coloured line represents a single individual in the simulation. The grey shaded area indicates the transition phase, starting at timestep $t = 20,001$, when the individuals were removed for the treatment scenario.

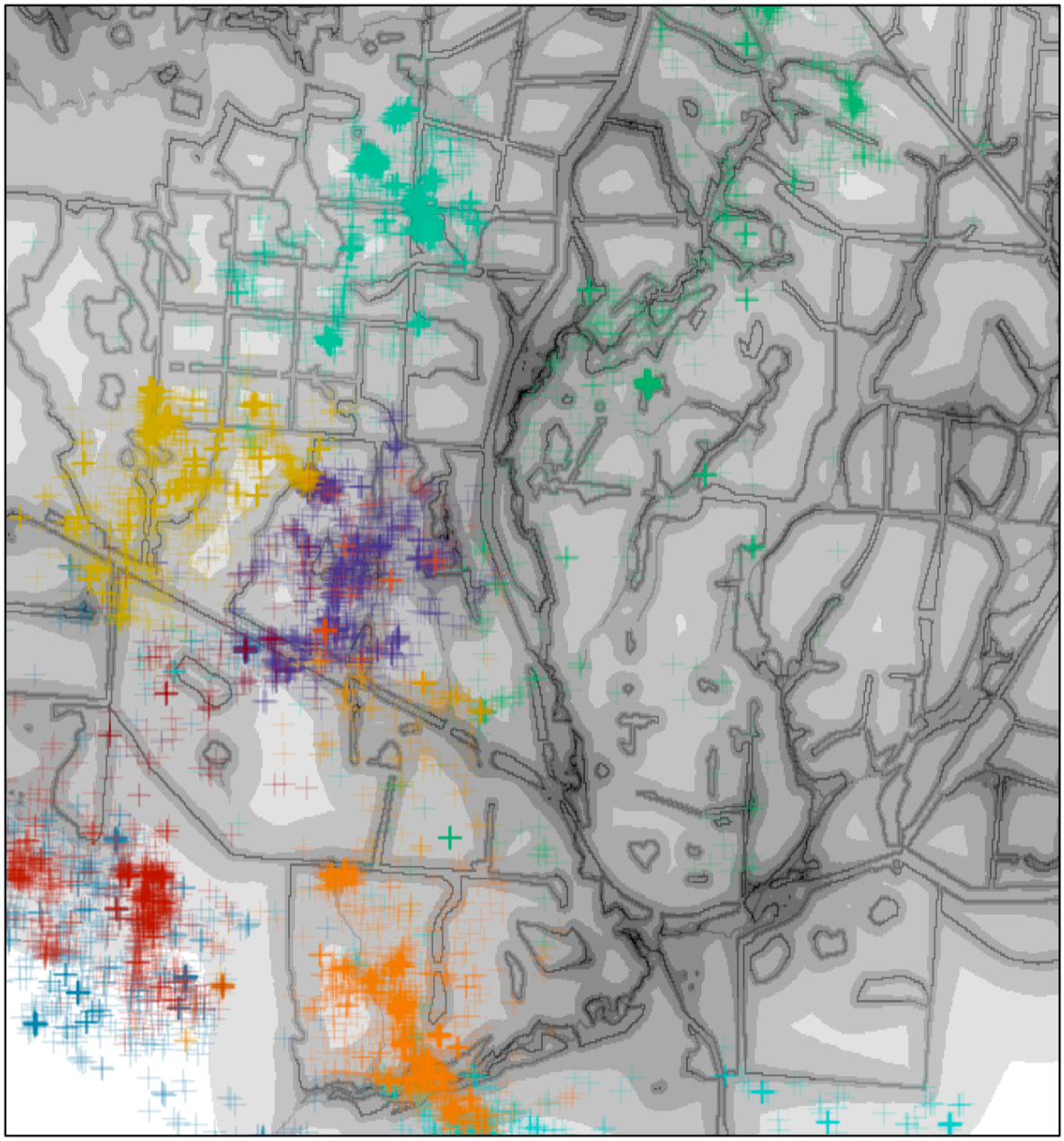

Figure A.3: Feral cat locations. GPS-locations of 6 adult female (warm colours) and 5 adult male feral cats (cool colours). The background represents the resource map, which was derived by calculating the 1–($\log_2$+1) scaled Euclidean distance from three environmental layers (water courses, vegetation and buildings).

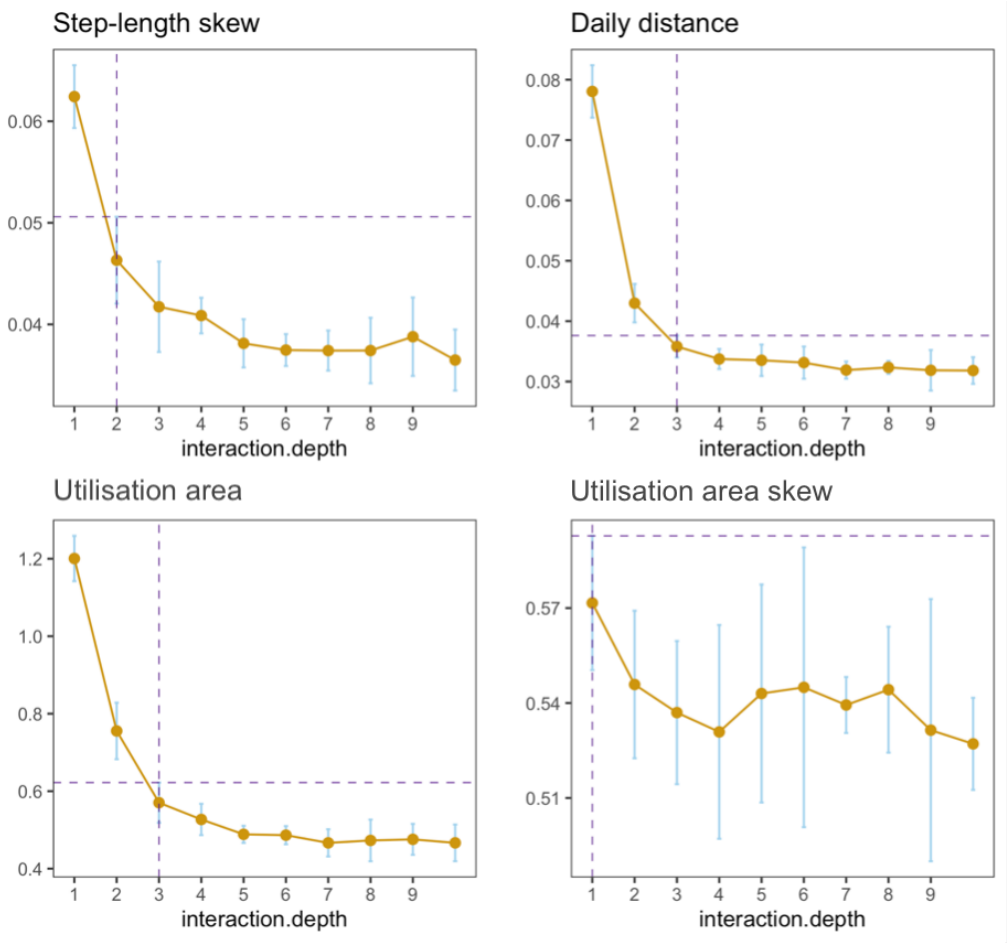

Figure A.4: Estimated prediction error curves and their standard errors for boosted regression tree (BRT) models of each summary statistic. Each curve is plotted as a function of interaction depth (i.e., tree complexity). The estimates of prediction error and their standard errors were obtained by fivefold cross-validation ('CV'). The least complex model within one standard error of the best is chosen, indicated by the purple vertical dashed lines. Note that we did not perform regularisation for step-length and UD overlap as CV deviance was less than 0.01 at tree complexity of 1.

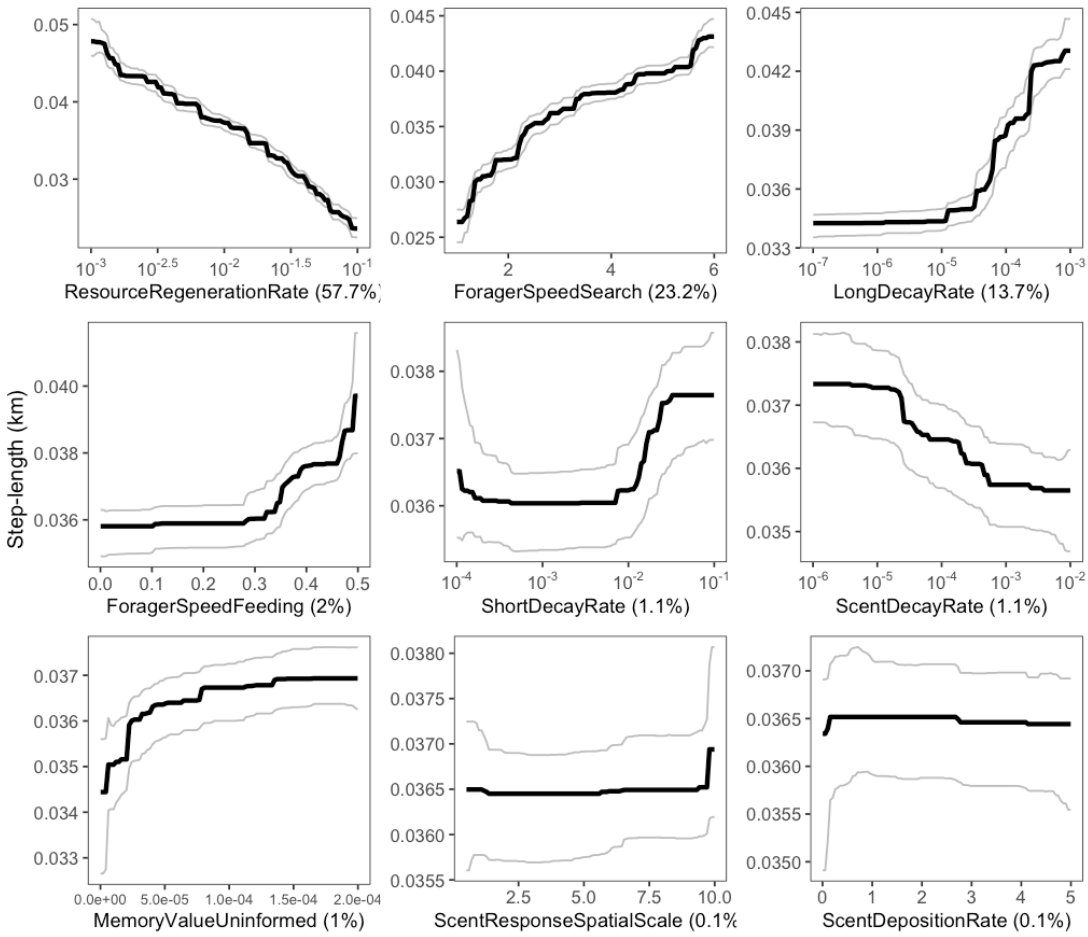

Figure A.5: Partial effects of input parameters on step-length as generated from our boosted regression tree (BRT) analysis. Partial dependency plots show the effect of a given explanatory variable on step-length, while holding the effects of other explanatory variables at their average. We used 500 bootstrap replicates to calculate the 95% confidence intervals, depicted in grey. Note that several of the xaxes are on a log-10 scale.

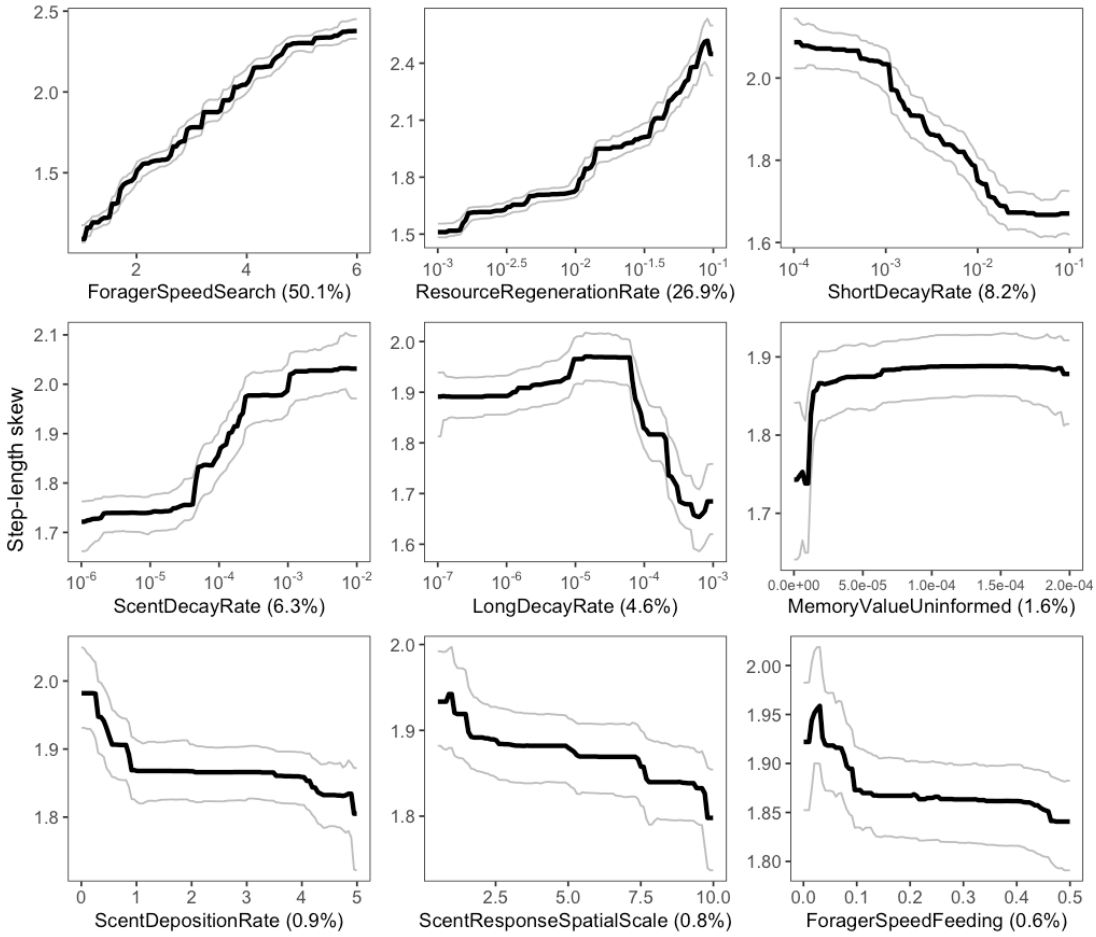

Figure A.6: Partial effects of input parameters on step-length skew as generated from our boosted regression tree (BRT) analysis. Partial dependency plots show the effect of a given explanatory variable on step-length skew, while holding the effects of other explanatory variables at their average. We used 500 bootstrap replicates to calculate the 95% confidence intervals, depicted in grey. Note that several of the xaxes are on a log-10 scale.

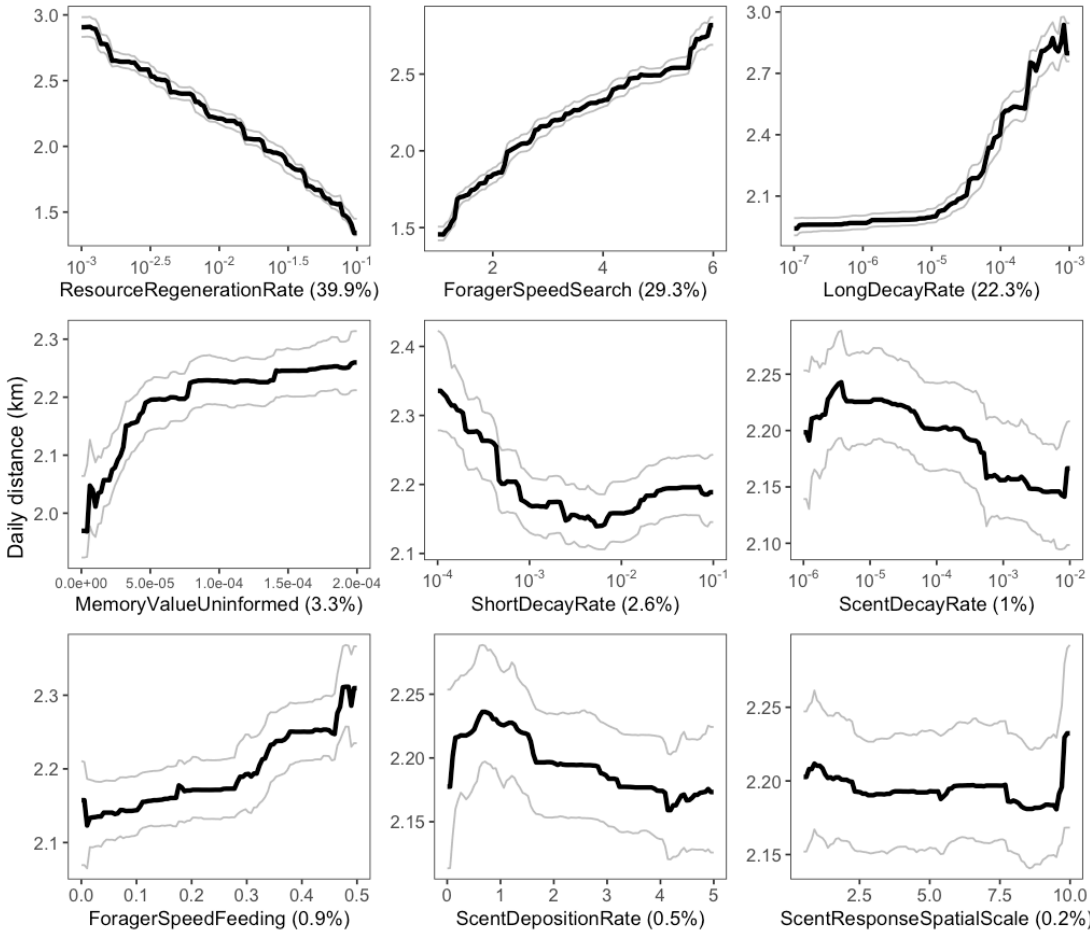

Figure A.7: Partial effects of input parameters on daily distance (covered) as generated from our boosted regression tree (BRT) analysis. Partial dependency plots show the effect of a given explanatory variable on daily distance, while holding the effects of other explanatory variables at their average. We used 500 bootstrap replicates to calculate the 95% confidence intervals, depicted in grey. Note that several of the xaxes are on a log-10 scale.

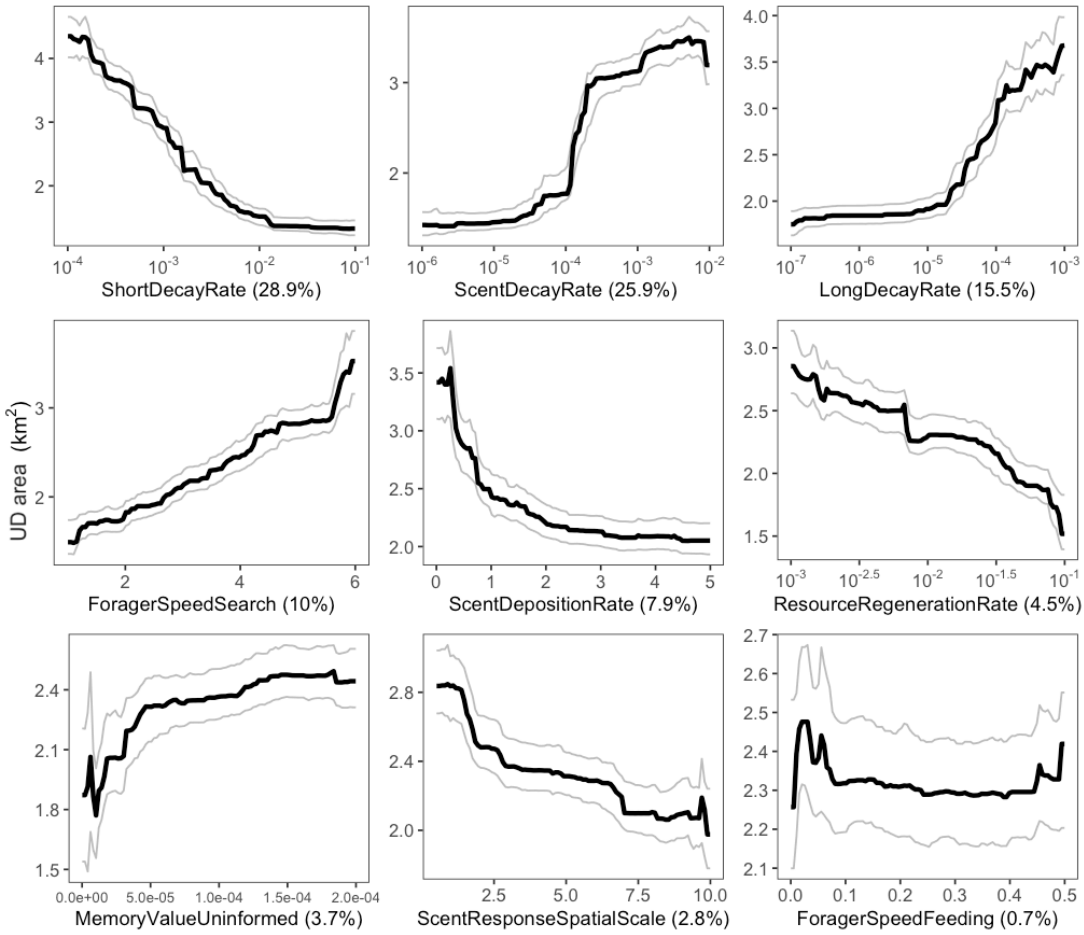

Figure A.8: Partial effects of input parameters on utilisation distribution (UD) area as generated from our boosted regression tree (BRT) analysis. Partial dependency plots show the effect of a given explanatory variable on UD area, while holding the effects of other explanatory variables at their average. We used 500 bootstrap replicates to calculate the 95% confidence intervals, depicted in grey. Note that several of the xaxes are on a log-10 scale.

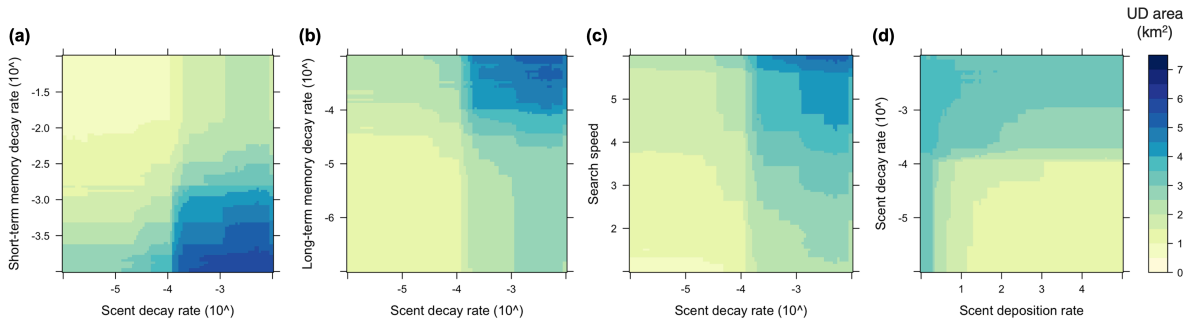

Figure A.9: Pairwise parameter interactions explaining home-range size. (a) scent decay rate and short-term memory decay rate, (b) scent decay rate and long-term memory decay rate, (c) search speed and scent decay rate, and (d) scent deposition rate and scent decay rate. Darker shades indicate larger home-range area as predicted from the boosted regression tree (BRT) model. Interaction sizes for each interaction are 75 (a), 43, (b), 34(c), 32(d).

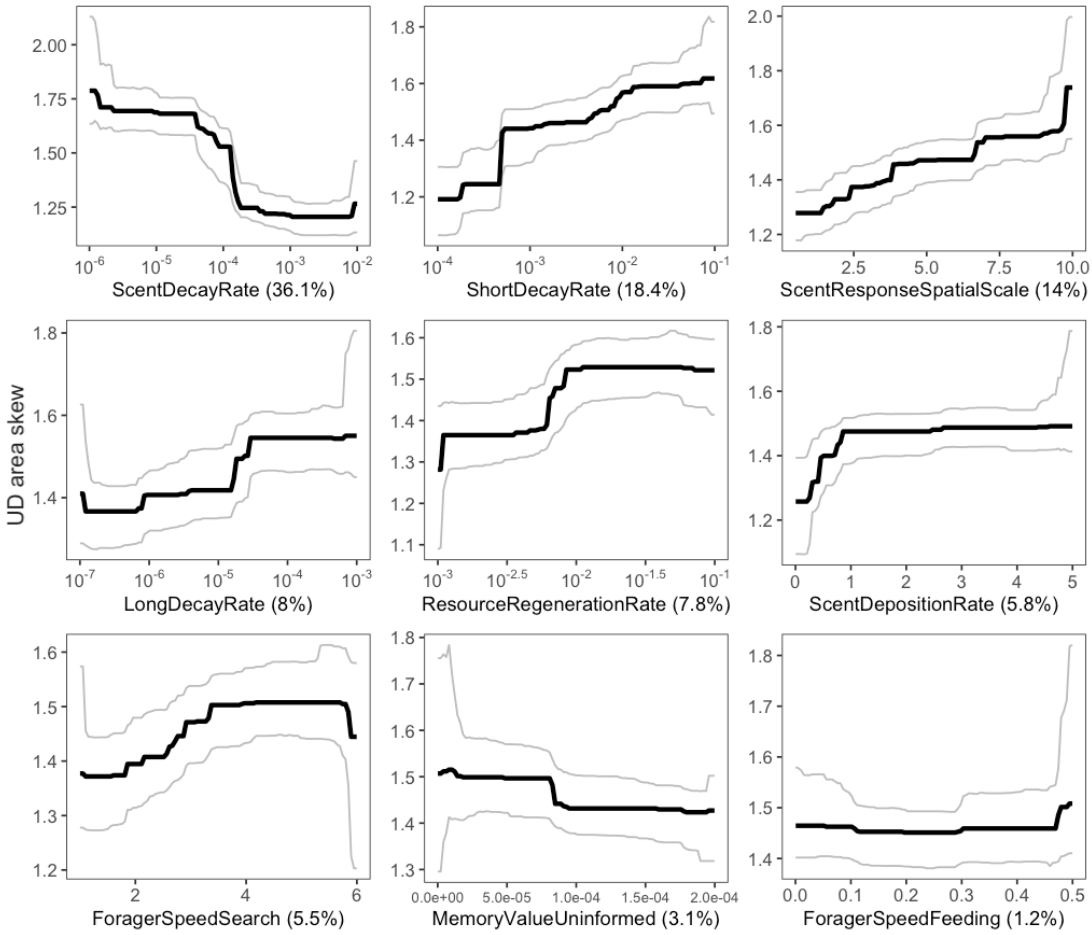

Figure A.10: Partial effects of input parameters on utilisation distribution (UD) area skew (distribution skewness) as generated from our boosted regression tree (BRT) analysis. Partial dependency plots show the effect of a given explanatory variable on UD area skew, while holding the effects of other explanatory variables at their average. We used 500 bootstrap replicates to calculate the 95% confidence intervals, depicted in grey. Note that several of the xaxes are on a log10 scale.

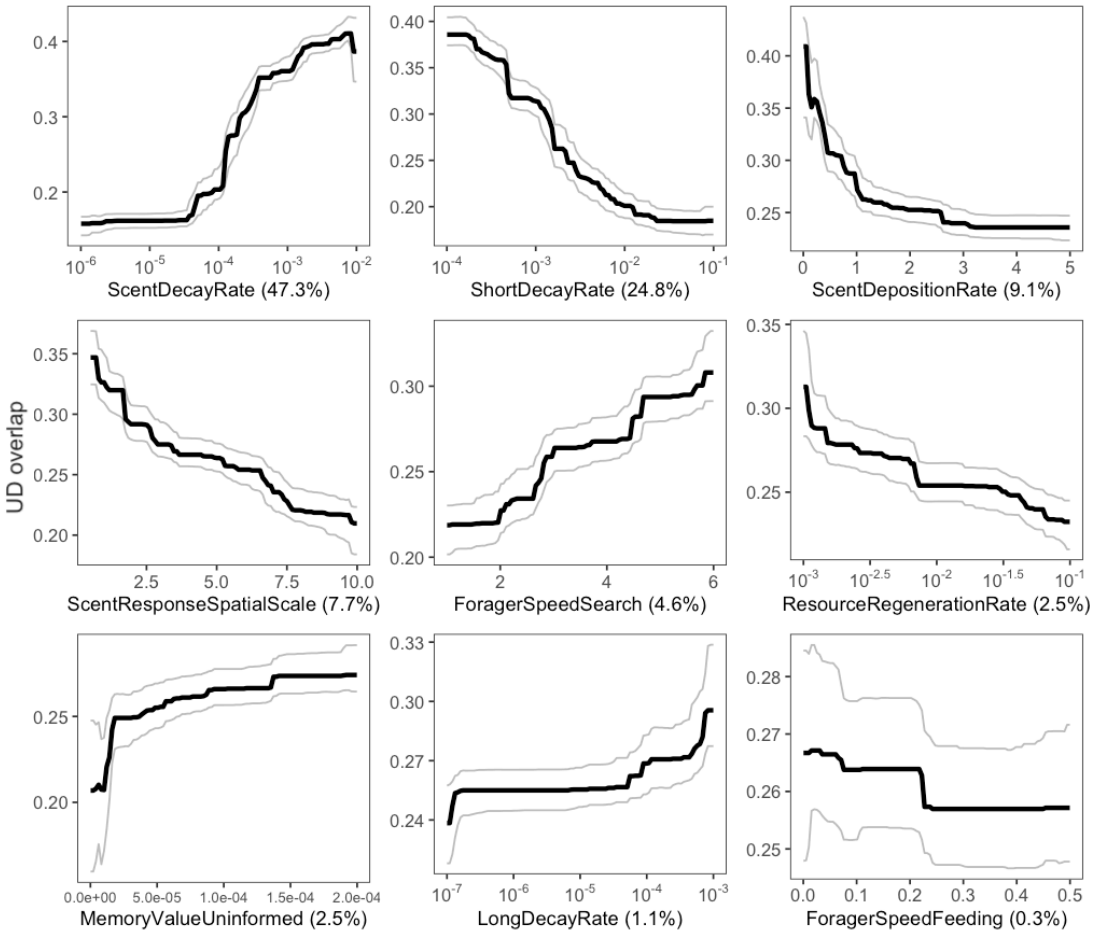

Figure A.11: Partial effects of input parameters on utilisation distribution (UD) overlap (mean of maximum individual pairwise % overlap of 95% home-range area) as generated from our boosted regression tree (BRT) analysis. Partial dependency plots show the effect of a given explanatory variable on UD overlap, while holding the effects of other explanatory variables at their average. We used 500 bootstrap replicates to calculate the 95% confidence intervals, depicted in grey. Note that several of the xaxes are on a log-10 scale.

B

Supplementary information: Chapter 3

Table B.1: Summary of detection histories for 100 replicates with an occasion length of one day, which translates to 30 occasions ($T = 30$). Values represent the mean and standard deviation (in brackets).

Survey summary	Females	Males
Number of independent detections	76.2 (9.8)	71.1 (8.8)
Individuals detected	29.8 (2.8)	23.2 (2.0)
Individuals detected once	9.4 (2.7)	5.4 (2.1)
Average detections per detected individual	2.6 (0.3)	3.1 (0.4)
Traps visited	52.3 (4.7)	50.1 (5.0)
Average traps visited per detected individual	1.9 (0.2)	2.4 (0.3)
Average traps visited per individual per occasion (T = 30)	0.09 (0.01)	0.10 (0.01)

Table B.2: Mean, standard deviation (SD) and coefficient of variation (CV) of $\hat{\sigma_{\text{det}}}$.

Scenario	Model	Females			Males		
		Mean	SD	CV	Mean	SD	CV
A			$N = 60$			$N = 40$	
	Basic						
	Null	16.9	2.5	0.15	20.9	3.8	0.18
	Covariate	16.9	2.5	0.15	20.9	3.8	0.18
	RSF						
	Null	16.6	2.5	0.15	20.6	3.8	0.19
	Covariate	16.6	2.5	0.15	20.5	3.8	0.18
	Transience						
	Null	13.8	2.3	0.17	15.6	3.0	0.19

Scenario	Model	Females			Males		
B			$N = 54$			$N = 36$	
	Basic						
	Null	13.9	2.3	0.17	18.0	3.0	0.17
	Covariate	13.9	2.3	0.17	18.0	3.0	0.17
	RSF						
	Null	13.6	2.4	0.18	17.8	3.2	0.18
	Covariate	13.5	2.4	0.17	17.6	3.1	0.17
	Transience						
	Null	10.9	2.3	0.21	12.8	2.7	0.21
C			$N = 48$			$N = 32$	
	Basic						
	Null	12.3	1.8	0.15	16.0	2.4	0.15
	Covariate	12.3	1.8	0.15	16.0	2.3	0.15
	RSF						
	Null	12.0	1.9	0.16	15.8	2.5	0.16
	Covariate	12.0	1.8	0.15	15.6	2.4	0.15
	Transience						
	Null	9.9	2.1	0.21	11.9	2.4	0.20

Table B.3: Average relative bias (RB), coverage and coefficient of variation (CV) of $\hat{A_{0.95}}$ with respect to hourly and daily measures of $A_{0.95}$ (population mean).

Scenario	Model	Females					Males				
		Hourly		Daily			Hourly		Daily		
		RB	Coverage	RB	Coverage	CV	RB	Coverage	RB	Coverage	CV
A		$N =$ 60					$N =$ 40				
	Basic										
	Null	0.53	0.44	0.12	0.82	0.29	0.48	0.58	0.08	0.79	0.41
	Covariate	0.52	0.33	0.11	0.65	0.29	0.48	0.40	0.08	0.57	0.41
B		$N =$ 54					$N =$ 36				
	Basic										
	Null	0.53	0.56	0.13	0.83	0.35	0.52	0.53	0.13	0.82	0.35
	Covariate	0.51	0.43	0.12	0.75	0.34	0.51	0.33	0.12	0.59	0.35
C		N = 48					N = 32				
	Basic										
	Null	0.42	0.70	0.08	0.85	0.30	0.42	0.65	0.07	0.84	0.29
	Covariate	0.41	0.64	0.07	0.81	0.29	0.41	0.45	0.07	0.65	0.29

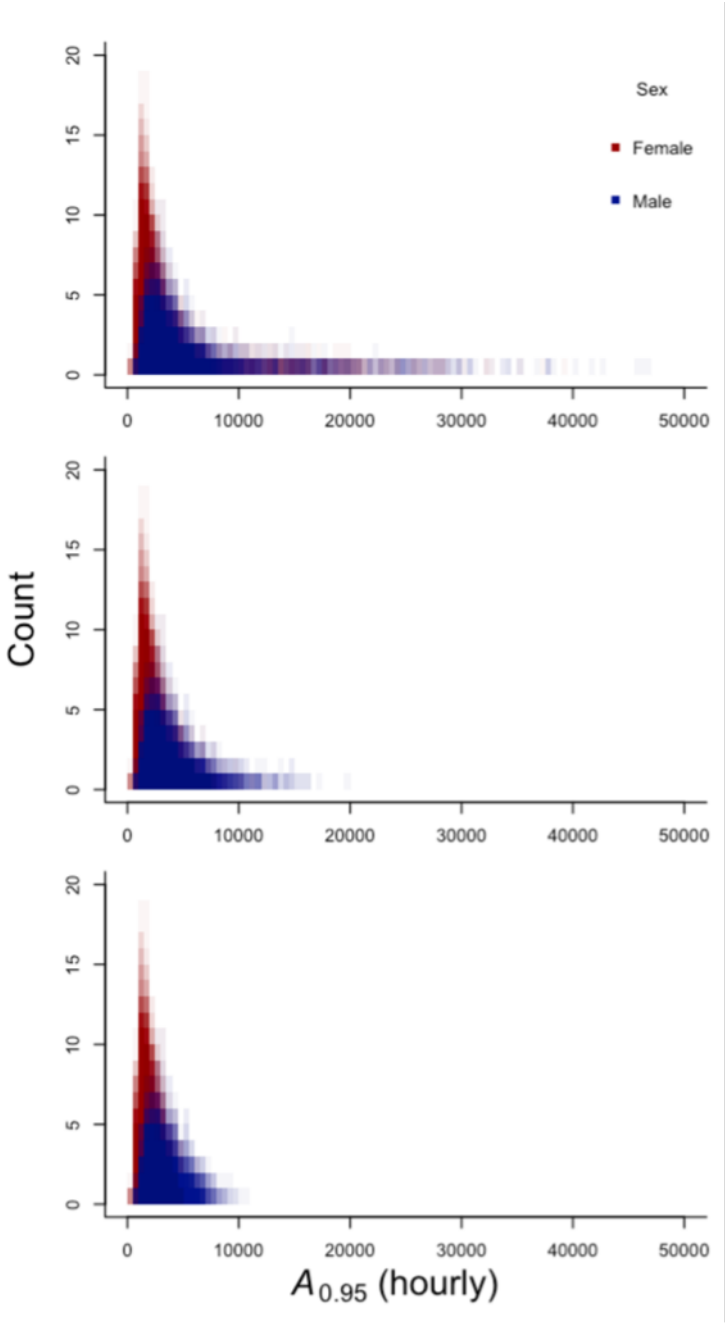

Figure B.1: Area of use (hourly-sampled) distribution in scenario A (full dataset), B (10% widest-ranging individuals of each sex removed) and C (20% widest-ranging individuals of each sex removed). Each panel shows 100 overlaid replicate-specific distributions (represented as histograms with translucent fill).

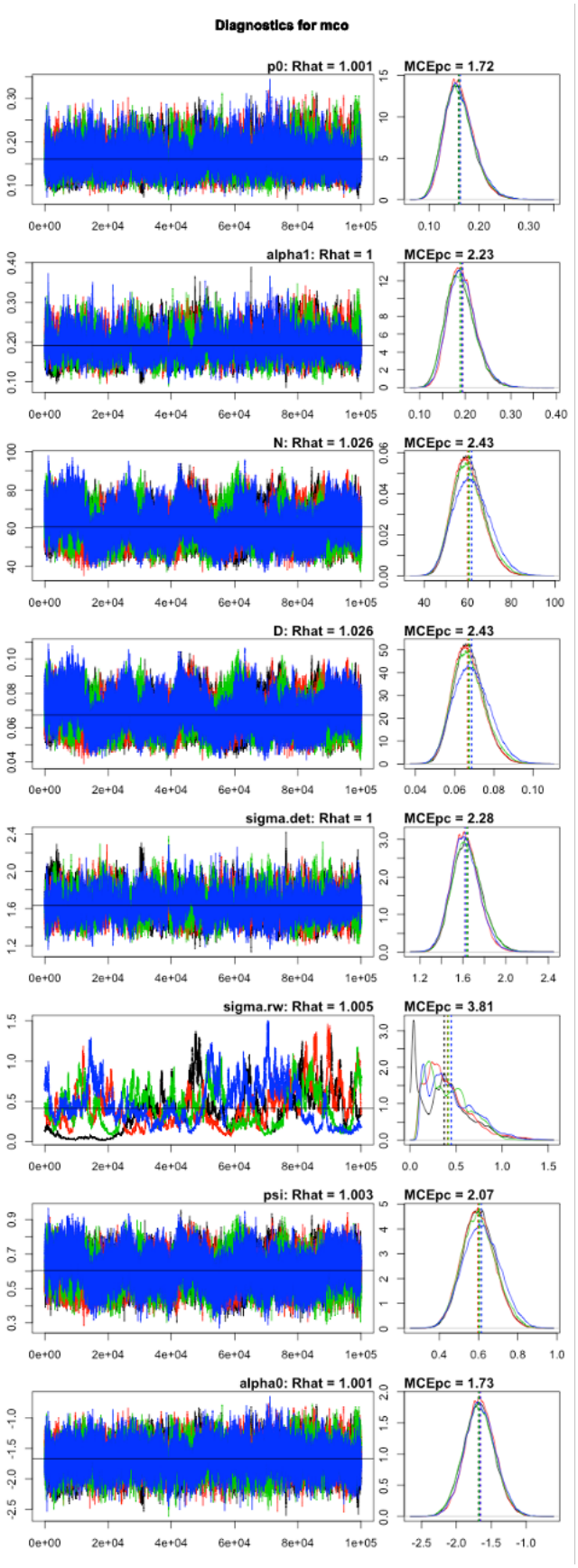

Figure B.2: Diagnostic plots of parameters from one female replicate where trace-plot of $\hat{\sigma}$ show poor mixing, despite $\hat{R}(\hat{\sigma}) \leq 1.1$ ($N = 60$; trap effort of 100, $J = 100$).

Table B.4: Results of fitting the transience model with complete transience to female and male datasets (100 replicates each) from the original trap density ($J = 100$) and double the trap density ($J = 196$, spaced 14 units apart with a circular detection zone of 0.2 unit in radius, set in the centre of the simulation landscape with a 59-unit buffer from the boundaries of the landscape).

Trap density	Parameter	Females		Males	
		Mean	$\hat{R}$	Mean	$\hat{R}$
Original		$N = 60$		$N = 40$	
	N	60.5	1.008	40.1	1.003
	$p0$	0.20	1.004	0.22	1.004
	σ_{det}	13.8	1.006	15.6	1.003
	σ	9.70	1.030	14.6	1.010
	α_0	-1.46	1.005	-1.35	1.003
	α_1	-0.31	1.006	0.24	1.004
Double					
	N	60.1	0.999	38.8	1.001
	$p0$	0.21	1.001	0.23	1.000
	σ_{det}	12.9	1.001	14.5	1.000
	σ	11.0	1.001	15.8	1.002
	α_0	-1.38	1.001	-1.24	1.000
	α_1	0.31	1.001	0.25	1.000

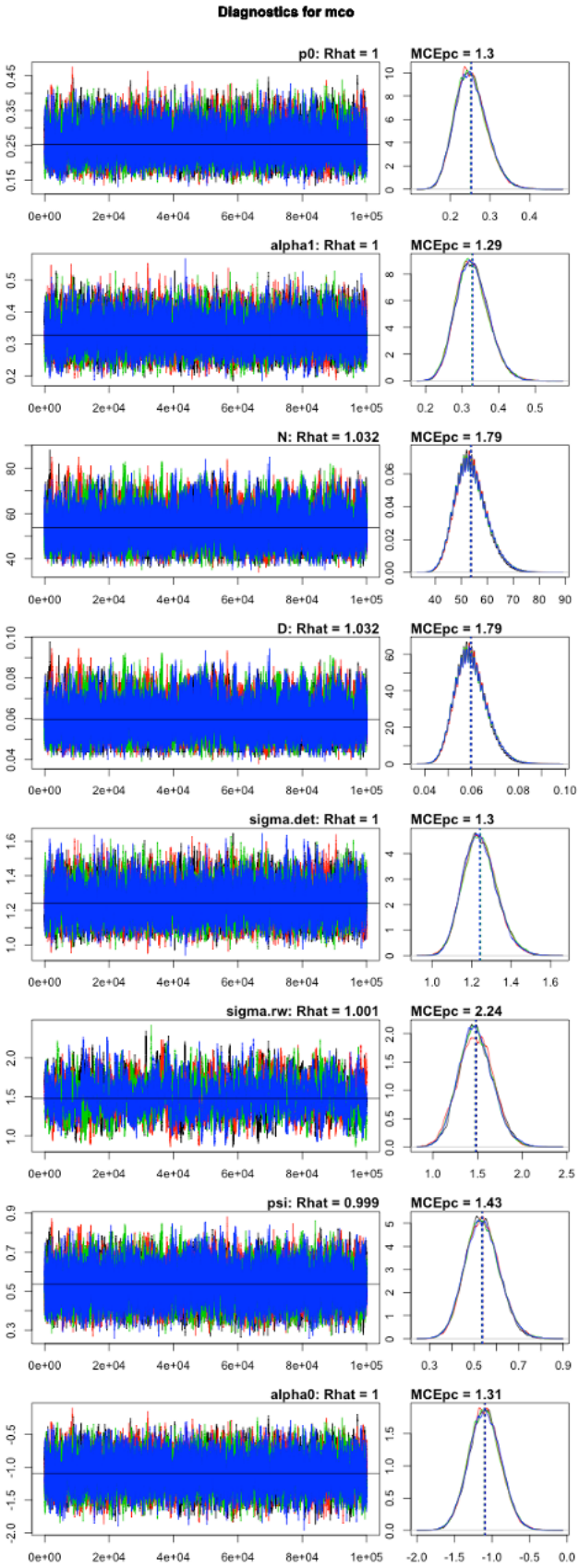

Figure B.3: Diagnostic trace plots of parameters from the same female replicate (Figure B.2) with double the trap density ($N = 60$; trap effort of 196, $J = 196$).

C

Supplementary information: Chapter 4

Table C.1: Simulated animal density scenarios and examples of species roughly corresponding to density values used in simulations.

Density	Species	Density (per 100 km^2)	Reference
High	Mouse deer spp.	200–628	O'Brien et al. (2003)
	Lesser mousedeer	900–3,800	Heydon and Bulloh (1997)
	Lesser mousedeer	8,100	Gray (2018)
	Agouti	6,700–7,000	Beck-King et al. (1999)
	Agouti	10,000	Aliaga-Rossel et al. (2008)
	Long-tailed porcupine	1,426	Ahmad et al. (2021)
Medium	Gray brocket	560	Rivero et al. (2004)
	Capybara	950	Alho and Rondon (1987)
	Red Muntjac	187	Sukmasuang (2001)
	Red Muntjac	310	Srikosamatara (2009)
	Malay civet	217	Colon (2002)
	Pampas fox	110–150	Luengos Vidal et al. (2012)
Low	Crab-eating fox	78	Faria-Corrêa et al. (2009)
	Malayan tapir	7	Siti (2010)
	Malayan tapir	9.5	Rayan et al. (2012)

Density	Species	Density (per 100 km^2)	Reference
	Leopard	7*	Simcharoen et al. (2008)
	Leopard	5	Athreya et al. (2013)

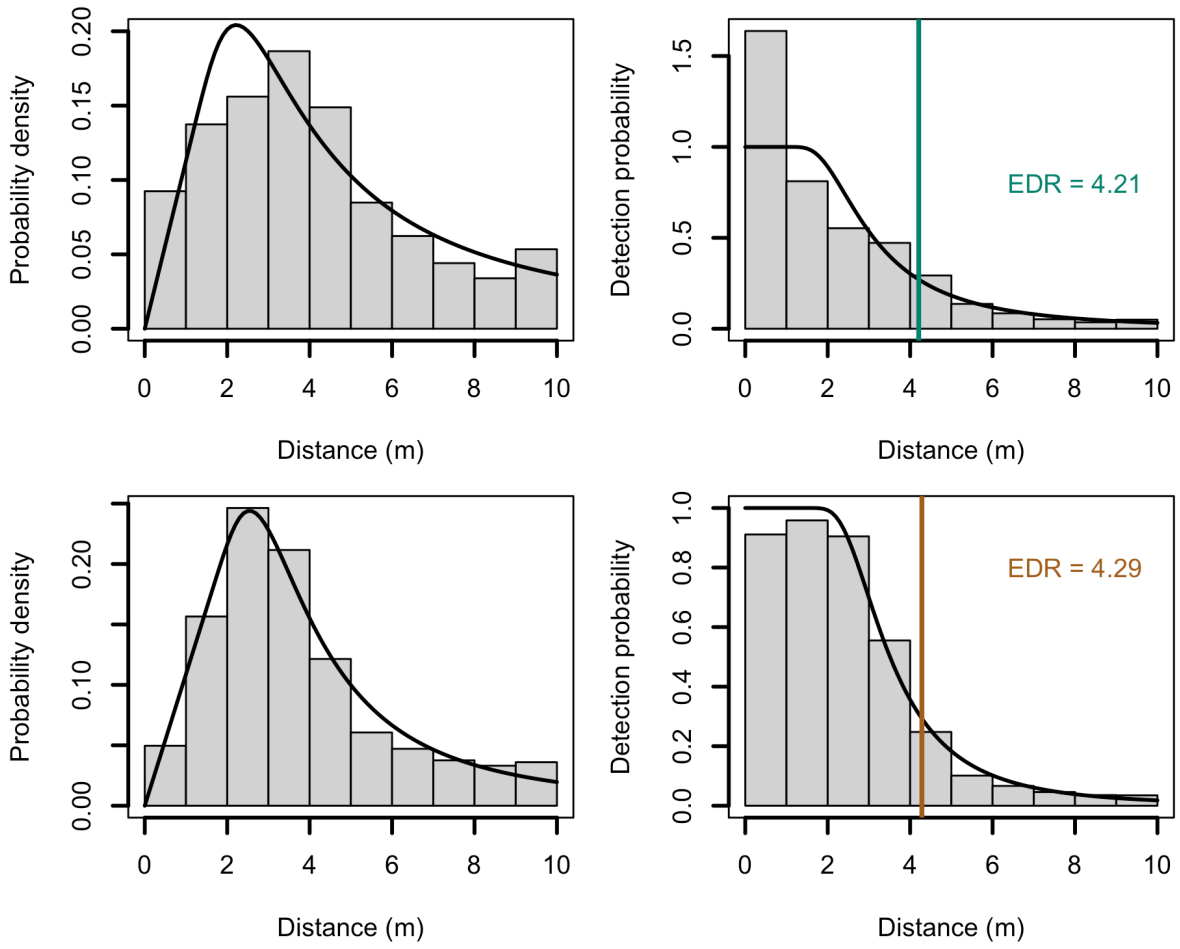

Figure C.1: Example radius/distance dataset from the high-density group100 scenario fitted to a hazard-rate model with no adjustments. Top panel shows the estimated probability density function (left) and detection function (right). Bottom panel shows the estimated probability density function (left) and detection function (right) for CTDS's distance data.

Table C.2: Simulated animal movement scenarios and examples of species roughly corresponding to parameter values used in simulations. Home-range and movement speed values represent the mean and standard deviation (in brackets), or a range of values. Our simulated speed are faster than those reported in literature because we simulated movement at a higher temporal resolution (5-min timesteps).

Density (movement rate)	Species	Home-range size (kmˆ2)	HR method	Movement speed (m/h)	Fix interval	Reference
High (slow)	Agouti	0.026 (0.003)	100% MCP	69.2 (17.9)	30 min	Aliaga-Rossel et al. (2008)
	Lesser mousedeer	0.051	100% MCP	21.9 (19.3)	2 h	Matsubayashi et al. (2003)
	Long-tailed porcupine	0.105 (0.07)	100% MCP			Matsukawa et al. (2018)
	Gray brocket	0.34–1.0*	95% MCP	110 (182)**; 53.2 (69.6)***	15 min	Grotta-Neto et al. (2019, 2020)
Medium (moderate)	Capybara	0.87 (0.06)	??% aKDE	164 (54)	4 h	Lopes et al. (2021)
	Pampas fox	1.40 (0.96)	95% MCP			Luengos Vidal et al. (2012)
	Malay civet	1.10 (0.58)	95% MCP	300	30 min	Colon (2002)
	Red Muntjac	2.78 (0.74)	95% MCP	271	1 h	Sukmasuang (2001)
	Leopard cat	2.8–5.8	100% MCP	305	1–4h	Schmidt et al. (2003)
Low (fast)	Malayan tapir	17.8	100% MCP	220	1 h	Siti (2010)
	Crab-eating fox	12.8	100% MCP	1820	15 min	Juarez and Marinho-Filho (2002)
	Golden jackal	26.3	95% MCP	1680 (310)	15 min	Charaspet et al. (2019)
	Leopard	26 (8.2)	95% FK			Simcharoen et al. (2008)
	Leopard	8–15	95% FK	339 (9.5)	1 h	Odden et al. (2014)

based on one individual tracked continuously from 19000100 for two days

* based on 15-min fixes, ** open habitat, *** closed habitat

Table C.3: Movement simulation parameters used in each population scenario.

		Individual				Group centroid				Centroid distribution (m)		Realised values	
		Step-length (m/h)		Turning angle		Step-length (m/h)		Turning angle		Min. dist	Border buffer	Speed (m/h)	Home-range size (km2)
Behaviour	Group size	a	b	kappa	w	a	b	kappa	w				
Sol	1			0.6	0.5	–	–	–	–	0	50		0.12
Group20	20	576	360	6,3[brw,crw]	–	420	300	6	0.85	100	200	576	2.4
Group100	100			4,3[brw,crw]	–	420	300	4	1	1500	750		57
Sol	1			0.6	0.57	–	–	–	–	50	250		1.4
Group5	5	1200	750	8,3[brw,crw]	–	960	600	2	0.7	1000	250	1200	3
Group25	25			6,3[brw,crw]	–	960	600	0.75	0.85	2500	750		4
Sol	1	2160		0.65	0.6	–	–	–	–	750	1000	2160	17

Table C.4: Summary of encounters for each method. Values represent the mean and standard deviation (in brackets) across all replicates from each population scenario under high trap effort (100 replicates each; $J = 100$). Density scenarios — hi: high; med: medium; lo: low. Behaviour scenarios — sol: solitary; g: group; #: individuals per group.

Method	Parameter	hi_sol	hi_g20	hi_g100	med_sol	med_g5	med_25	lo_sol
REM	Encounters per cameras (y/cam)	21.6 (20.2)	22.6 (22.6)	23.3 (15.9)	3.7 (3.8)	3.7 (4.5)	3.5 (5.7)	0.24 (0.55)
	Group size per encounter (g/y)	1.00 (0.05)	1.18 (0.5)	1.68 (1.44)	1.00 (0.01)	1.02 (0.14)	1.09 (0.33)	1.00 (0)
REST	Encounters per cameras (y/cam)	8.7	8.8	8.3	1.5	1.5	1.4	0.08
CTDS	Encounters per cameras (y/cam)	93.8	100.1	105.8	9.6	9.5	9.2	0.45

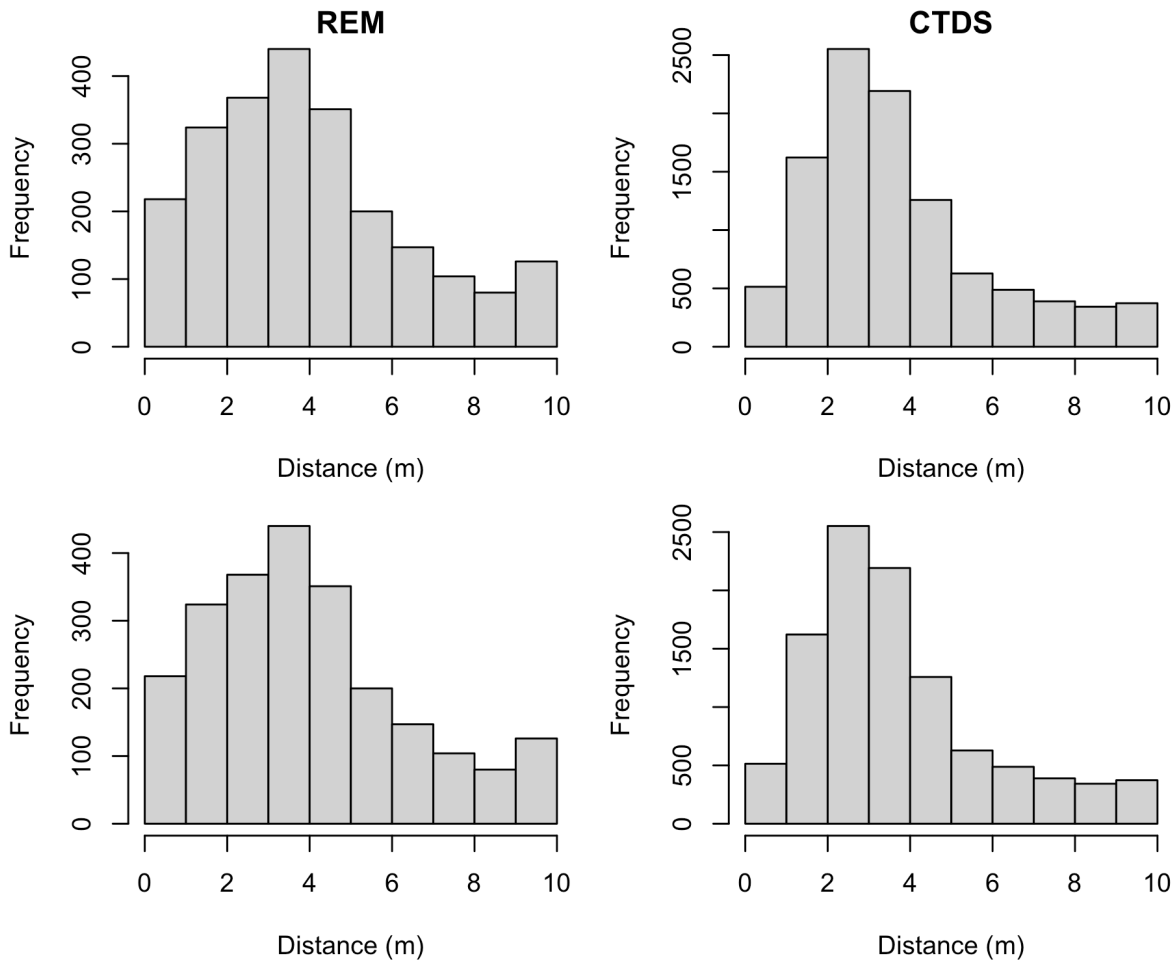

Figure C.2: Frequency distribution of radius/distance data from the high-density group100 scenario (using same replicate as in Figure C.1) under perfect detection (top panel) and imperfect detection (bottom panel) for REM (left panel) and CTDS (right panel). Note that radius/distance data under imperfect detection is a subset of the data from that under perfect detection, after being subjected to our simulated detection function.

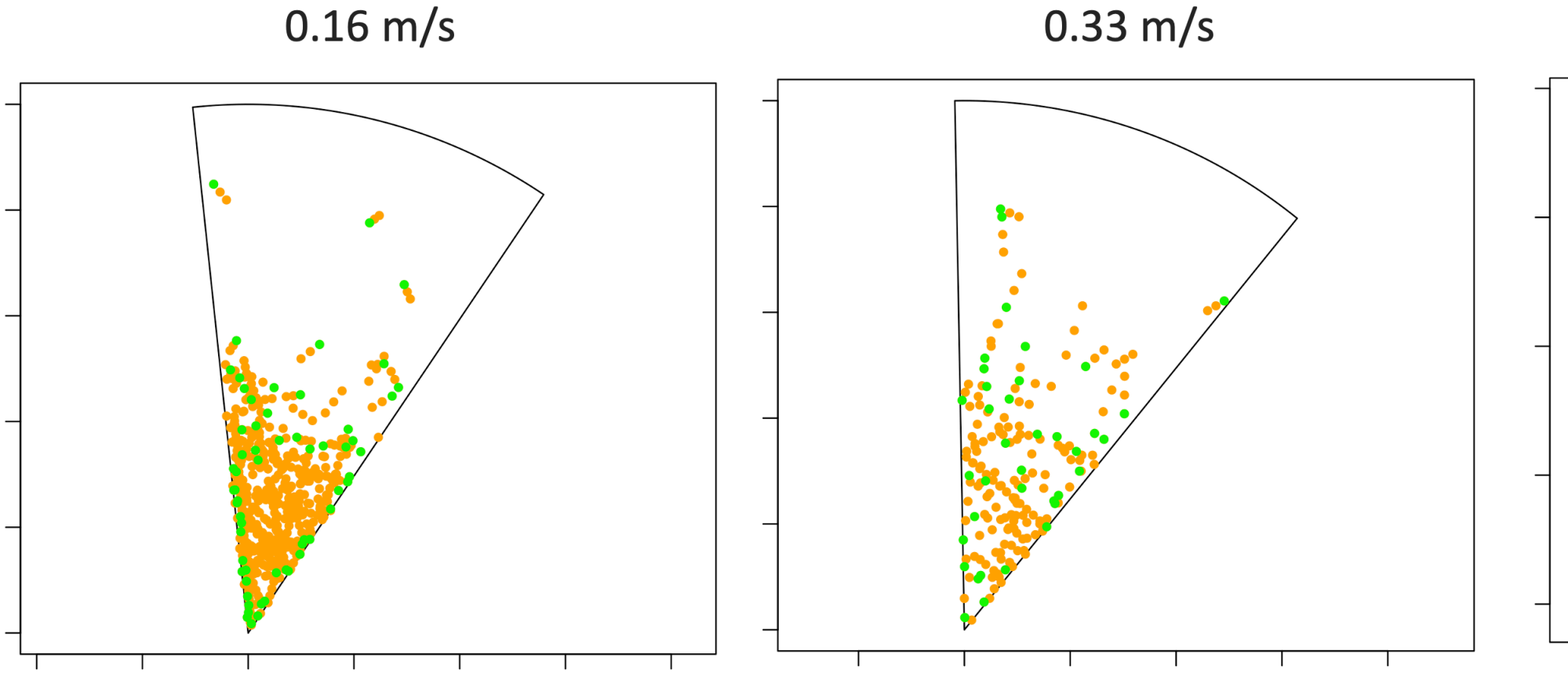

Figure C.3: Animal positions for all detections (orange) and positions for only first detection of sequence (green; i.e., radius data) relative to the camera-trap's field of view (circular sector polygon) from one example simulation for each of the following population scenario – population with mean speed of 0.16 (left), 0.33 (centre) and 0.60 m/s (right).

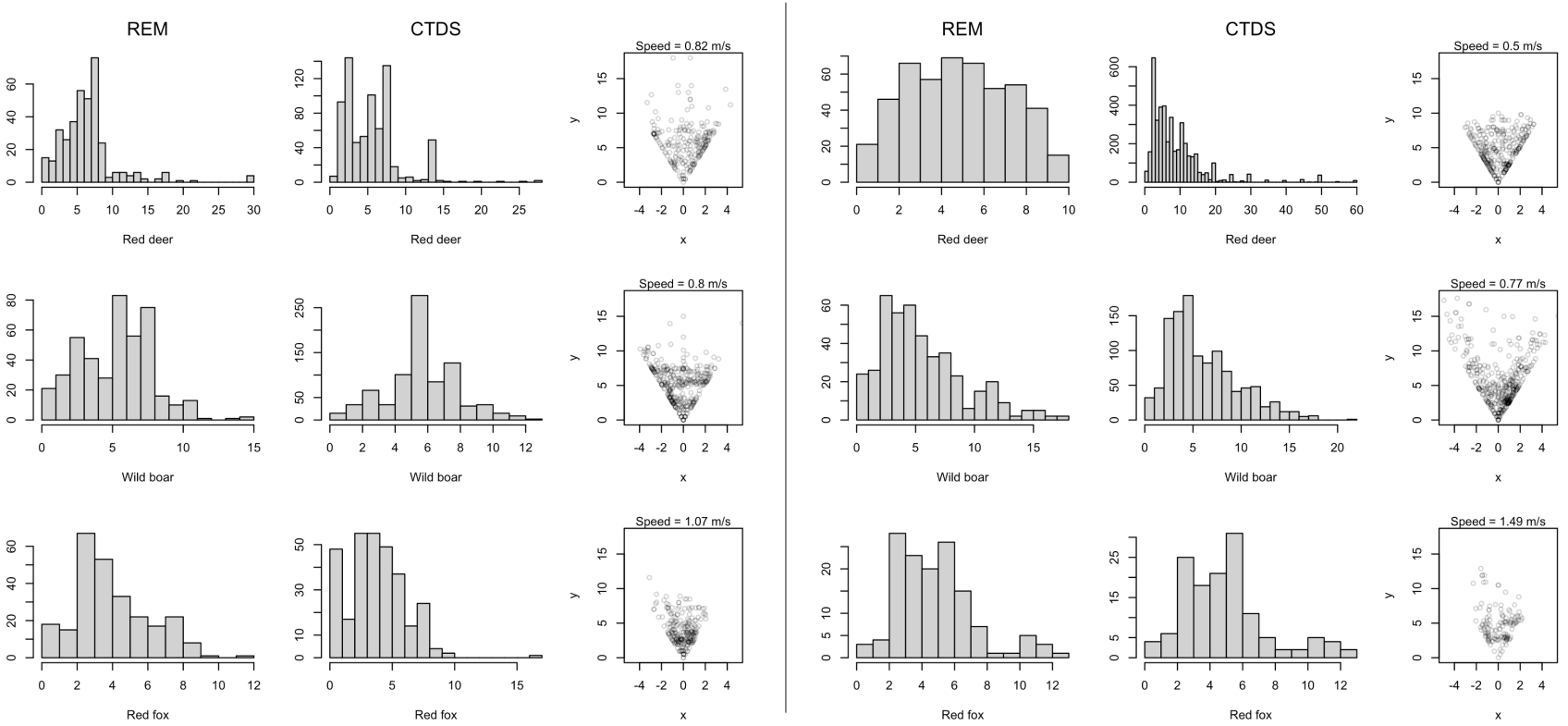

Figure C.4: Frequency distributions of random encounter model (REM) and camera-trap distance sampling (CTDS) distance data from three species (red deer, wild boar, red fox), from two different sites (left: A; right: B). The third panel of each site plot show the locations of animals when the camera-traps were triggered (i.e., REM data). Speeds displayed are the mean speeds of each population. Data from Palencia et al.(2021a). Note that most group captures only recorded the angle of one animal and those locations could not be plotted.

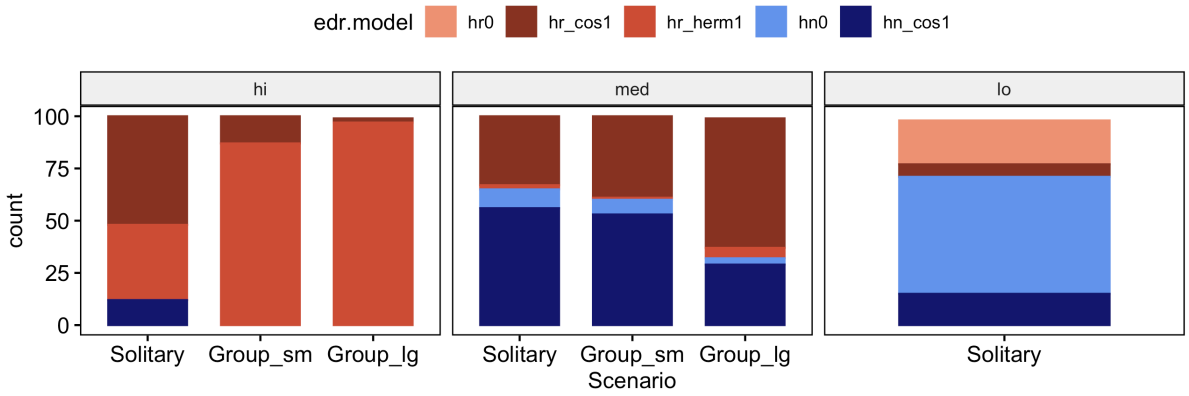

Figure C.5: Counts of detection models (*hr*: hazard-rate, *hn*: half-normal; *cos*: cosine, *herm*: hermite, *poly*: polynomial; 0: no adjustment, 1: 1st order adjustment) selected for each replicate dataset by scenario. The selected model was the one with the lowest AIC value. Detection models were fitted to radius (r) data for density estimation under REM. Note that we did not fit more than one adjustment term because we simulated a monotonically decreasing detection function (i.e., data generating process) with distance from the CT.

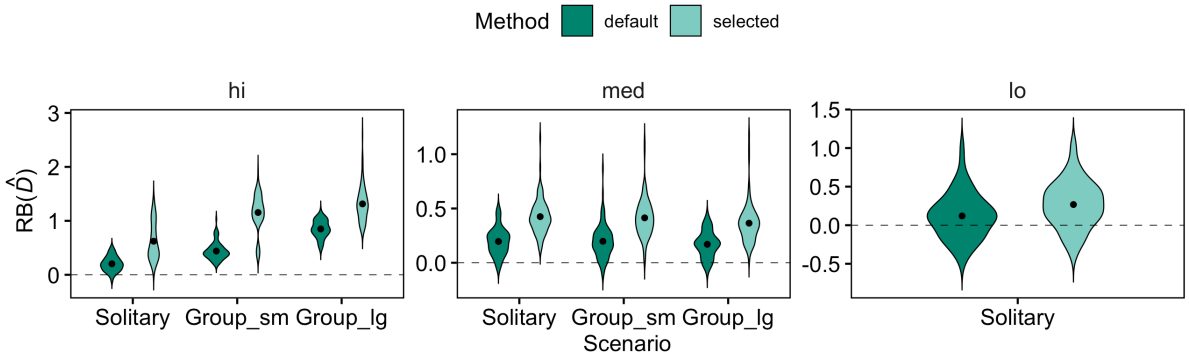

Figure C.6: Comparison of relative bias of estimated density derived from effective detection radius (EDR, mathematically noted as r) estimation under *default* vs. model selection (*selected*) procedures for REM. Violin plots (hi: high-density; med: medium-density; lo: low-density) represent the distribution of relative bias from converged models out of 100 replicate data sets (black point representing the overall mean) of solitary and group scenarios.